

PHYSICOMECHANICAL PROPERTIES
STUDY OF POLYLACTIC ACID (PLA) IN
MULTI-SINGLE PLANE CONFIGURATIONS
VIA FUSED DEPOSITION MODELLING (FDM)



اونيورسيتي مليسيا قهغ السلطان عبدالله
UNIVERSITI MALAYSIA PAHANG
AL-SULTAN ABDULLAH

MASTER OF SCIENCE

UNIVERSITI MALAYSIA PAHANG
AL-SULTAN ABDULLAH

UNIVERSITI MALAYSIA PAHANG AL-SULTAN ABDULLAH

DECLARATION OF THESIS AND COPYRIGHT

Author's Full Name : LYDIA A/P SANDANASAMY
Date of Birth : 11/09/1995
Title : PHYSICOMECHANICAL PROPERTIES STUDY OF
POLYLACTIC ACID (PLA) IN MULTI-SINGLE PLANE
CONFIGURATIONS VIA FUSED DEPOSITION
MODELLING (FDM)
Academic Session : SEM II 2023/2024

I declare that this thesis is classified as:

- CONFIDENTIAL (Contains confidential information under the Official Secret Act 1997)*
- RESTRICTED (Contains restricted information as specified by the organization where research was done)*
- OPEN ACCESS I agree that my thesis to be published as online open access (Full Text)

I acknowledge that Universiti Malaysia Pahang Al-Sultan Abdullah reserves the following rights:

1. The Thesis is the Property of Universiti Malaysia Pahang Al-Sultan Abdullah
2. The Library of Universiti Malaysia Pahang Al-Sultan Abdullah has the right to make copies of the thesis for the purpose of research only.
3. The Library has the right to make copies of the thesis for academic exchange.

Certified by:

S. Lydia

(Student's Signature)

New IC/Passport Number
Date: 13/02/2024



Prof. Madya Ir. Dr. Wan Sharuzi Wan Harun
PhD, PEng, MEng, CEng MIMechE, PTech
Pensyarah
Fakulti Teknologi Kejuruteraan Mekanikal & Automatif
Universiti Malaysia Pahang
20600, Pekan, Pahang
Tel : + 6 09 424 6358 Mobile : + 6 019 358 0058
E-mail : sharuji@ump.edu.my Website : www.ump.edu.my

(Supervisor's Signature)
Assoc.Prof.Ir.Ts.Dr Wan Sharuzi
Bin Wan Harun

Name of Supervisor
Date: 13/02/2024

NOTE: * If the thesis is CONFIDENTIAL or RESTRICTED, please attach a thesis declaration letter.

THESIS DECLARATION LETTER (OPTIONAL)

Librarian,
Universiti Malaysia Pahang Al-Sultan Abdullah,
Lebuh Persiaran Tun Khalil Yaakob,
26300, Gambang, Kuantan, Pahang.

Dear Sir,

CLASSIFICATION OF THESIS AS RESTRICTED

Please be informed that the following thesis is classified as RESTRICTED for a period of three (3) years from the date of this letter. The reasons for this classification are as listed below.

Author's Name

Thesis Title

Reasons

(i)

(ii)

(iii)



Thank you.

Yours faithfully, **اونيفورسيتي مليسيا فهغ السلطان عبدالله**
UNIVERSITI MALAYSIA PAHANG
AL-SULTAN ABDULLAH

(Supervisor's Signature)

Date:

Stamp:

Note: This letter should be written by the supervisor and addressed to the Librarian, *Universiti Malaysia Pahang Al-Sultan Abdullah* with its copy attached to the thesis.



SUPERVISOR'S DECLARATION

We hereby declare that we have checked this thesis and in our opinion, this thesis is adequate in terms of scope and quality for the award of the degree of Master of Science.

Prof. Madya Ir. Dr. Wan Sharuzi Wan Harun
PhD, PEng, MScM, CEng, MIMechE, PTech
Pensyarah
Fakulti Teknologi Kajian Mekanikal & Automatik
Universiti Malaysia Pahang
28600, Pekan, Pahang.
Tel : + 6 09 424 8358 Mobile : + 6 019 956 0038
E-mail : wsharuzi@ump.edu.my Website : www.ump.edu.my

(Supervisor's Signature)

Full Name : ASSOC. PROF. IR. TS. DR. WAN SHARUZI BIN WAN HARUN

Position : ASSOCIATE PROFESSOR

Date : 13/02/2024

(Co-supervisor's Signature)

Full Name : DR ISMAYUZRI BIN ISHAK

Position : LECTURER

Date : 13/02/2024



DR. ISMAYUZRI BIN ISHAK
PENSYARAH KANAN
FAKULTI TEKNOLOGI KEJURUTERAAN
PEMBUATAN & MEKATRONIK
UNIVERSITI MALAYSIA PAHANG
Tel: 09-424 8360 Faks: 09-424 8361

فہمغ السلطان عبداللہ
UNIVERSITI MALAYSIA PAHANG
AL-SULTAN ABDULLAH



STUDENT'S DECLARATION

I hereby declare that the work in this thesis is based on my original work except for quotations and citations which have been duly acknowledged. I also declare that it has not been previously or concurrently submitted for any other degree at Universiti Malaysia Pahang Al-Sultan Abdullah or any other institutions.

S. Lydia

(Student's Signature)

Full Name : LYDIA A/P SANDANASAMY

ID Number : MTM21002

Date : 13/02/2024



اونيورسيتي مليسيا فهغ السلطان عبدالله
UNIVERSITI MALAYSIA PAHANG
AL-SULTAN ABDULLAH

PHYSICOMECHANICAL PROPERTIES STUDY
OF POLYLACTIC ACID (PLA) IN
MULTI-SINGLE PLANE CONFIGURATIONS VIA
FUSED DEPOSITION MODELLING (FDM)

LYDIA A/P SANDANASAMY



Thesis submitted in fulfillment of the requirements

اونيورمليتي مليسيا تيمبڠ السلطان عبدالله
for the award of the degree of

Master of Science
UNIVERSITI MALAYSIA PAHANG
AL-SULTAN ABDULLAH

Faculty of Mechanical and Automotive Engineering Technology

UNIVERSITI MALAYSIA PAHANG AL-SULTAN ABDULLAH

MARCH 2024

ACKNOWLEDGEMENTS

The author would like to express heartfelt gratitude and acknowledgement to their supervisor, Assoc. Prof. Ir. Ts. Dr. Wan Sharuzi Bin Wan Harun, and co-supervisor, Dr. Ismayuzri Bin Ishak, for their invaluable guidance, germinal ideas, continuous encouragement, and unwavering support, which have been instrumental in the realization of this research. The author has consistently been impressed by their exceptional professionalism and progressive vision, further enhancing their appreciation.

Furthermore, the author extends sincere thanks to their lab supervisors, Mr. Zurkarnain and Mr. Aidil Shafiza Bin Safiee, as well as the staff of the Material Lab, for their guidance and provision of essential laboratory equipment throughout the research journey.

The author acknowledges a profound debt of gratitude towards their parents, who have shown unwavering love, unwavering belief and made significant sacrifices throughout their life. The author is particularly thankful for their parents' sacrifice, patience, and understanding, which were crucial in enabling the successful completion of this work. The author also wishes to extend special thanks to their siblings and friends, whose unwavering support and presence throughout this journey have been invaluable.



اونيورسيتي مليسيا قهغ السلطان عبدالله
UNIVERSITI MALAYSIA PAHANG
AL-SULTAN ABDULLAH

ABSTRAK

Pemodelan pemendapan bersatu (FDM) adalah salah satu proses pembuatan yang termasuk dalam kategori pembuatan aditif (AM). Ia merupakan teknologi pencetakan 3D yang canggih untuk menghasilkan bahan plastik. Teknik ini semakin populer di kalangan ahli akademik dan profesional perniagaan untuk penyelidikan dan pembangunan kerana ia mudah digunakan, murah dan mampu memproses polimer termoplastik seperti acrylonitrile butadiene styrene (ABS), asid polilaktik (PLA), polikarbonat (PC) dan nilon. Kaedah FDM menggunakan penyemperitan leburan lapisan demi lapisan bagi filamen plastik untuk menghasilkan struktur 3D. Walau bagaimanapun, sifat anisotropik adalah isu utama dalam bahagian-bahagian yang dicetak menggunakan FDM yang menghadkan aplikasinya. Kajian ini bertujuan untuk mengkaji sifat mekanikal dan fizikal sampel cetakan FDM-PLA dengan melaksanakan pelapisan berbilang satah (multiplane) dan dibandingkan dengan lapisan satah tunggal. Parameter proses yang penting dikenal pasti dengan penyiasatan menyeluruh kajian terdahulu. Dalam kajian ini, eksperimen utama dijalankan dengan menggunakan polimer Asid Polilaktik (PLA). Sifat mekanikal diukur dari segi kekuatan tegangan dan kekuatan lentur, manakala sifat fizikal diukur dalam ketepatan ketumpatan dan dimensi. Sifat mekanikal dan fizikal sampel cetakan PLA dianalisis dengan mengubah orientasi pembinaan dan corak isian. Analisis eksperimen menunjukkan bahawa pelaksanaan multiplane telah meningkatkan sifat mekanikal dan fizikal sampel cetakan FDM dengan ketara. Parameter yang paling ketara mempengaruhi sifat mekanikal ialah orientasi pembinaan. Hasil kajian ini mendapati bahawa kekuatan tegangan berbilang satah (0° , 0°) pola sepusat dan garisan menunjukkan kekuatan tegangan yang lebih tinggi masing-masing iaitu 52.5 MPa dan 51.0 MPa, berbanding satah tunggal, iaitu 35.2 MPa dan 30.2 MPa masing-masing. Hasil eksperimen lenturan menunjukkan kedua-dua corak sepusat dan garisan orientasi pembinaan 0° dan 0° lapisan berbilang satah menunjukkan hasil yang lebih tinggi, 88.8 MPa dan 88.3 MPa, berbanding satah tunggal, iaitu 42.8 MPa dan 46.0 MPa. Keputusan kekuatan tegangan telah dibuktikan dalam analisis morfologi. Dalam membandingkan satu dan berbilang satah untuk sifat fizikal, ketumpatan dan ketepatan dimensi, satah berbilang menunjukkan hasil yang lebih baik daripada satah tunggal untuk ketumpatan. Sebaliknya, bagi ketepatan dimensi, kedua-dua satah tunggal dan berbilang satah adalah berhampiran nilai nominalnya. Kesimpulannya, penyelidikan ini telah menunjukkan bahawa pelaksanaan lapisan berbilang satah boleh meningkatkan sifat mekanikal dan fizikal sampel PLA yang menggunakan cetakan FDM dengan ketara berbanding dengan lapisan satah tunggal. Kajian ini memberikan gambaran menyeluruh tentang kesan parameter pemrosesan pada sifat mekanikal dan fizikal bahagian-bahagian yang dicetak menggunakan FDM, yang boleh membantu mengoptimumkan proses untuk mendapatkan hasil yang lebih baik. Penemuan penyelidikan ini boleh membantu dalam pelbagai bidang yang menggunakan teknologi FDM selaras dengan matlamat SDG khususnya yang berkaitan dengan matlamat 9 yang menekankan kepada industri, inovasi dan infrastruktur dengan penggunaan teknologi yang bersih dan mesra alam, seperti perubatan, automotif, aeroangkasa, dan produk pengguna. Tambahan pula, teknologi ini boleh digunakan untuk julat aplikasi yang lebih luas dengan menambah baik ciri-ciri bahagian-bahagian yang dicetak menggunakan FDM. Kajian ini menjadi penyumbang kepada pemajuan teknologi pembuatan aditif dan memberikan pemahaman yang lebih baik tentang potensi dan faedah pelaksanaan pelapisan berbilang satah.

ABSTRACT

One of the manufacturing processes included in this category of additive manufacturing (AM) is fused deposition modelling (FDM), and it is becoming popular among academics and business professionals for research and development. It is a sophisticated 3D printing technology for producing plastic materials, and this technique has recently risen in popularity as it is simple to use, inexpensive, and capable of processing thermoplastic polymers like acrylonitrile butadiene styrene (ABS), polylactic acid (PLA), polycarbonate (PC) and nylon. The FDM method uses layer-by-layer melt-extrusion of a plastic filament to produce 3D structures. However, anisotropic properties are the major issue in the FDM printed parts that limits their applications. Therefore, this research aims to study the mechanical and physical properties of FDM-PLA printed samples by implementing multiplane layering. Hence, the implementation of multiplane was compared with single-plane layering. In order to achieve the goal, significant process parameters are identified with a thorough investigation of prior studies. In this research, the primary experiment is conducted by using Polylactic Acid (PLA) polymer. The mechanical properties are measured in terms of tensile strength and bending strength, whereas physical properties are measured in density and dimensional accuracy, respectively. Thus, the mechanical and physical properties of PLA printed samples were analysed by varying the building orientation and infill pattern. The experimental analysis shows that implementing multiplane has significantly enhanced the mechanical and physical properties of the FDM printed samples. The most significant parameter that affects the mechanical properties is building orientation. From the results, it can be seen that the tensile strength of multiplane (0° , 0°) of concentric and line patterns exhibits higher tensile strengths of 52.5 MPa and 51.0 MPa, respectively, compared to the single plane, which are 35.2 MPa and 30.2 MPa respectively. From the bending results, both concentric and lines pattern of building orientation 0° and 0° multiplane layering show higher results, 88.8 MPa and 88.3 MPa, compared to single-plane, which are 42.8 MPa and 46.0 MPa. Hence, the tensile strength results are proven in the morphology analysis. In comparing single and multiplane for the physical properties, density and dimensional accuracy, multiplane shows better results than single plane for density. In contrast, as for dimensional accuracy, both single-plane and multiplane are near their nominal value. In conclusion, this research has shown that implementing multiplane layering can significantly improve FDM printed PLA samples' mechanical and physical properties compared to single-plane layering. The study provides insight into the effects of processing parameters on the mechanical and physical properties of FDM printed parts, which can help optimise the process for better results. The findings of this research can be helpful in various fields that utilise FDM technology in line with sustainable development goals (SDG) goals particularly related to goal 9 that emphasize on industry, innovation and infrastructure with greater adoption of clean and environmentally sound technology, such as medical, automotive, aerospace, and consumer products. Furthermore, the technology can be utilised for a broader range of applications by improving the properties of FDM printed parts. This study contributes to advancing additive manufacturing technology and provides a better understanding of the potential benefits of implementing multiplane layering.

TABLE OF CONTENT

DECLARATION	
TITLE PAGE	
ACKNOWLEDGEMENTS	ii
ABSTRAK	iii
ABSTRACT	iv
TABLE OF CONTENT	v
LIST OF TABLES	ix
LIST OF FIGURES	x
LIST OF SYMBOLS	xiii
LIST OF ABBREVIATIONS	xiv
LIST OF APPENDICES	xvi
CHAPTER 1 INTRODUCTION	1
1.1 Research Background	1
1.2 Problem Statement	3
1.3 Objectives	4
1.4 Research Scope	4
1.5 Thesis Outline	5
CHAPTER 2 LITERATURE REVIEW	7
2.1 Introduction	7
2.2 Additive Manufacturing (AM)	7
2.2.1 Material Extrusion (ME)	9
2.2.2 Material Jetting (MJ)	9
2.2.3 Powder Bed Fusion (PBF)	10
2.2.4 Sheet Lamination (SL)	11



اونيورسيتي مليسيا قهغ السلطان عبدالله
UNIVERSITI MALAYSIA PAHANG
AL-SULTAN ABDULLAH

2.2.5	Vat Photo Polymerisation	12
2.2.6	Binder Jet (BJ)	12
2.2.7	Direct Energy Deposition (DED)	13
2.3	Fused Deposition Modelling (FDM)	14
2.3.1	Fused Deposition Modelling Printing Process	15
2.3.2	Benefits of Fused Deposition Modelling	17
2.4	Material Anisotropy	18
2.5	Multiplane in Fused Deposition Modelling	18
2.6	Polymer and Polylactic Acid (PLA)	20
2.7	Processing Parameter of FDM	21
2.7.1	Nozzle Temperature	22
2.7.2	Bed Temperature	22
2.7.3	Layer Height	23
2.7.4	Printing Speed	24
2.7.5	Build Orientation	25
2.7.6	Infill Density	26
2.7.7	Infill Pattern	26
2.7.8	Raster Angle	27
2.7.9	Nozzle Diameter	28
2.8	Air Gap	29
2.9	Void	29
2.10	Physical and Mechanical Properties in FDM	31
2.10.1	Tensile Strength	31
2.10.2	Bending Strength	32
2.10.3	Dimensional Accuracy	33
2.10.4	Density	34



2.11	Morphology Analysis	34
2.12	Summary	35
CHAPTER 3 METHODOLOGY		36
3.1	Introduction	36
3.2	Research Methodology	37
3.3	Polylactic Acid (PLA) Filament	38
3.4	Selection and Calibration of 3D Printer	39
3.5	Sample Design	40
3.6	Processing Parameter and Sample Condition	42
3.7	Sample Fabrication of Single-Plane and Multiplane	44
3.8	Mechanical Testing	47
3.8.1	Tensile Test	47
3.8.2	Bending Test	48
3.9	Physical Properties	49
3.9.1	Density	50
3.9.2	Dimensional Accuracy	50
3.10	Morphology Analysis	51
3.11	Preliminary Results of Thermal Analysis	54
3.11.1	Differential Scanning Calorimetry (DSC)	54
3.11.2	Thermogravimetric Analysis (TGA)	56
CHAPTER 4 RESULTS AND DISCUSSION		58
4.1	Introduction	58
4.2	Conditions of Fabricated Samples	58
4.3	Dimensional Accuracy	60
4.4	Density	63



4.4.1	Density of Single-Plane and Multiplane for Concentric Pattern	63
4.4.2	Density of Single-Plane and Multiplane for Line Pattern	65
4.5	Tensile Strength Test	68
4.6	Bending Test	74
4.7	Scanning Electron Microscope (SEM)	77
CHAPTER 5 CONCLUSION		82
5.1	Introduction	82
5.2	Conclusion	82
5.3	Recommendation	84
REFERENCES		86
APPENDICES		101
LIST OF PUBLICATIONS		116



اونيورسيتي مليسيا قهغ السلطان عبدالله
UNIVERSITI MALAYSIA PAHANG
AL-SULTAN ABDULLAH

LIST OF TABLES

Table 2.1	Effects of processing parameter on voids	30
Table 3.1	Manufacturer data sheet of PLA material	38
Table 3.2	Specifications of Creality Ender-3 printer	40
Table 3.3	Constant processing parameter	42
Table 3.4	Manipulated processing parameter	43
Table 3.5	Summary of sample condition for single-plane and multiplane	44
Table 4.1	Parameters of tensile and bending fabricated samples	59
Table 4.2	Dimensional accuracy results of single-plane vs multiplane for concentric pattern	60
Table 4.3	Dimensional accuracy results of single-plane vs multiplane for line pattern	61
Table 4.4	Density results of single-plane and multiplane for concentric pattern	63
Table 4.5	Density results of single-plane and multiplane for line pattern	66
Table 4.6	Summary of tensile data for concentric pattern	68
Table 4.7	Summary of tensile data for line pattern	71

LIST OF FIGURES

Figure 2.1	Types of additive manufacturing process	8
Figure 2.2	Material extrusion process	9
Figure 2.3	Diagram of material jetting process	10
Figure 2.4	Powder bed fusion process	11
Figure 2.5	Schematic diagram of binder jetting process	13
Figure 2.6	Graphical representation diagram of DED process	14
Figure 2.7	Trend of utilization of PLA in FDM process from the year 2013-2021	15
Figure 2.8	Workflow of 3D printing process	16
Figure 2.9	Schematic representation of the FDM process	16
Figure 2.10	Graphical representation of toolpath layering (a) single-plane (b) multiplane	19
Figure 2.11	Layer height graphical representation	24
Figure 2.12	Different directions of build orientations	25
Figure 2.13	Types of infill pattern for FDM printed parts	27
Figure 2.14	Graphical representation of raster angle	28
Figure 2.15	Various types of raster orientation (a) $+45^\circ$, (b) 0° , (c) 90° , (d) $0^\circ/90^\circ$, (e) $+45^\circ/-45^\circ$, (f) $0^\circ/+45^\circ$, (g) $90^\circ/+45^\circ$, (h) $0^\circ/-45^\circ$	28
Figure 2.16	Formation of voids in between layers	31
Figure 2.17	SEM image of voids occurred in PLA-FDM printed parts	35
Figure 3.1	Flow chart of the overall process	37
Figure 3.2	White Polylite™ PLA filament with diameter of 1.75mm	39
Figure 3.3	Creativity Ender-3 printer	39
Figure 3.4	Tensile sample dimensions (ASTM D638-14)	41
Figure 3.5	Bending sample dimensions (ASTM D790-17)	41
Figure 3.6	Different infill pattern: (a) concentric, (b) line, used in this research	43

Figure 3.7	Illustration on how (a) multiplane samples are printed, (b) position of stopper	45
Figure 3.8	(a) Printing of tensile sample, (b) magnified view of sample printing	46
Figure 3.9	(a) Single-plane printed tensile sample, (b) multiplane printed tensile sample	46
Figure 3.10	(a) single-plane printed bending sample, (b) multiplane printed bending sample	47
Figure 3.11	(a) INSTRON 3369 machine universal testing machine, (b) Sample during testing	48
Figure 3.12	Bending sample during testing	49
Figure 3.13	Density test setup and weighing scale machine (Precisa, Switzerland)	50
Figure 3.14	Digital vernier calliper (Mitutoyo, Malaysia)	51
Figure 3.15	Grinding and polishing machine (Topper, China)	52
Figure 3.16	Various designations of sandpaper	52
Figure 3.17	Optical microscope (Olympus, Japan)	53
Figure 3.18	Scanning Electron Microscope (HITACHI TM3030 PLUS)	54
Figure 3.19	Differential Scanning Calorimetry machine (Perkin Elmer DSC 8000, USA)	55
Figure 3.20	Heat flow changes of PLA	55
Figure 3.21	Thermogravimetric and DTG curves about temperature variations	56
Figure 4.1	Fabricated (a) tensile and (b) bending samples for single-plane and multiplane	59
Figure 4.2	Dimensional accuracy of single-plane vs multiplane of bending sample for concentric pattern	61
Figure 4.3	Dimensional accuracy of single-plane vs multiplane of bending sample for line pattern	62
Figure 4.4	Relative density of single-plane vs multiplane for concentric pattern	64
Figure 4.5	Optical micrographs of (a) single-plane 0°, (b) multiplane 0°, 0°	64
Figure 4.6	Optical micrographs of (a) single-plane 45°, (b) multiplane 45°, 0°	64

Figure 4.7	Optical micrographs of (a) single-plane 90°, (b) multiplane 90°, 0°	65
Figure 4.8	Relative density of single-plane vs multiplane for line pattern	66
Figure 4.9	Optical micrographs of (a) single-plane 0°, (b) multiplane 0°, 0°	67
Figure 4.10	Optical micrographs of (a) single-plane 45°, (b) multiplane 45°, 0°	67
Figure 4.11	Optical micrographs of (a) single-plane 90°, (b) multiplane 90°, 0°	67
Figure 4.12	Ultimate tensile strength of single-plane vs multiplane for concentric pattern	69
Figure 4.13	Young's modulus of single plane vs multiplane for concentric pattern	69
Figure 4.14	Stress-strain curves of tensile concentric pattern for single-plane and multiplane tensile samples	70
Figure 4.15	Ultimate tensile strength of single-plane vs multiplane for line pattern	72
Figure 4.16	Young's modulus of single-plane vs multiplane for line pattern	72
Figure 4.17	Stress-strain curves of line pattern for single-plane and multiplane tensile samples	73
Figure 4.18	Flexure stress of single-plane vs multiplane for concentric pattern	75
Figure 4.19	Flexure stress of single-plane vs multiplane for line pattern	75
Figure 4.20	Single-plane fractured cross-section SEM images of tensile test samples (a) outer structure of 90° concentric pattern, (b) void in concentric pattern	77
Figure 4.21	Single-plane fractured cross-section SEM images of tensile test samples (a) outer structure of 90° lines pattern, (b) delamination between layers, (c) void	78
Figure 4.22	Multiplane fractured cross-section SEM images of tensile test samples (a) outer structure of 0°, 0° concentric pattern, (b) air gap between layers, (c) void, (d) magnified view of void	79
Figure 4.23	Multiplane fractured cross-section SEM images of tensile test samples (a) outer structure of 0°, 0° lines pattern, (b) void, (c) magnified view of the void	80

LIST OF SYMBOLS

°	Degree
°C	Degree Celsius
N ₂	Nitrogen gas
%	Percentage
ε	Strain



اونيورسيتي مليسيا قهغ السلطان عبدالله
UNIVERSITI MALAYSIA PAHANG
AL-SULTAN ABDULLAH

LIST OF ABBREVIATIONS

AM	Additive Manufacturing
ABS	Acrylonitrile butadiene styrene
ASTM	American Society for Testing and Materials
BJ	Binder Jetting
CAM	Computer Aided Manufacturing
CAD	Computer Aided Design
DTG	Derivative thermogravimetric
DMD	Direct Metal Deposition
DSC	Differential Scanning Calorimetry
DED	Direct Energy Deposition
DMA	Dynamic Mechanical Analysis
DLP	Digital Light Processing
FDM	Fused Deposition Modeling
FDA	Food and Drug Administration
G-Code	Geometric code
GPa	Gigapascal
IJM	Inkjet Modelling
Kn	Kilonewton
Kg	Kilogram
LOM	Laminated Object Manufacturing
ME	Material Extrusion
MJ	Material Jetting
mm	Millimeter
MP	Multipane
MPa	Megapascal
MFMS	Multifunctional Material System
OM	Optical Microscope
PLA	Polylactic Acid
PVA	Polyvinyl
PBF	Powder Bed Fusion
PA	Polyamide

SEM	Scanning Electron Microscope
SDG	Sustainable Development Goals
SLS	Selective Laser Sintering
SLA	Stereolithography
STL	Standard Tessellation Language
SP	Single Plane
3D	Three-Dimensional
3DP	Three-Dimensional Printing
2D	Two dimensional
TGA	Thermogravimetric Analysis
TA	Thermal Analysis
UAM	Ultrasound Additive Manufacturing



اونيورسيتي مليسيا قهغ السلطان عبدالله
UNIVERSITI MALAYSIA PAHANG
AL-SULTAN ABDULLAH

LIST OF APPENDICES

Appendix A: Fabricated tensile samples for concentric pattern	102
Appendix B: Fabricated tensile samples for line pattern	104
Appendix C: Fabricated bending samples for concentric pattern	106
Appendix D: Fabricated bending samples for line pattern	108
Appendix E: Density results of concentric pattern for single-plane and multiplane	110
Appendix F: Density results of line pattern for single-plane and multiplane	113



اونيورسيتي مليسيا قهغ السلطان عبدالله
UNIVERSITI MALAYSIA PAHANG
AL-SULTAN ABDULLAH

CHAPTER 1

INTRODUCTION

1.1 Research Background

Additive manufacturing (AM) is a technique of merging several layers of materials to fabricate a 3D model. It requires the use of a computer-based 3D model and a 3D printer via a process for developing a physical model that is based on the original model concept (Bikas et al., 2016; Gu et al., 2013; Valvez et al., 2020). AM is capable of developing parts or items that are typically small and of unique designs, as well as those produced in small quantities (Gu et al., 2013). The manufacturing industries have embraced the technique extensively due to its cost- and time-saving benefits (Bikas et al., 2016). Over the past few years, AM has been widely used for creating prototypes and parts with high fracture surfaces (Valvez et al., 2020). Compared to most modelling approaches, it creates goods at a faster rate and with a higher dimensional precision (Dhinakaran et al., 2020).

This 3D printing (3DP), in particular, is an AM technique geared for fabricating a wide range of structures and complex geometries from 3D model data (Ngo et al., 2018). It is a class of computer-aided manufacturing (CAM), wherein the process consists of printing successive layers of materials in the design space over time and are formed on top of each other (Bhagia et al., 2021; Ngo et al., 2018). This technology was developed by Charles Hull in 1986 in a process known as stereolithography (SLA), followed by developments such as, inkjet printing, fused deposition modelling (FDM) and powder bed fusion (PBF). The 3DP technology, which involves various materials, equipment and methods, has evolved over the years and is equipped with the capacity to transform logistics and manufacturing processes (Ngo et al., 2018). It is a highly versatile fabrication system that can be enforced to various materials, such as polymers, metals, ceramics and others (Cano-Vicent et al., 2021b). Advantages offered by the technology include a precise control of the intricate structure and minimal waste generated during 3D printing manufacture (Vatani et al., 2015).

With regards to FDM, it is one of the most popular commercial 3D printing technologies today (Bhagia et al., 2021). The basic concept of its manufacturing process is simply melting the raw materials and using them to build new shapes (Kristiawan et al., 2021). FDM is commonly utilised in AM techniques that produce practical prototypes of various thermoplastics due to its ability to yield high-quality and complex goods safely. Besides FDM, different types of AM techniques exist, such as SLA, direct metal deposition (DMD), selective laser sintering (SLS), and inkjet modelling (IJM). Each technique is different in terms of production methods and materials accordingly (Dhinakaran et al., 2020). Currently, a variety of materials are available for FDM-3DP, including ceramics, metals (e.g. titanium, stainless steel, gold, and silver) and polymers. Polymers, in particular, comprise PLA, polyamide (PA), acrylonitrile butadiene styrene (ABS), and polyvinyl alcohol (PVA) (Vatani et al., 2015). Among these materials, PLA has made significant progress within the 3D printing field due to its biodegradability (Navarro et al., 2006; Rezwan et al., 2006).

Biodegradable polymers are gaining much attention especially to manufacture environmentally friendly materials as an alternative to petroleum-based products. PLA is a particularly promising candidate in view of its sustainability and attractive mechanical properties (Zhu et al., 2013). It is well-known for its high modulus, high strength, and optical transparency compared to other synthetic polymers. However, PLA also exhibits low thermal stability and low crystallisation ability (Murphy & Collins, 2018). Nevertheless, it has been documented that among a range of biodegradable plastics, it is not only widely available but also safe to be decomposed after its usage without polluting the environment (Taib et al., 2022). Moreover, PLA is currently a biodegradable polymer approved for use by the Food and Drug Administration (FDA) for various biomedical applications. Fabrication of most of the reported PLA-based scaffolds via rapid prototyping currently require the molecular modification of the PLA matrix (Melchels et al., 2009; Xiong et al., 2002).

Accordingly, multiplane printing utilises a combination of multiple printing planes to undertake the layering for printing a 3D object, whereby the planes for layering can be in any of three orthogonal planes. However, most conventional FDM printers utilise a horizontal layer-upon-layer technique to print such objects (Ishak et al., 2019).

Therefore, this research aims to evaluate the mechanical properties of PLA-printed parts by implementing multiplane layering printing techniques in FDM.

1.2 Problem Statement

FDM is a rapidly growing AM technology that is expanding quickly due to its capacity to create functional parts with intricate geometries (Chacón et al., 2017). Many polymeric parts that are fabricated by using various AM techniques, such as FDM, SLS, DLP, and SLA exhibits material anisotropy. Any material that exhibits a difference in material property (mechanical, electrical or thermal) across different parts of the material are considered as material anisotropy. In FDM printing, anisotropy of material properties has been the most significant issue till date based on researchers (Zohdi & Yang, 2021) and from all the types of anisotropy, mechanical anisotropy is one of the major issue (Dizon et al., 2018) where 3D-printed parts that were printed by using FDM process are anisotropic (Ishak et al., 2019).

Moreover, FDM is a complex process associated with difficulties in determining the optimal attributes due to numerous conflicting parameters affecting the component and material qualities. Process parameters such as build orientation, layer thickness, raster angle, raster width, infill density, infill pattern, and printing speed plays a significant role in determining the printed part quality and mechanical properties (Chacón et al., 2017; Domingo-Espin et al., 2015; Mohamed et al., 2015). According to researchers, the influence of these parameters on the resulting mechanical properties is imperative as these factors is crucial for functional parts (Chacón et al., 2017). Thus, the selection of the appropriate processing parameter is vital in determining the printed samples properties.

Single-plane layering, in particular, denotes the process employed by conventional 3D printers in which 3D geometry is transformed into contours in 2D, simplifying the 3D printing whereas multiplane printing entails layering 3D objects throughout multiple printing planes. However, based on previous researchers that have been done, the implementation of multiplane are primarily used in robot arms as the conventional printers, only have the ability to translate only in three directions: x, y, and z. Consequently, the translational motion alone limits printing to a single-plane layering process. Moreover, the use of conventional 3D printers renders multiple-plane layering

unachievable, contrary to 3D parts requiring this type of layering render a multiplane layering platform necessary (Ishak et al., 2019).

1.3 Objectives

This study aims to fabricate multi-single plane PLA samples using FDM. The objectives of this research are as follows:

- i. To investigate the effect of two infill pattern (concentric, line) on the mechanical properties (tensile strength, bending strength) and physical properties (dimensional accuracy, density) of PLA samples
- ii. To analyse the mechanical properties (tensile strength, bending strength) and physical properties (dimensional accuracy, density) of fabricated PLA samples for different building orientations, including multi-plane ($0^\circ 0^\circ, 45^\circ 0^\circ, 90^\circ, 0^\circ$) and single-plane ($0^\circ, 45^\circ, 90^\circ$)
- iii. To determine the relationship between building orientation and the properties of PLA samples through a morphological approach, employing optical microscope (OM) and scanning electron microscope (SEM) analysis

By addressing these objectives, this research is underpinned by the goal of gaining insight pertaining the impact of infill pattern, building orientation, and multi/single-plane layering on the mechanical and physical properties of FDM-printed PLA samples. Additionally, the morphological analysis performed by using OM and SEM provides a detailed understanding of the structural characteristics held by the samples regarding their properties.

1.4 Research Scope

- i. PLA filament in white colour, with a diameter of 1.75 mm (± 0.05 mm), was selected as the material for this study
- ii. The research employed FDM, a 3D printing technique, using the Creality Ender-3 machine as the printing equipment.
- iii. PLA samples were fabricated by varying the infill pattern (concentric, line) and building orientation ($0^\circ 0^\circ, 45^\circ 0^\circ, 90^\circ, 0^\circ$) for multiplane and ($0^\circ, 45^\circ, 90^\circ$) for single-plane configurations. A layer height of 0.2mm,

nozzle temperature of 190°C, bed temperature of 60°C, and printing speed of 15mm/s were maintained during the printing process.

- iv. The mechanical properties of the printed samples were evaluated through tensile tests following the ASTM D638-14 type IV standard and bending tests following the ASTM D790-17 standard.
- v. The physical properties, including dimensional accuracy and density, were assessed for the printed samples.
- vi. The morphology of the printed samples was analyzed using optical microscopy (OM) and scanning electron microscopy (SEM) techniques, providing a detailed assessment of the tensile and density characteristics.
- vii. To ensure reliable results, five samples were printed for each condition, allowing the calculation of average values for each test. Consequently, 120 samples were printed to assess the tensile and bending properties, while 36 were printed to evaluate the density properties.

1.5 Thesis Outline

This thesis comprises five chapters, each serving a specific purpose in presenting the research findings and analysis. The following is an enhanced description of each chapter:

Chapter 1: Introduction The first chapter provides a comprehensive overview of the research, including the background information, the problem statement that motivated the study, clearly defined objectives, and the scope of the research. It sets the stage for the subsequent chapters by highlighting the significance and relevance of the research topic.

Chapter 2: Literature Review Chapter 2 critically evaluates relevant journal articles and research papers about 3D printing technology, specifically focusing on Fused Deposition Modelling (FDM). It delves into various aspects, such as materials used, processing parameters, and the mechanical and physical properties associated with FDM technology. This chapter provides a solid foundation of existing knowledge and is a reference point for the current research.

Chapter 3: Methodology Chapter 3 elaborates on the materials and methods employed in the research. It explains the rationale behind the material selection and provides detailed insights into mechanical testing (tensile and bending), physical testing (dimensional accuracy and density), and morphology analysis (OM and SEM). This chapter ensures transparency and clarity regarding the experimental procedures carried out in the study.

Chapter 4: Results and Discussions Chapter 4 presents and discusses the results of the tests and analyses. It comprehensively examines dimensional accuracy, density, tensile strength, bending strength, and morphology analysis. The chapter thoroughly interprets and discusses the results, drawing connections to the research objectives and shedding light on noteworthy findings or trends.

Chapter 5: Conclusion and Recommendations In the final chapter, a summary of the research findings is presented, encapsulating the key outcomes and insights obtained throughout the study. Additionally, this chapter offers suggestions for future improvements or areas that warrant further exploration. It serves as a conclusion to the thesis, highlighting the contributions made by the research and indicating potential directions for future research endeavours.

CHAPTER 2

LITERATURE REVIEW

2.1 Introduction

An introduction to AM is presented in this chapter. First, a thorough analysis of the various AM processes that have been developed is delineated. A description of FDM, which is the most popular AM process, and its advantages follow after. Subsequent sections offer an overview of polymers, multiplanes, and PLA, while finally, an overview of FDM's processing parameters, mechanical and physical properties, and morphology analysis is elaborated in detail.

2.2 Additive Manufacturing (AM)

The AM technique is a trendy technology for creating 3D products based on 3D computer aided design (CAD) models (Singh et al., 2022). A fast-developing and sophisticated manufacturing technique, it renders the production of complex geometric structures and physical models possible at a low cost and great accuracy. AM utilises a layer-by-layer technique to create objects using 3D designs rather than conventional methods such as casting and cutting (Shanmugam et al., 2021). In recent years, the technology has emerged as the key towards creating lighter and stronger parts through a transformative approach to production (Singh et al., 2022). Its real benefits make it possible for manufacturing complicated structures for various applications. Currently, the AM technology is used in a variety of engineering applications, including mechanical (Dilberoglu et al., 2017), biomedical (Harun et al., 2018), construction (Camacho et al., 2018), aerospace (Kumar & Nair, 2017) food industries (Lipton et al., 2015), and in academic research.

Material extrusion, direct energy deposition, sheet lamination, vat photopolymerisation, binder jetting, powder bed fusion, and material jetting are the seven main categories of AM/3DP techniques (Daminabo et al., 2020; Lee, 2017), as shown in Figure 2.1. Among these, material extrusion 3D printing based on FDM technology is

implemented to produce polymer-based structures and models due to the convenience of producing intricate geometrical parts, fast production, variation of build methods, range of engineering polymers, easy removal of support, and cost-effective (Awasthi & Banerjee, 2021; Ian Gibson, 2015).



Figure 2.1 Types of additive manufacturing process

Source: (Solomon et al., 2021)

Several main advantages of AM over traditional production comprise quality, innovation, cost, speed, and transformation (Cano-Vicent et al., 2021b). It is a potent instrument for reducing supply chain complexity in view of it permitting and facilitating the creation of products in moderate- to mass quantities that can be uniquely customised accordingly. The necessity for adequate materials is essential to the selection requirements for this technology (Attaran, 2017; Bourell et al., 2017). Polymer-based composites have advanced to the "state-of-the-art" status in the material system design and development for 3DP applications as a result of the increased demand for lightweight, highly functional and cost-effective product systems (Gao et al., 2015; González et al., 2017; Scheithauer et al., 2015).

2.2.1 Material Extrusion (ME)

The ME procedure employs a continuous thermoplastic or composite material filament to build 3D objects. It is a layer-by-layer process in which the thermoplastic material is force over the nozzle and fed over the build plate, resulting in the object being built at constant pressure and speed. With FDM as the primary technique in this process, its cost-effectiveness and low production time compared to other methods are well-documented. Accordingly, the key benefits of the process include inexpensive initial and ongoing costs, compact equipment, easily understood printing method, and uncomplicated replacement of printing filament (Morissette et al., 2000; Rajan et al., 2022; Smay & Lewis, 2012; Travitzky et al., 2014).

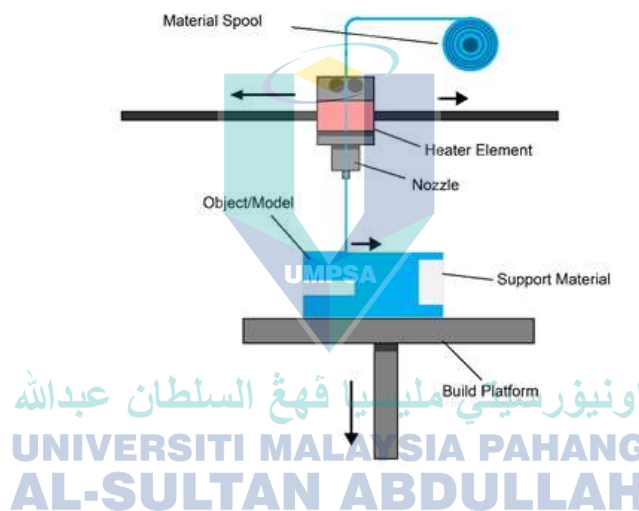


Figure 2.2 Material extrusion process

Source: (Ahangar et al., 2019)

2.2.2 Material Jetting (MJ)

A technique for AM, MJ utilises liquid photopolymer to manufacture functional parts by selectively curing them. Polymer liquid droplets are deposited on the build plate using a piezo print head and ultraviolet lamps to solidify the polymer. This technique is similar to inkjet printing wherein the droplets are directly deposited onto a substrate (Calvert, 2001; De Gans et al., 2004; Le, 1998; Rajan et al., 2022). Compared to the vat-photo polymerisation method, this particular process can print huge components. Due to its benefits in printing products with high dimensional precision and minimal surface roughness, the MJ technology has grown in popularity and been adopted by various

industries, including manufacturing, aircraft, and biomedicine (Gülcan et al., 2021). Researchers have experimented with direct ink jetting of ceramic nano ink suspensions (Blazdell, 2003; Blazdell & Evans, 2000; Blazdell et al., 1995; Slade, 1998; Zhao et al., 2003), metals (Ko et al., 2010) and semiconductors (Elliott et al., 2013) to produce finished products with an improved functionality. However, this process is hindered by a primary drawback, namely its inappropriateness for function prototypes. In addition, the products are more brittle, and only a few materials such as waxes and polymers may produce parts with great accuracy (Rajan et al., 2022).

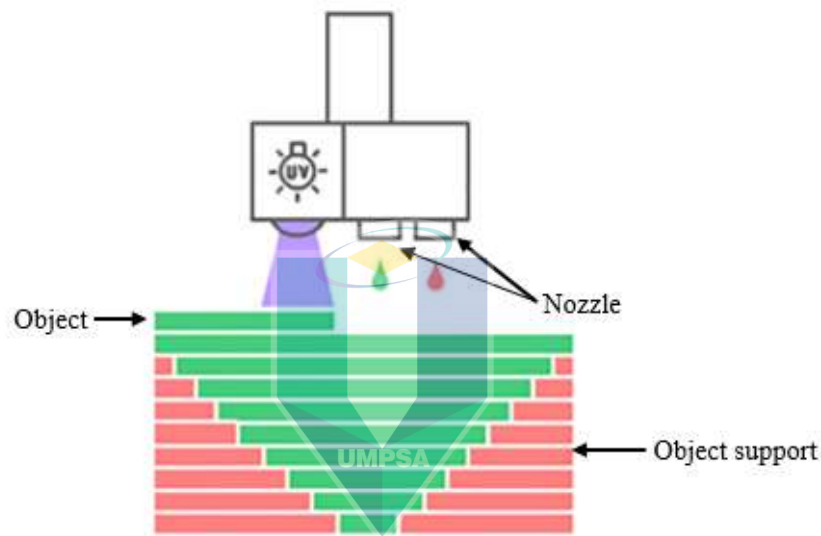


Figure 2.3 Diagram of material jetting process

Source: (Ahangar et al., 2019)

2.2.3 Powder Bed Fusion (PBF)

PBF is one of the most widely used AM processes that uses powder-based materials in which the materials are first sintered using heat, a laser or an electron beam after being fed over the base plate. Then, a rolling mechanism spreads the subsequent layer of powder after each layer has been scanned (Soundararajan et al., 2021). Deckard and Beaman (1990) have invented a polymer PBF method, which is commonly used to manufacture polyamides and polymer composites (Bertrand et al., 2007). The main techniques behind the PBF method denote SLS, selective laser melting (SLM) and electron beam melting (EBM) (Daminabo et al., 2020). Here, PBF is utilised to create complicated structures without extra support by reheating the preceding layers to reduce anisotropy (Rajan et al., 2022; Singh et al., 2020). Benefits offered by the method include

relatively low cost caused by the lack of a supporting structure, the utilisation of various materials, and the recycling of leftover powders. In contrast, its drawbacks include the comparatively slow speed, protracted print time and post-processing, high power consumption, poor structural qualities, and uneven surface texture. Furthermore, the method can indirectly produce metal (Deckers et al., 2012) and ceramic (Bertrand et al., 2007) melting polymer blends; the produced pieces need high-temperature post-processing to thoroughly sinter the structural powder completely.

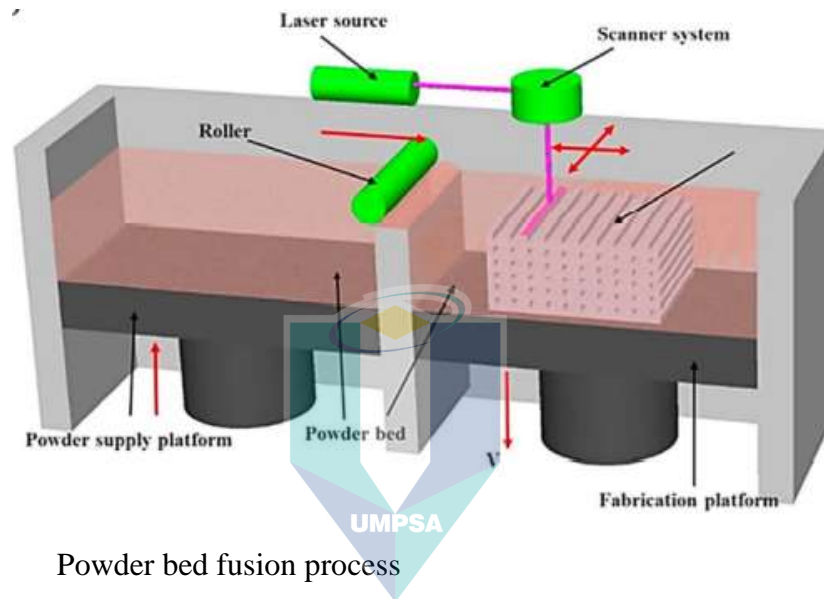


Figure 2.4 Powder bed fusion process

Source: (Ngo et al., 2018)

اونيورسيتي مليسيا قهغ السلطان جابا
 UNIVERSITI MALAYSIA PAHANG
 ALIOTTAN ABDULLAH

2.2.4 Sheet Lamination (SL)

The AM process known as SL involves bonding the foils or sheets of materials together to yield a product. Before laminating, raw materials (worksheets) are cut by cutter or laser by their geometry. The sheets are then piled on top of each other and joined together via diffusion instead of melting (Rajan et al., 2022). The superior technologies in the AM category comprise ultrasound additive manufacturing (UAM) and laminated object manufacturing (LOM) (Forster & Forster, 2015; Li et al., 2019; Ligon et al., 2017). Material handling is easy, with low operation costs and fast processing speed, resulting in a reasonably quick processing speed and the materials may be handled quickly and affordably. The SL method, in particular, can implement several materials such as metals, polymer, paper and ceramic. It offers key benefits like the ability to function as a hybrid production system, use of ceramic and composite fibre materials, and the absence of support structures. Contrarily, limitations encountered with the technique include the

limited availability of a few materials and the need to remove extra materials after lamination. Additionally, the lamination procedure affects how strong the bonding is, and in some instances, adhesive bonds lack the durability and strength needed for long-term use (Lee et al., 2017; Mitchell et al., 2018; Zhang et al., 2018).

2.2.5 Vat Photo Polymerisation

Vat photo polymerisation is a technique where 3D objects are generated by selective curing of liquid resin through targeted ultraviolet light. This category encompasses a variety of lithography-based AM techniques wherein UV lasers are used to selectively polymerise UV-curable resins, thereby producing a layer of solidified material such as digital light stereolithography (DLP). During laser exposure, the mixed metal resin undergoes a chemical reaction to solidify and small monomers are then linked together like a chain during the photochemical process to form solids. Hence, this method offers high surface quality and precision (Forster & Forster, 2015; Gao et al., 2015; Li et al., 2019; Ligon et al., 2017). However, drawbacks such as high equipment cost, lengthy time required for post-processing and resin removal, and limited availability of materials should be considered (Wong & Hernandez, 2012).

2.2.6 Binder Jet (BJ)

In this process, a liquid binding agent is dispensed on powder to generate a 2D pattern on a layer. To do this, the bonding agent is applied by dropping over the powder using the print head once the powder is evenly disseminated around the bed. The required shape is then solidified using an electrical heater (Meteyer et al., 2014; Zhang et al., 2018; Ziaee & Crane, 2019). The powder bed descends after the production of the first layer, following which the powder is dispersed over the previously printed layer, and then the process resumes. Moreover, the BJ process utilises various techniques, including dynamic binder/powder interaction, powder deposition, printing techniques and post-processing techniques. Therefore, it can be tailored for use to nearly any powder with high output rates, with a track record of effectively processing several materials, including ceramics, metals, and polymers (Ziaee & Crane, 2019). As printed objects are made of bonded powder, infiltration during post-processing is necessary for them to have enough strength (Gao et al., 2015). Thus, this technology can process any powdered material that can be properly dispersed and moistened. To date, researchers have

processed several metals (Williams et al., 2011), ceramics (Sachs, 1992), foundry sand and polymer materials by using this method (Gao et al., 2015).

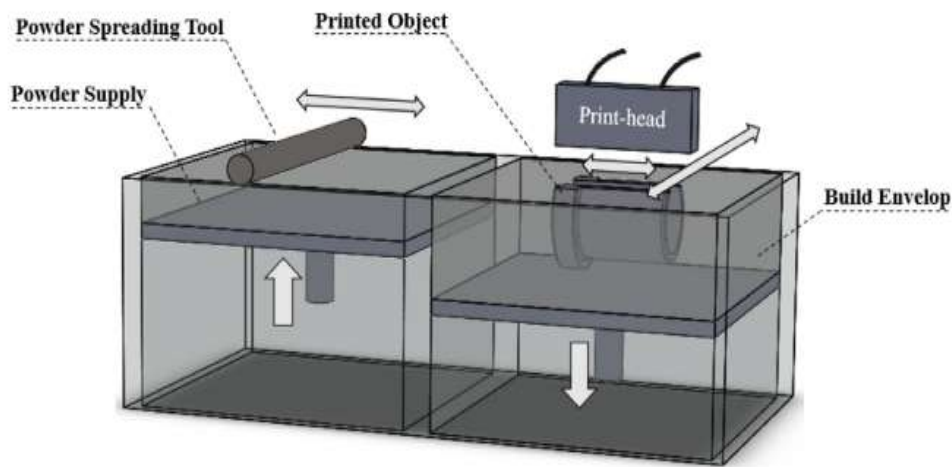


Figure 2.5 Schematic diagram of binder jetting process

Source: (Ziaee & Crane, 2019)

2.2.7 Direct Energy Deposition (DED)

The process involves melting materials deposited by using concentrated thermal energy like a laser, electron beam, or plasma arc to produce 3D objects. A robotic arm or gantry system typically operates the energy source and material feed nozzle, while a moveable chamber and a laser are fixed within. When the laser operates, it melts the metal powder and solidifies the layer generated while the metal powder is simultaneously sent into the nozzle to the targeted location (X. Yao et al., 2020; Zhang et al., 2018). The moveable chamber can move in several directions and is not fixed to one axis. DED processes can be categorised into two types, which are metal powder and metal wire, depending on the feedstock utilised. Furthermore, different kinds of substrates can be employed in DED implementation as opposed to PBF, thus offering numerous advantages such as manufacturing products with great precision, reduced void development, and increased density, among others. In general, the main techniques employed in this method are direct light fabrication (DLF), laser-engineered net shaping (LENS), and DMD (Ribeiro et al., 2020). Additionally, the benefits of this technology include a high build rate and fast production time, multi-material can be employed, and minimal material waste, whereas its limitations are expensive capital cost, low build

resolution, and the absence of a support structure (Gao et al., 2015; Wilson et al., 2014; Ye & Shin, 2014).

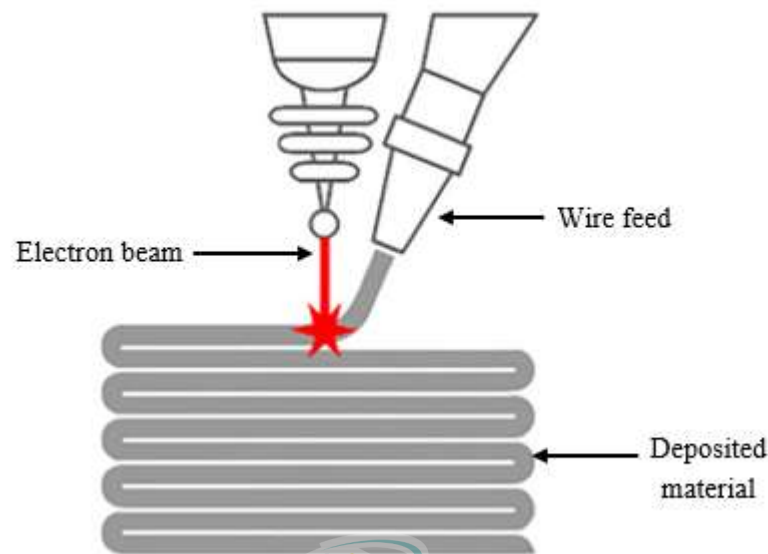


Figure 2.6 Graphical representation diagram of DED process

Source: (Sheoran & Kumar, 2020)

2.3 Fused Deposition Modelling (FDM)

The objective of AM in the current market is to make high-quality parts at low costs, increase productivity, and reduce lead times. With 3D printing, for example, FDM that has been invented over 20 years ago remains the second most popular technique after stereolithography (Jain & Kuthe, 2013; Mogan et al., 2021). It is also one of the manufacturing processes included in AM engineering classes, rendering it increasingly popular among academics and business professionals for R&D purposes (Kristiawan et al., 2021). Furthermore, the technology utilises a rapid prototype (RP) computer to build porous material parts by using the layer-by-layer manufacturing process (NKOMO et al., 2017).

Due to its non-laser application and economical to use and maintain, FDM has emerged as a research highlight in 3D printing (Liu et al., 2019). A 3D design programme is typically used in FDM to generate a digital design, which is then sliced into several layers or laminations. The printer receives this layer of data and uses it to recreate the design layer by layer until the entire model is obtained. In theory, low melting point filaments such as ABS, PA, PLA and PC denote the commonly used options (Liu et al.,

2019). Moreover, the type of material and the processing parameters encompass the most crucial factors in determining the mechanical properties of FDM printed parts. Examples of processing parameters include raster angle, printing speed, infill density, layer time, printing orientation, extrusion temperature and rate, nozzle transverse speed, and bed temperature (Ansari, 2021; Cuan-Urquizo et al., 2019; Riddick et al., 2016; Yang & Yeh, 2020). The FDM technique is employed in various manufacturing industries, such as aerospace (Mogan et al., 2021), automobile, biomedical (Cano-Vicent et al., 2021a), smart home appliances, stationeries and training aid, and creative gifts (Liu et al., 2019).

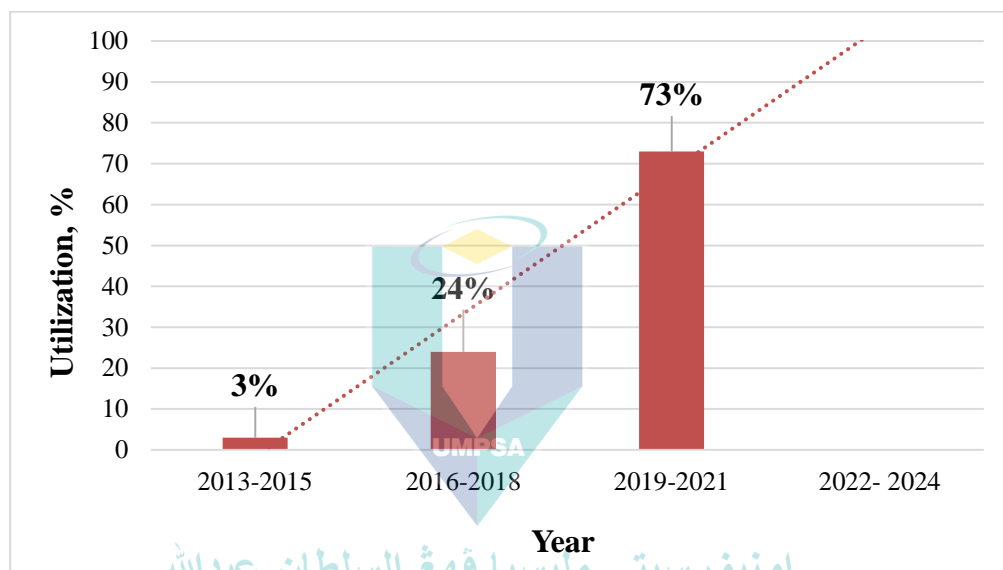


Figure 2.7 Trend of utilisation of PLA in FDM process from the year 2013-2021

Figure 2.7 indicates the trend of FDM, whereby the utilisation of its processes for PLA processing has been incremental from 2013 – 2021. The data was obtained based on a research matrix table in which 150 journals were evaluated, with expectations for a continuous increasing trend in the upcoming years. Although the FDM method has numerous benefits in comparison with other AM technologies, including cost-effectiveness, researchers are now moving towards FDM to study the process further thoroughly (Sachini Wickramasinghe et al., 2020).

2.3.1 Fused Deposition Modelling Printing Process

FDM involves depositing polymeric materials layer by layer and one on top of the other until the desired shape is achieved (Saroia et al., 2019). It is made of a polymeric filament delivered from a coil, which melts as it travels through the extruder until the

melting point is attained before being laid down one layer at a time on the print bed by CAD drawing. Layers will be deposited successively until the desired product is printed, whereby the deposited layers fuse to form a bonding (Awasthi & Banerjee, 2021). Hence, the quality of the bonds, which are formed via molecule diffusion, neck growth, and contact between two surfaces, can be used to determine the integrity of the layers (Bellehumeur et al., 2004; Singh et al., 2017; Sun et al., 2008). The workflow of the 3D printing process is shown in Figure 2.8 below, and also a schematic representation of the FDM process in Figure 2.9.

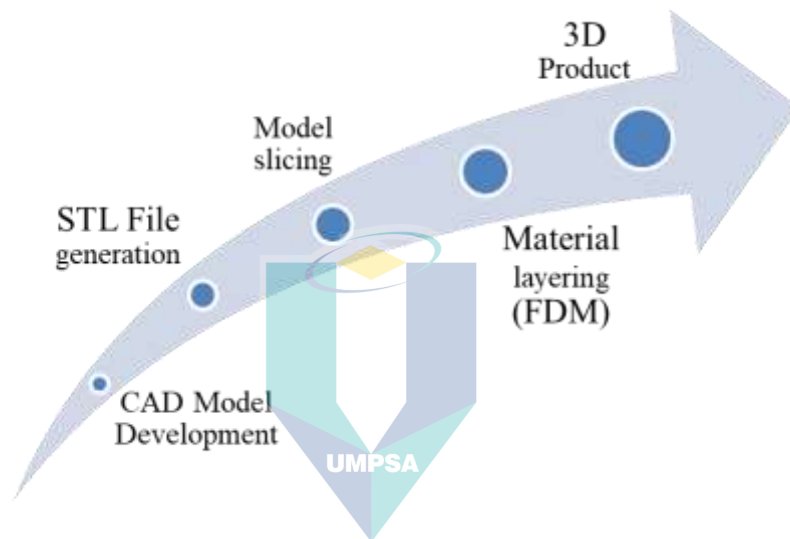


Figure 2.8 Workflow of 3D printing process

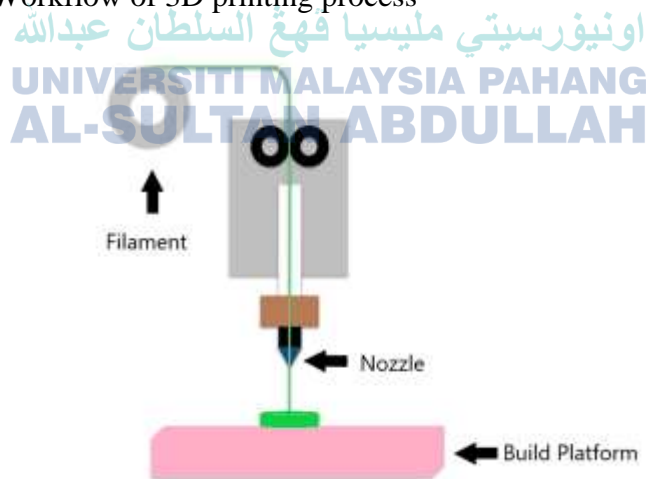


Figure 2.9 Schematic representation of the FDM process

Source: (Mogan et al., 2021)

An extruder is the portion where the plastic filament is heated to its melting point before forming the designed part through a process known as extrusion. Several components comprise the parts of a 3D printer, one of which being the extrusion motor, which moves the filament and pulls it from the spool during printing. The filament is transported to the hot end or tip of the extruder by a pulley and a lever on the 3D printer. Moreover, a Bowden tube is typically installed at the extruder inlet to minimise filament breakage, while the device also features a fan to cool the extruder. The polymeric material is melted at the hot end located at the extrusion output and the extruder is mounted on a carriage that enables x and y movement. In this manner, the extruder moves to form the design as the part is being produced. Some printers even feature two or three extruders, allowing them to print with numerous filaments simultaneously (Chia & Wu, 2015). Hot bases, often referred to as hotbeds, describe platforms with a heating system that can warm the printer base to a specific temperature so that the temperature differences between the hot end and the print bed are minimised when the molten material falls on it. This will help to prevent defects like temperature-related breakage in printed parts or warping brought on by the first layer of a part deforming and detaching from the printing bed (Kristiawan et al., 2021).

2.3.2 Benefits of Fused Deposition Modelling

FDM's primary advantages over conventional manufacturing are its ability to enable quick prototyping and on-demand manufacture. Geometric freedom, lack of tooling, low inventory demand, less material waste, and unattended operation for the manufacture of personalised designs denote other perks it offers (Sathies et al., 2020). Additionally, redistributed manufacturing, which is vital for lowering the carbon footprint and enabling future intelligent manufacturing methods, is made possible by AM techniques such as FDM (Cano-Vicent et al., 2021b). The ability to modify the matrix architecture comprising its geometry, orientation, size, shape, and interconnection and to produce structures with variable designs and compositions depending on the material used are extra benefits highlighted (Alafaghani, 2018; Rezaei et al., 2016; Tagliaferri et al., 2019).

2.4 Material Anisotropy

Material anisotropy can be found in many polymeric parts produced via different technologies of AM such as FDM, SLA, SLS and DLP; this study defined the terminology in the scope of three categories: (a) mechanical anisotropy; (b) electrical anisotropy; and (c) thermal anisotropy. The mechanical anisotropy reported for parts printed via the FDM method is the highest amongst all other AM methods, with it able to go as high as almost 50%. The significant factor that causes the material anisotropy, particularly of the mechanical type, is the lack of interlayer bonding adhesion between adjacent rasters. This is a consequence of insufficient diffusion and neck growth between the layers (Zohdi & Yang, 2021). During FDM printing, the thermoplastic filament is fed by the drive wheels into the heating chamber and once it reaches the melting point, is extruded via the nozzle. It is subsequently solidified and gradually deposited on the platform layer by layer. Even though the deposition lines can be incorporated into adjacent lines, fissures between the cylindrical lines indicate inter and intra-layer deformation (Baker et al., 2017). The extruded material rapidly cools from its melted state to achieve the printer chamber temperature, resulting in the development of inner stresses responsible for the weak bond between two deposition lines and thus causing delamination or part fabrication failure. Such structure inhomogeneity results in impaired mechanical strengths in the parts produced via FDM. Meanwhile, another factor leading to anisotropy can be related to the significant air voids, which form between adjacent cylindrical lines while printing (Zohdi & Yang, 2021). Although these air voids can be reduced in size by changing the printing parameters (e.g. air gaps), the negative effect and the presence of these voids cannot be removed fully; this pinpoints the main challenge with parts produced via FDM (Cooke et al., 2011; Monzón et al., 2017).

2.5 Multiplane in Fused Deposition Modelling

Single-plane layering is used in conventional 3D printing to manufacture objects, simplifying the process by transforming 3D geometry into 2D contours. In contrast, the process of multiplane printing involves layering 3D objects throughout multiple printing planes. To print the 3D part in this way, the printing planes for the layers can

be in any one of three orthogonal planes (Ishak et al., 2019). Figure 2.10 illustrates the toolpath layering for single-plane and multiplane layering accordingly.

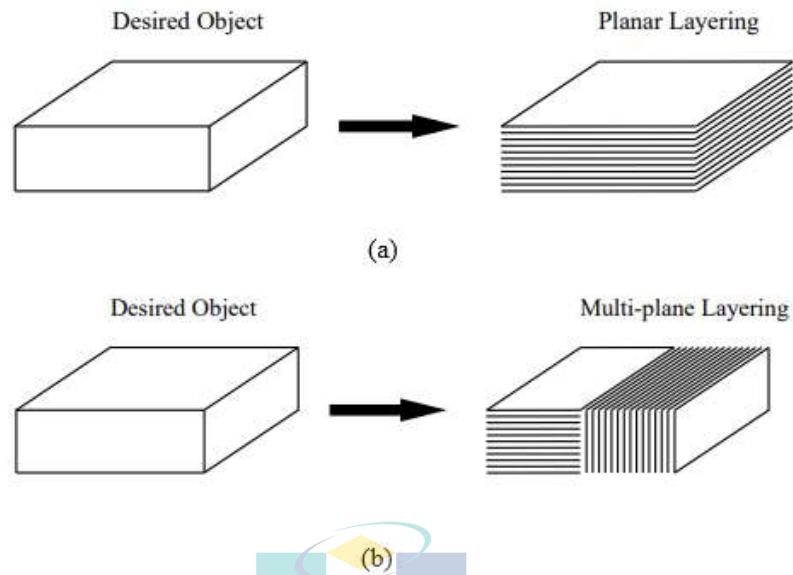


Figure 2.10 Graphical representation of toolpath layering (a) single-plane
(b) multiplane

Source: (Bin Ishak et al., 2016)

In-depth reviews of literature describe how robot arms are primarily used in the implementation of multiplane. Compound fabrication, for example, was first developed in which an industrial robot arm was implemented as the fabrication platform. To build 3D objects, compound fabrication combines subtractive, formative, and additive methods. Similarly, a part can be 3D printed using an inclined build platform (Keating & Oxman, 2013). Similarly, another researcher have also employed a robot arm platform to print 3D objects, whereby the platform allows the printing of parts with many planes (Ishak et al., 2019). Additionally, the works of few scholars have utilised the robot arm platform for non-planar layering (Alsharhan et al., 2017; Shembekar et al., 2018). From the literature review, it can be clearly concluded that the implementation of multiplane has been mostly undertaken using a robot arm while no research has been done by using a conventional 3D printer for the same type of implementation.

2.6 Polymer and Polylactic Acid (PLA)

Due to their adaptability and suitability to various 3D printing techniques, polymers are regarded as the most extensively utilised materials in the industry and typically occur in the form of thermoplastic filaments, powder, or resin (Kristiawan et al., 2021). Several industrial fields, including aerospace, medicine, architecture and toy fabrication, have explored the capability of 3D printing polymers and composites for several years. In particular, the capability for customising geometry with high accuracy is one advantage of employing 3D printing to fabricate composites (Ngo, 2018). Furthermore, the process may be more affordable for bespoke products than other conventional formative techniques like moulding.

Nevertheless, the characteristics of pure polymer products made by 3D printers tend to limit their use to conceptual prototypes. In view of this, various techniques and materials have been developed for producing advanced polymer composites with superior performance concurrent with ongoing research addressing the poor mechanical properties of such polymers (Takezawa, 2017; XinWang, 2017). Moreover, more opportunities are now available to investigate the possible uses for polymer-based material systems. This is attributable to the current levels of research and advancement in composites, nanomaterials, and biomaterials (Christ et al., 2017), which are aided by better metrological methodologies (Scheithauer et al., 2015; Tofail et al., 2018).

Multifunctional material systems (MFMSs) such as polymer composites in the form of hydrogels, polymer blends, nano-based polymer composites and many more continue to be an up-and-coming area for advancing the development of production systems meeting the sustainability and high-performance requirements of global supply chains, particularly in light of tightening governmental regulations and rising demand from developing economies (Pappu et al., 2019; Thakur et al., 2019).

As a renewable energy source derived from maize starch or cane sugar, PLA is distinguishable from most thermoplastic polymers. In contrast, many plastics are produced by polymerising semi-renewable petroleum sources (de Ciurana et al., 2013). A greener and lower-costing alternative to petroleum-based plastics, PLA has become increasingly popular over the last few years (Vink et al., 2003) and offers less carbon footprint (Dorgan et al., 2001). Made from natural sources, it is biodegradable,

recyclable, biocompatible, renewable, and compostable (Gruber et al., 2000; Rasal et al., 2010). Moreover, it can be manufactured using existing manufacturing machinery, which is created and used for materials in the oil and gas industry, following the similarities of its properties to that of polystyrene, polyethylene, and polypropylene. Consequently, production is relatively cost-effective. PLA, otherwise also known as polymer proteins, has the second-highest production capacity among all bioplastics (de Ciurana et al., 2013).

Owing to the simplicity of its processing (Garlotta, 2001), favourable thermal characteristics (Ahmed et al., 2009), and biodegradability (Mu~noz, 2020), this material is frequently utilised in various AM processes, typically in the form of 3D printing filament that is purchasable. Additionally, the ease with which PLA fuses makes AM suitable for various intriguing applications (Jerez-mesa, 2017), rendering it present in environmentally-friendly medical products, containers, tissue engineering, biosensors, biodegradable plastics, packaging, and paper coatings, for example (Farah et al., 2016; Mu~noz, 2020). Without a heated bed, PLA may be printed at temperatures between 160 and 230 °C and boasts cheap costs, non-toxicity, and is rigid and brittle simultaneously (Cano-Vicent et al., 2021b).

2.7 Processing Parameter of FDM

Processing parameters denote the most researched aspect of FDM 3DP (Kabir et al., 2020) in which the appropriate attributes deem the success of AM as underpinned by its capacity to satisfy consumer demands (Mohamed et al., 2015). According to Kumar *et al.* (2021), the mechanical performance of 3D-printed prototypes is significantly influenced by the FDM input parameters (Kumar et al., 2021). Therefore, finding the ideal processing parameters is the top priority of a production engineer as it is crucial for various reasons. They include: for maintaining quality, strengthening dimensional accuracy, preventing undesirable wastes, reducing the amount of scrap, and improving the production rates, while lowering costs and minimising manufacturing time concurrently. Due to the number of competing elements affecting the quality of the part and material qualities, FDM emerges as a very complex process that makes determining the appropriate parameters a challenge (Mohamed et al., 2015). In addition, the characteristics of build parts and their production efficiency are heavily influenced by several parameters (Dey & Yodo, 2019; Solomon et al., 2021). Accordingly, the influence

of process parameters on mechanical properties, namely the tensile strength, compression strength, and bending strength of test specimens, have been extensively investigated (Popescu et al., 2018). Here, the anisotropic behaviour of PLA components made via FDM must be taken into account when choosing the process parameters as the build orientation parameters pose a significant impact on the anisotropy of the printed parts (Chacón et al., 2017; Hanon, Marczis, et al., 2021; Laureto & Pearce, 2018).

2.7.1 Nozzle Temperature

Extrusion temperature refers to the temperature maintained inside the heating nozzle of the FDM before a material is extruded (Dey & Yodo, 2019). One of the most investigated process parameters is the nozzle temperature, as reflected in research done by Cojocaru *et al.* (2017). The scholars have reported that most researchers would select nozzle temperatures ranging from 175°C to 275°C, whereas those utilising PLA materials most frequently opt for temperatures ranging from 190°C to 220°C in view of these values correlating with PLA melting temperature (Cojocaru et al., 2022). Meanwhile, Behzadnasab *et al.* (2020) have demonstrated that the use of printing temperature higher than 240°C results in an uneven flow of material from the printing head nozzle (Behzadnasab et al., 2020). Furthermore, the viscosity of the material used for printing is affected, henceforth impacting the characteristics of the part. To prevent any changes of the filament material fluidity and potentially affecting the component manufacturing, an ideal temperature must be maintained (Solomon et al., 2021). Wang *et al.* (2007) have shown that the internal tension formed as the material is extruded through the nozzle cools down from its initial temperature, a phenomenon associated with the glass transition temperature to the chamber's temperature. Due to the fluctuation in deposition speed, this internal stress may cause inter and intra-layer deformation and potentially result in the failure of the manufactured part (Wang et al., 2007).

2.7.2 Bed Temperature

Heated beds are a necessity for 3D printing: it is essential to adjust the temperature of printers that have them, even if they are not found on all such printers. It is crucial to select the heated bed's temperature to avoid warping, wherein its role in keeping the plastic warm and avoid warping enhances the printing quality (Mogan et al., 2021). Typically, the build plate temperature is set between 50°C to 60°C during the printing of

PLA material; however, heat flows render it challenging to consistently maintain the temperature in open-space 3D printers. Thus, the temperature is generally higher in the centre of the build plate than it is at the edges (Cojocaru et al., 2022). Furthermore, the importance of heating the printer bed to temperatures around the PLA glass transition temperature (T_g), or about 60 °C, should not be dismissed and this is commonly acknowledged by authors (Liu et al., 2019).

2.7.3 Layer Height

The quantity of material deposited during a single pass along the vertical axis of an FDM machine is called the layer height. Material deposition heights do not exceed the nozzle diameter of an extruder typically as the value is purely dependent on the diameter of the extruder tip (Mogan et al., 2021). Nevertheless, the primary cause of poor part resolution in the FDM technique is linked to the choice in choosing a thicker layer thickness (Patil et al., 2021). By selecting layer thickness of a higher value, the part resolution is decreased; however, it also leads to reduced production time. Contrastingly, selecting and working with a layer thickness of a smaller value results in higher part resolution while also taking up a longer printing time (Cojocaru et al., 2022). Typically, the layer height in FDM falls between the range of 0.05mm to 0.4mm (M. Kumar et al., 2019). Therefore, a lower layer thickness should be chosen to obtain a good surface quality (Patil et al., 2021).

Several studies have highlighted that implementing a low layer thickness enhances the surface quality and dimensional accuracy of the printed part (Roberson et al., 2015). The experimental study by De Toro *et al.* (2019), in particular, has demonstrated how the layer height is inextricably linked to the bending and impact properties of the tested component. Consequently, the scholars have recommended a lower layer thickness for better-bending properties and a higher layer thickness for better impact properties (de Toro et al., 2019). Moreover, an experiment conducted by Nabipour *et al.* (2021) have opted for adjusting several parameters, namely the layer thickness, nozzle diameter, nozzle temperature and raster angle to determine the manner in which these printing attributes affect the tensile strength. The results showed that implementing a lower layer thickness would contribute to an enhanced tensile strength due to stronger adhesion present between layers. Additionally, the analysis of variance (ANOVA)

analysis performed revealed the impact of layer thickness changes on the tensile strength of the printed samples (Nabipour & Akhondi, 2021).

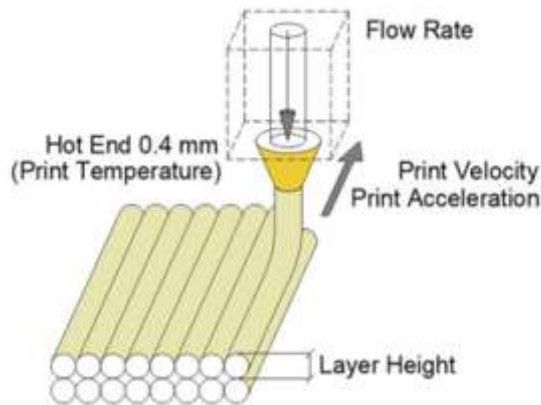


Figure 2.11 Layer height graphical representation

Source: (Barrios & Romero, 2019)

2.7.4 Printing Speed

Printing speed impacts the mechanical characteristics of an object, whereby it can be described as the traversal speed of the build nozzle as material deposition occurs on the build platform along the XY plane (Kačergis et al., 2019). However, high-speed printing may degrade the mechanical attributes of a part by causing inadequate layer bonding. It also significantly impacts the material cooling and melting rates and printing time, leading to poor layer adhesion (Mogan et al., 2021). Furthermore, the printing speed dominates the build component deformation (Kačergis et al., 2019). A quicker extrusion process generates a large amount of residual stress during the material deposition, whereas printing thinner layers is associated with negligible impact on the printing speed (van Manen et al., 2018). Here, Cojocar *et al.* (2022) have explained that as the printing speed increases, the production process takes less time overall while also leading to poor dimensional accuracy. Similarly, higher printing speeds lessen the degree of bottom layer solidification when adding additional layers, possibly resulting in sliding processes between the subsequent deposited layers, especially at the edges, and considerable dimensional deviations (Cojocar et al., 2022). Meanwhile, Farazin *et al.* (2022) are of the opinion that mechanical properties are less affected by the printing speed compared to other processing parameters (Farazin & Mohammadimehr, 2022).

2.7.5 Build Orientation

Building orientation explains how the indicated component is altered on the build platform concerning the three principal axes of the specified machine tool, namely X, Y, and Z. For instance, using an FDM printer and two printing directions, scholars have printed two test samples for the PA12 filament category (Feng et al., 2019). Figure 2.12 shows the different directions of the build orientation. One of the key determinants of the anisotropic behaviour shown by PLA-FDM printed parts is the 3D model placement on the build platform of the printer. Here, build orientations XY and YX are referred to as "flat build orientations", XZ and YZ as "on-edge build orientations", and ZX and ZY as "upright build orientations" in various sources (Nyiranzeyimana et al., 2021). Compared to the flat build and on-edge orientations, the mechanical properties shown by the upright build orientations are significantly lower. Thus, the interlayer fracture that takes place in the upright printed samples is the element causing such a mechanical behaviour. Moreover, as the tilt angle increases, the mechanical characteristics at tilted samples relative to the build plate also decrease. In comparison to the horizontally printed samples, upright printed samples display significantly lower mechanical strength. Additionally, increasing the sample positioning angle in relation to the build plate yields decreasing mechanical properties (Cojocaru et al., 2022).

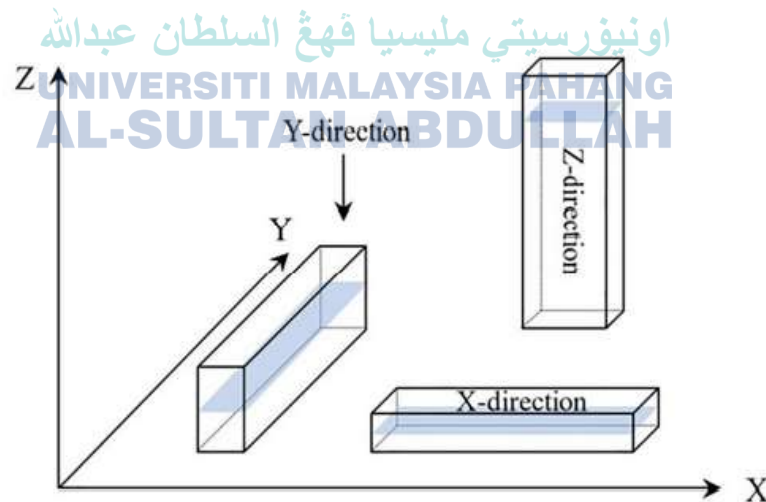


Figure 2.12 Different directions of build orientation

Source: (Solomon et al., 2021)

2.7.6 Infill Density

The infill density indicates the material volume printed on the specified component, wherein it directly dominates the properties of the printed component. Less density significantly impacts mechanical qualities, whereas a denser infill takes longer to manufacture but shows superior mechanical properties compared to the former type (Solomon et al., 2021). The effects of 3D printing process parameters on the bending and tensile strength of materials have been examined by Gunasekaran *et al.* (2020) in which results depicted a high ultimate tensile value for the PLA sample printed with 100% infill density. As the sample was printed layer by layer, improved bonding and increased load distribution were observed, as opposed to those printed with varied infill densities. The results further demonstrated that the PLA sample printed with 100% infill density resulted in 53 MPa tensile strength, while those printed with infill densities of 25%, 50%, and 75% generated 39 MPa, 43 MPa, and 47 MPa, respectively (Gunasekaran et al., 2021). Additionally, as the infill density increases, the physical characteristics of the printed sample are improved, whereby high infill densities result in a minimum layer thickness, leading to excellent layer bonding. This phenomenon is due to the inter-layer adhesion between two successive layers; as the infill density increases, the mechanical strength also increases (Hodžić et al., 2020).

2.7.7 Infill Pattern

Infill pattern is the process used to print the internal design of the printed component in which numerous kinds are available, such as grid, line, triangle, concentric, tri-hexagonal, and zigzag (Qattawi et al., 2017). In an experimental study, Baich *et al.* (2015) have demonstrated the importance of correlating the influence of the infill pattern to the mechanical properties. A different pattern may yield superior results for tensile, bending, or compressive properties, whereas the same pattern may not hold well for a component exposed to different sorts of loads. Therefore, it is essential to correlate the infill pattern to their mechanical properties, which may play an essential role in determining the properties of fabricated components (Baich & Manogharan, 2015).

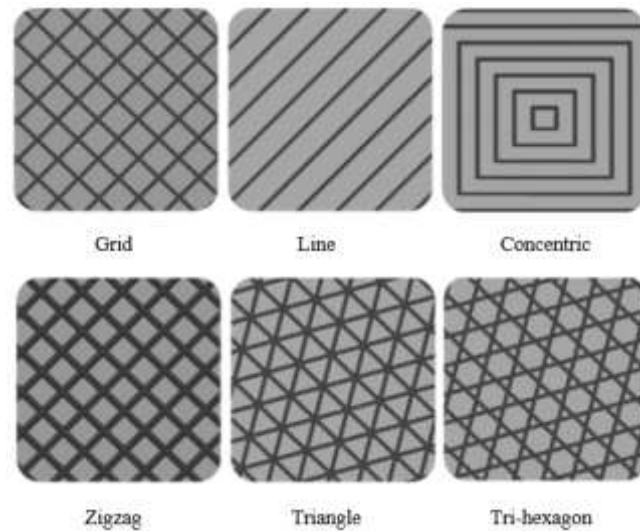


Figure 2.13 Types of infill pattern for FDM printed parts

Source: (Solomon et al., 2021)

2.7.8 Raster Angle

This element indicates the direction of material deposition along the build region across the x-axis of the FDM machine used. Raster angle ranges from 0 to 90 degrees (Rayegani & Onwubolu, 2014) and refers to the angle between the raster tool path and the x-axis of the build path after material deposition. The standard raster angles permitted are 0–90° or 0–90° in 15° steps. For instance, a selection of 45° will produce a raster tool path in the first bottom layer that is inclined at 45° to the x-axis, whereby the tool path direction will alternate in each layer above that (Masood, 2014). Several raster parameters, including raster angle, how it alternates between two successive layers, the width of a raster line, the distance between two successive raster lines, the number of wall lines, and the separation between the raster and the wall lines, are among those that affect the mechanical behaviour (Tronvoll et al., 2018). The anisotropic mechanical behaviour and component failure in 3D-FDM printing are influenced by the raster angle, which can be divided into two types: unidirectional raster and alternating raster. Unidirectional raster refers to the same raster angle being maintained for all succeeding layers, whereas alternating raster denotes the raster angle that varies between layers, typically by 90 degrees. The importance of analysing the mechanical behaviour in relation to the raster angle and the build orientation of the sample is thus undeniable (Khosravani & Reinicke, 2020; Samykano, 2021).

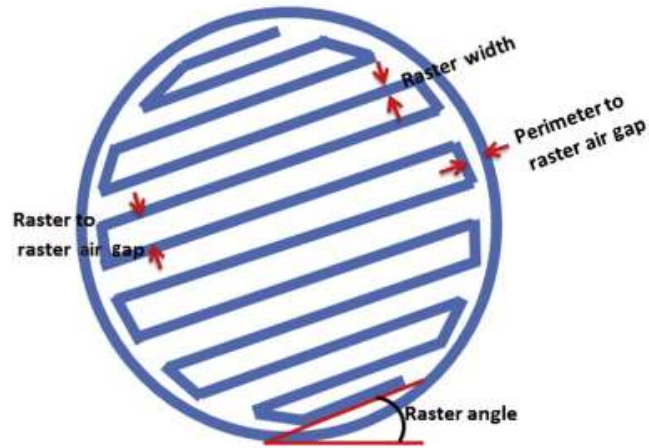


Figure 2.14 Graphical representation of raster angle

Source: (Masood, 2014)

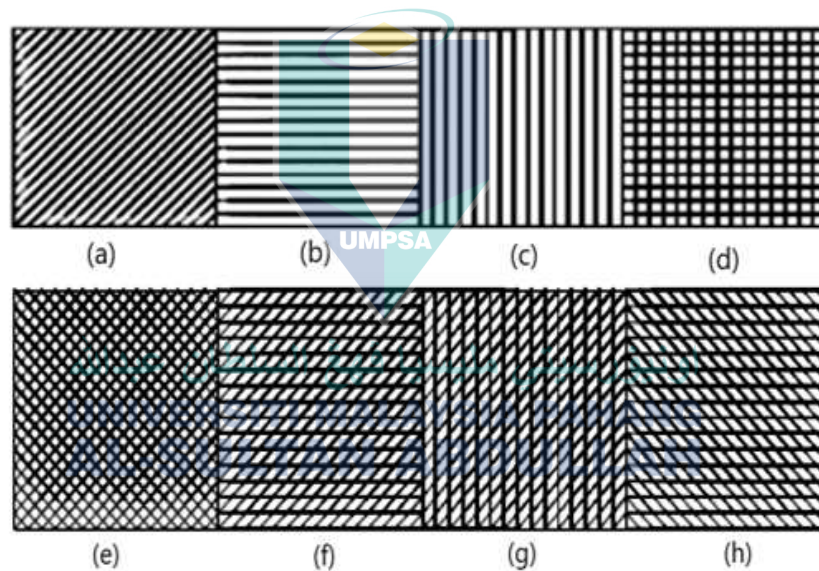


Figure 2.15 Various types of raster orientation (a) $+45^\circ$, (b) 0° , (c) 90° , (d) $0^\circ/90^\circ$, (e) $+45^\circ/-45^\circ$, (f) $0^\circ/+45^\circ$, (g) $90^\circ/+45^\circ$, (h) $0^\circ/-45^\circ$

Source: (Sheoran & Kumar, 2020)

2.7.9 Nozzle Diameter

The nozzle diameter significantly impacts the width of the sample which is attributable to its direct influence on the pressure drop along the liquefier (Wu et al., 2015). Turner *et al.* (2014) have experimentally showed that the nozzle's L/D (length to diameter) ratio further affects how much pressure is dropped, reporting increasing drops

as the D value decreases (Turner et al., 2014). Therefore, selecting the ideal nozzle diameter is crucial to maintaining a proper and constant flow of the extruding material. To optimise the nozzle diameter value, a thorough analysis must be conducted and takes into account all elements influencing the process. Additionally, the nozzle diameter significantly impacts the time of extrusion, whereby the time required to complete the extrusion decreases as the nozzle diameter increases. Thus, nozzle diameter has been demonstrated to notably influence geometrical inaccuracy (Solomon et al., 2021).

2.8 Air Gap

The air gap illustrates the separation between two adjacent bead depositions and its value can be zero, positive, or negative. Zero air gap indicates the deposited materials just touch each other, whereas positive values position loosely packed structures wherein rapid assembly of the given component is essential. Material deposition in successive runs is made apart in positive air gaps. Contrarily, a negative air gap can be used when denser structures are required and time is not an issue. Due to the partial occupancies of the beads, negative air gaps result in a denser component (Ahn et al., 2002; Rayegani & Onwubolu, 2014). Ahn *et al.* (2002), in particular, have investigated the effects of air gap, road/raster width, model temperature, material colour, and raster orientation on the tensile and compressive properties of PLA/ABS materials generated by the FDM process (Ahn et al., 2002). The resulting analysis showed that the mechanical characteristics of FDM-produced objects appeared to be parameter-dependent and anisotropic (i.e. displayed better characteristics in the deposition direction of the filaments). The scholars have also noted that raster orientation and air gap pose a significant impact on the material mechanical properties.

2.9 Void

Void is the formation between layers during printing in which the element together with rough surfaces and inadequate fibre-to-matrix bonding denote the three most prevalent flaws in printed objects (S. Wickramasinghe et al., 2020). In FDM parts, various shapes and sizes of voids may be observed and are often categorised based on how they are formed. These voids are the primary cause of porosity in FDM parts and regarded as impossible to be completely eradicated (Ghorbani et al., 2022). In an experiment, it has been found that the particular reason for the circumstance is due to no

pressure being applied during the FDM process, rendering the completed parts having larger void regions inside the printed structure (Dawoud et al., 2016). In fact, a majority of studies have demonstrated that increasing the layer height of a print causes large voids to form in the microstructure, thus lowering the tensile strength of the print parts (Abbas et al., 2018; Aworinde et al., 2019; Luzanin et al., 2019). Hence, it is suggested that smaller layer thicknesses can be used to limit these void regions as they strengthen the bond between layers and lessen the interlayer distortion leading to micro gaps in the structure (Chockalingam et al., 2016; Priya et al., 2019). Table 2.1 summarises the effects of processing parameter on voids in detail.

Table 2.1 Effects of processing parameter on voids

Processing Parameter	Void size	Outcome	Reference
Printing speed	Large	By using a high printing speed resulted in larger voids	(Abbott et al., 2018)
Bed temperature	Small	High bed temperature resulted in small void	(Aliheidari et al., 2018; Wang et al., 2017)
Layer thickness	Small	By implementing a thinner layer thickness results in small void	(Aliheidari et al., 2018; Wang & Gardner, 2017)
Infill density	Reduced void	Higher infill density leads to reduced voids	(Abeykoon et al., 2020)
Nozzle temperature	Small	High nozzle temperature results in small voids	(Aliheidari et al., 2018; Petersmann et al., 2020)
Build orientation	Occurrence of voids	The voids growth are in upright, flat and on-edge orientations	(Hernandez-Contreras et al., 2020)

In contrast to traditionally manufactured parts, FDM-printed parts suffer from weak and anisotropic mechanical characteristics due to inherent flaws, including the occurrence of voids and weak layer-to-layer adhesion (Tao, 2021). Several factors can cause void formation during printing, such as gaps between the layers and beads, air traps in the structure, and uneven filament diameter. The nature of printing formation of voids

renders them unavoidable to some extent, whereby those present between the layers are larger and differ according to the layer thickness and air gap. Contrarily, voids present inside the filament are smaller and more difficult to control by altering the processing parameters (M. Kumar et al., 2019). Numerous experiments have shown that by reducing the layer thickness, gaps between layers causing the printed part to fail via delamination can be minimised (Bledzki & Jaszkievicz, 2010; Rodríguez et al., 2001).

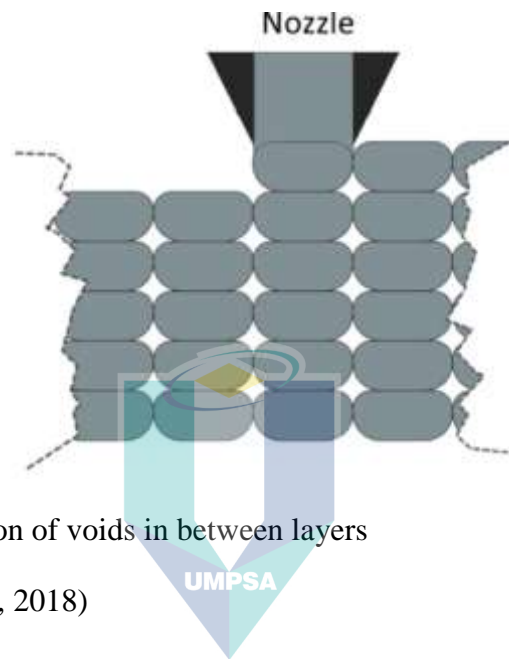


Figure 2.16 Formation of voids in between layers

Source: (Tronvoll et al., 2018)

2.10 Physical and Mechanical Properties in FDM

The behaviour of a material under different loading modes such as tensile, shear, impact, and pressure can be determined using its mechanical characteristics. Infill density, raster angle, and building orientation comprise a few of the structural and material characteristics. The mechanical characteristics of FDM products, in particular, also depend on production factors including extrusion temperature, nozzle speed, bed temperature, and printing speed. Meanwhile, mechanical strengths such as tensile and bending strengths are discovered to be extremely anisotropic in the FDM process (Garg & Bhattacharya, 2017).

2.10.1 Tensile Strength

Compared to other FDM-printed part qualities, the tensile strength of a part has received the most research and analysis efforts. The build orientation, for example, is the

most critical process parameter and can pose a significant impact on the tensile strength of an FDM-printed part, according to prior research (Rajpurohit & Dave, 2019). Three distinct modes of tensile sample failure can be described, which are inter-layer, intra-layer, and in-layer failures. When a fracture develops at the boundary between two adjacent material layers and these material layers remain intact after the failure, an inter-layer failure mode is said to have occurred. Intra-layer mode, meanwhile, is defined as the cohesion between the adjacent strands within a layer, whereas in-layer failure happens when the fractured surface is not aligned with the raster angle or the interface between two consecutive layers (Spoerk et al., 2017; T. Yao et al., 2020). The tensile strength of the FDM-printed object is maximised when it is orientated at a 0° angle, either lying flat or on the edge of the build platform.

The extruded filament material or rasters are parallel to the direction of the applied tensile load in this arrangement. According to research, thinner layers and higher rasters result in a larger bonding area, thereby increasing the tensile strength (Rajpurohit & Dave, 2019; Sheoran & Kumar, 2020). Qattawi *et al.* (2017) have conducted an experimental investigation on the effects of process parameters on the mechanical properties of printed products by using a variety of processing settings. They include: infill pattern, printing speed, infill percentage, build direction, layer thickness, and set nozzle temperature (Qattawi et al., 2017). The scholars then described the negligible effect of the infill pattern, infill density, and printing speed on the tensile properties. Meanwhile, the impact of build orientation, printing speed, and layer thickness of PLA material have been assessed by Chacon *et al.* (2017). The resulting findings demonstrated strength as the most beneficial mechanical performance; it was reduced due to inter-layer failure, which was visibly observed in the upright sample. In contrast, trans-layer failure occurred on the on-edge sample. Additionally, as the layer thickness increased, the sample ductility was reduced, and as the printing speed increased, the bending and tensile strengths decreased (Chacón et al., 2017).

2.10.2 Bending Strength

Bending strength measures the capacity for a material to sustain a bending deflection when force is applied to the sample. Compared to tensile and compressive strength, bending strength is the FDM-printed part attribute that has received little

research. It is more challenging to analyse and determine the best process parameter for bending strength than it is for tensile or compressive strength as bending causes the part to encounter both compressive and tensile pressures on several layers. However, based on the studies conducted, it can be inferred that when the construction angle or orientation is 0° , the bending strength is at its highest (Akhoundi & Behraves, 2019). In the experiment by Chacon *et al.* (2017), several factors such as building orientation, layer thickness, and printing speed have been examined with regards to the bending strength. The scholars discovered that the strengths negatively correlated with the layer thickness and printing speed. Meanwhile, building orientation has posed a significant impact on the bending strength (Chacón *et al.*, 2017).

An assessment of the available literature has called for more research to be done in order to fully understand the impact of other process characteristics in determining the ideal arrangement of FDM process variables (Akhoundi & Behraves, 2019; X. Yao *et al.*, 2020). Moreover, Jaya *et al.* (2018) have stated that the bending properties of PLA material are significantly influenced by the layer thickness. The findings revealed that the bending strength decreased as the layer height was increased. Therefore, implementing a lower layer thickness would result in a high bending strength (Jaya Christiyani *et al.*, 2018). The bending strength is influenced by the printing speed and build orientation; implementing a lower printing speed causes the layers to be highly bonded, while the layer orientation should be along the x-axis to enhance the bending strength (Jaya Christiyani *et al.*, 2018). In an experiment by Durgun *et al.* (2014), investigation into the tensile and bending strength via varying the building orientation and raster angle has revealed that building orientation affects the mechanical strength (i.e. tensile, bending) of the FDM-printed parts more than the raster angle (Durgun & Ertan, 2014).

2.10.3 Dimensional Accuracy

The industry's general acceptability of the FDM process depends on its capacity to maintain a high degree of dimensional stability in the created product. This is attributable to the multiplicity of conflicting process factors throughout the process that pose an individual or cumulative impact on dimensional accuracy (Mohamed, 2017). Thus, in many industrial applications including medical devices, aircraft, and electronics, achieving great dimensional precision is a crucial quality feature (Shih, 2013). According to the present study, layer thickness is one of the most important and influential process

parameters for dimensional accuracy. By minimising the staircase effect of FDM-printed constructions, choosing a lower layer thickness enhances the resulting accuracy (Zharylkassyn et al., 2021).

Based on prior studies, it can be deduced that low extrusion temperature, fewer solid contours or outer shells, and lower print speeds all contribute to an increased dimensional accuracy (Sheoran & Kumar, 2020). However, process variables like the number of solid contours or outer shells, extrusion temperature, raster width, and infill density require more research as their effects on dimensional accuracy other than layer thickness have yet to be thoroughly investigated or studied. Furthermore, FDM-printed items experience dimension changes post-curing, whereby previous studies have shown that the dimensions of the build platform shrink in the X and Y directions while expanding in the Z direction. Therefore, the build orientation process parameter significantly impacts dimensional accuracy (Sood et al., 2009).

2.10.4 Density

One of the most crucial elements in establishing the characteristics of polymer composite materials is density, measured as the material's mass per unit volume. During the testing of composites, specimens are weighed in air and then suspended on a wire before submerged in water, following which the difference in density is noted (Saba et al., 2019). As material density is dependent on the printing temperature, the flow rate should be regulated based on the printing temperature to achieve excellent adhesion and connection between the printing layers (Damanpack et al., 2021).

2.11 Morphology Analysis

Physical characteristics such as malleability, hardness, wear resistance, and strength are strongly influenced by the microstructure of materials such as composites, metals, and polymers. A microstructure significantly impacts the physical and mechanical properties of certain materials due to various deformities present or absent. OM and SEM comprise the two primary forms of a microscope, whereby the last two centuries has seen the former being utilised as a simple device with limited capabilities. The beam type applied to a sample distinguishes between an SEM from an OM in which the latter involves applying a beam of light to a sample and analysing the effects of the light as it interacts with the sample. Moreover, the SEM examines the effects of electrons

on a sample by applying a beam of electrons to it. Nevertheless, small organics are rarely visible in OM and small solid pieces can be seen, whereas SEM provides grayscale images and a more detailed view (Mohammed & Abdullah, 2018). The SEM images of PLA are shown in Figure 2.17.

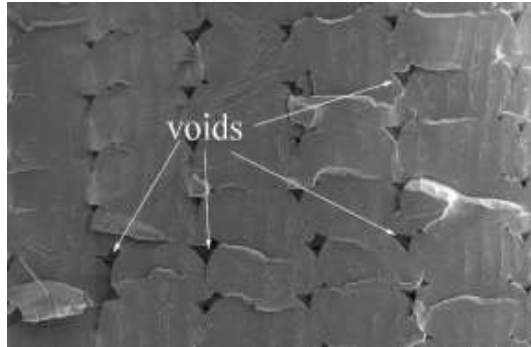


Figure 2.11 SEM image of voids occurred in PLA-FDM printed parts

Source: (Fekete et al., 2021)

2.12 Summary

The literature review conducted provides an in-depth discussion of AM, specifically the FDM process. The study emphasises the material anisotropy of FDM in which mechanical anisotropy emerges as a significant issue and according to researchers, the degree of mechanical anisotropy can reach up to 50% depending on the selection of process parameters. Therefore, process parameters such as build orientation, layer thickness, raster angle, width, infill density and pattern, and printing speed are highlighted as crucial in determining the part quality and mechanical properties. Furthermore, another important point that needed to be highlighted from the literature review is the implementation of multiplane are only done by using the robot arm due to the translational motion alone in conventional printer that limits its printing to a single-plane layering. However, the literature review must be substantiated with a comprehensive discussion on the existing research gaps in the context of FDM mechanical anisotropy and the role of process parameters in determining the mechanical properties. Thus, the study must further explore the research gap in this area to provide new insights and knowledge to the field.

CHAPTER 3

METHODOLOGY

3.1 Introduction

This chapter briefly explains the methods necessary in conducting the research comprehensively. The material, processing parameters, sample standards, and physical and mechanical testing for single-plane and multiplane samples are explained in detail. The techniques to achieve the objective of this research are also discussed, following which a flowchart elucidating a comprehensive review of the process of conducting this research is included.



اونيورسيتي مليسيا قهغ السلطان عبدالله
UNIVERSITI MALAYSIA PAHANG
AL-SULTAN ABDULLAH

3.2 Research Methodology

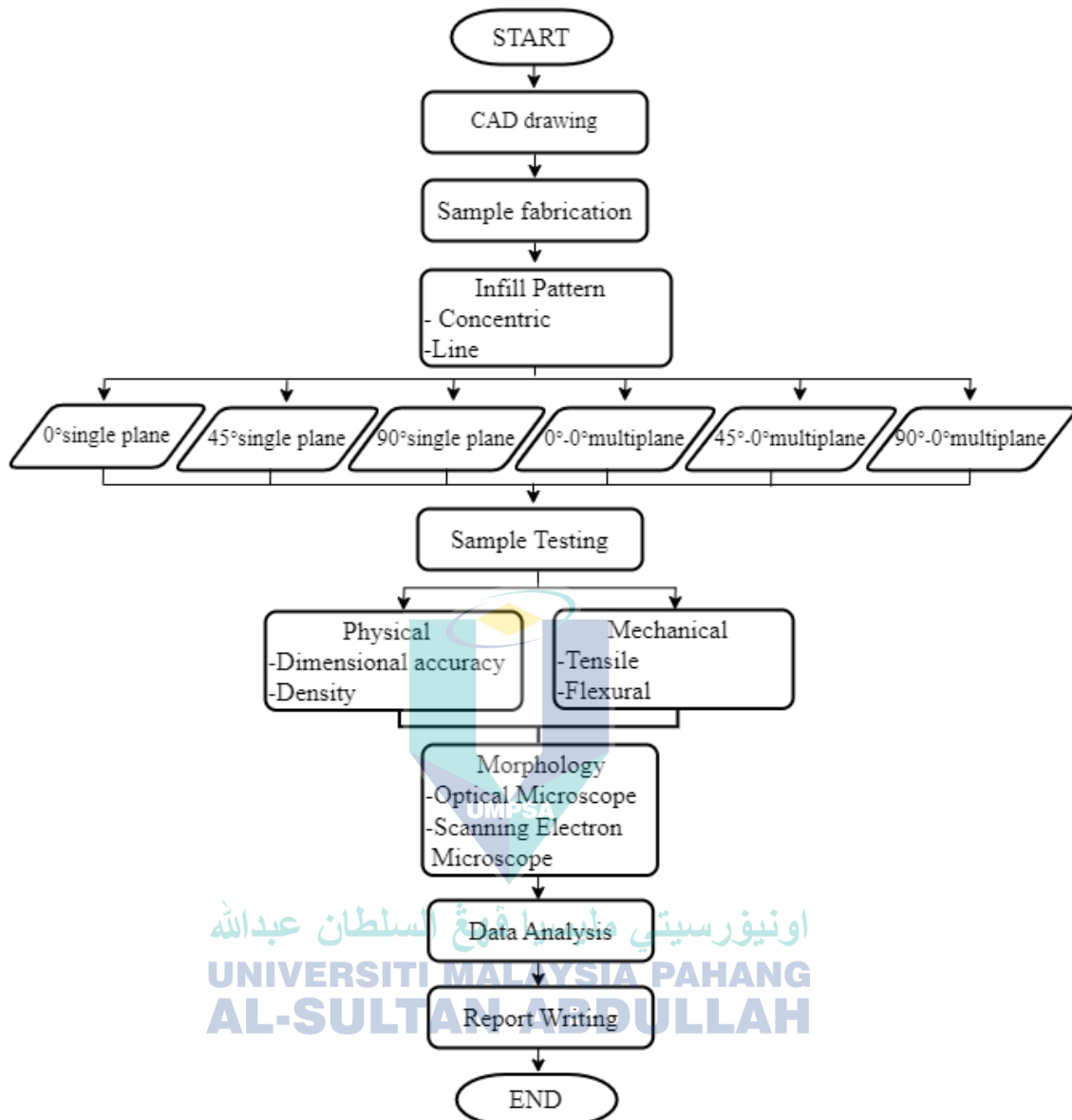


Figure 3.1 Flow chart of the overall process

The overall process for this research is shown in Figure 3.1. Firstly, the CAD models were drawn using SOLIDWORKS software according to the ASTM standard dimension. Then, the purchased PLA material was dried in an oven at a heating temperature of 75°C before the PLA filament underwent differential scanning calorimetry (DSC) and thermogravimetric analysis (TGA) testing. Then, the sample was fabricated by using various orientation angles. In general, there are two types of planes, which are the single-plane and multiplane, and the orientation angle for each plane varies. Thus, the orientation angles for the single-plane type were (0°, 45°, 90°) and for the

multiplane were (0°, 0°), (45°, 0°), and (90°, 0°), respectively. After the samples were printed according to the orientation angle and infill pattern, they underwent mechanical, physical, and microstructure testing. The data obtained from each test was subjected to an analysis before being reported in detail.

3.3 Polylactic Acid (PLA) Filament

Plastics are classified as thermoplastics or thermosetting plastics according to their formability. Biodegradable natural plastics, in particular, are made partly from renewable resources (e.g. starch) and could be produced either naturally or synthetically (Nampoothiri et al., 2010). PLA, however, is also hydrophobic and has a slow decomposition rate. Its high strength, elastic modulus, and biodegradability render PLA a commercially available bio-based polymer utilised in various applications (Sheoran & Kumar, 2020). Furthermore, PLA is a popular thermoplastic used in FDM due to its unique physical properties, namely easy processability, biodegradability, biocompatibility, and low cost.

In this research, commercially available white Polylite™ PLA 3D printing filament with a diameter of 1.75mm sourced from Polymaker is used as shown in Figure 3.2. The filament was purchased from Pebblereka 3D Print Company, Kuala Lumpur, Malaysia, and the manufacturer data sheet are presented in Table 3.1.

Table 3.1 Manufacturer data sheet of PLA material

Properties	Value
Extrusion temperature	190°C - 230°C
Tensile strength	46.6MPa
Young's Modulus	2.636GPa
Bending strength	85.1MPa



Figure 3.2 White Polylite™ PLA filament with diameter of 1.75mm

3.4 Selection and Calibration of 3D Printer

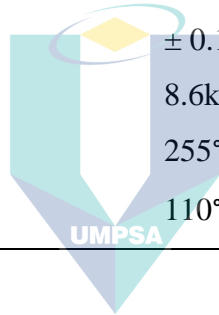
Selecting a suitable 3D printer based on its ability to print the chosen material and its varying parameters is vital. Therefore, the Creality Ender-3 machine was chosen to print the test samples in this research. Figure 3.3 depicts the Creality Ender-3 machine while Table 3.2 details the specifications of the 3D printer.



Figure 3.3 Creality Ender-3 printer

Table 3.2 Specifications of Creality Ender-3 printer

Properties	Specifications
Machine size	440mm x 410mm x 465mm
Printing size	220mm x 220mm x 250mm
Input	AC 100-256V 50-60Hz
Output	DC 24V 15A 360W
File format	G-code, STL(from cura convert to G-code)
Filament size	1.75mm
Layer height	0.1mm to 0.4mm
Nozzle diameter	0.4mm
Travel speed (max)	180mm/s
Working mode	Micro-SD (offline) or USB cable (online)
Precision	± 0.1 mm
Weight	8.6kg
Nozzle temperature (max)	255°C
Hotbed temperature (max)	110°C



Printer calibration was the first step even before printing could begin, whereby it was vital due to the lack of accuracy the printed samples could yield if calibration was not performed, as well as for ensuring the consistency. Hence, calibration of the printer was done by referring to the printer’s manual in view of the absence of any standards for this action. Firstly, the x, y, and z axes of the 3D printer were aligned carefully as their movement could affect the printing quality. The axis movement must be flawless to ensure the printing process effectiveness. Next, the x and z-axis rods were aligned horizontally at 180°, following which the heated bed was positioned by measuring its distance from the nozzle with a feeler gauge. This would ensure a constant distance between the nozzle and the heated bed and filament deposition on the bed uniformly and smoothly for each layer of the printing process.

3.5 Sample Design

The samples in this research were designed to achieve the goals and objectives specified in the beginning. Therefore, according to the ASTM standard, flat dog-bone

tensile shape and cuboid shape for the bending test were designed. Here, ASTM D638-14 type IV was used for tensile testing while ASTM D790-17 was implemented to carry out bending testing. Figures 3.4 and 3.5 show the dimensions for the tensile and bending samples, whereas Figure 3.6 illustrates how the multiplane samples are printed.

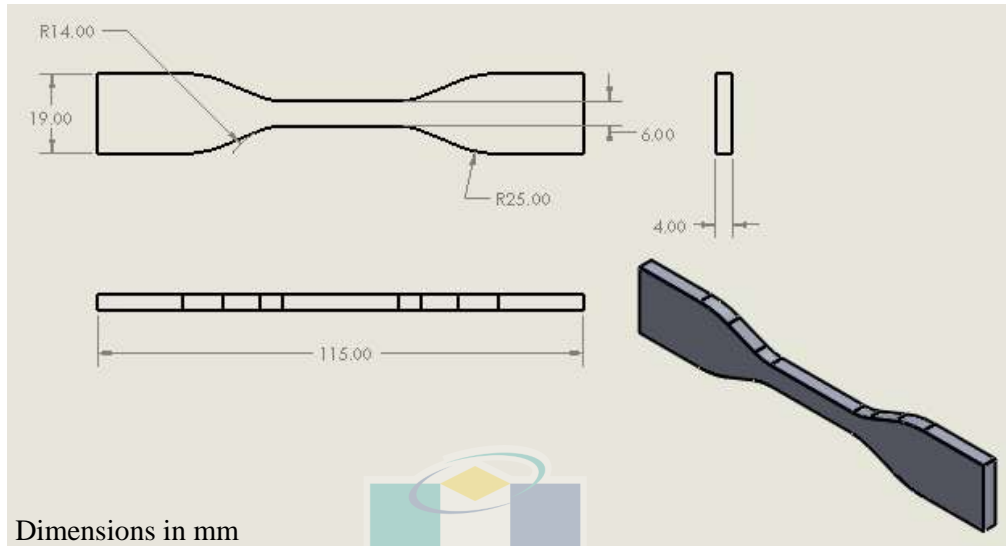


Figure 3.4 Tensile sample dimensions (ASTM D638-14)

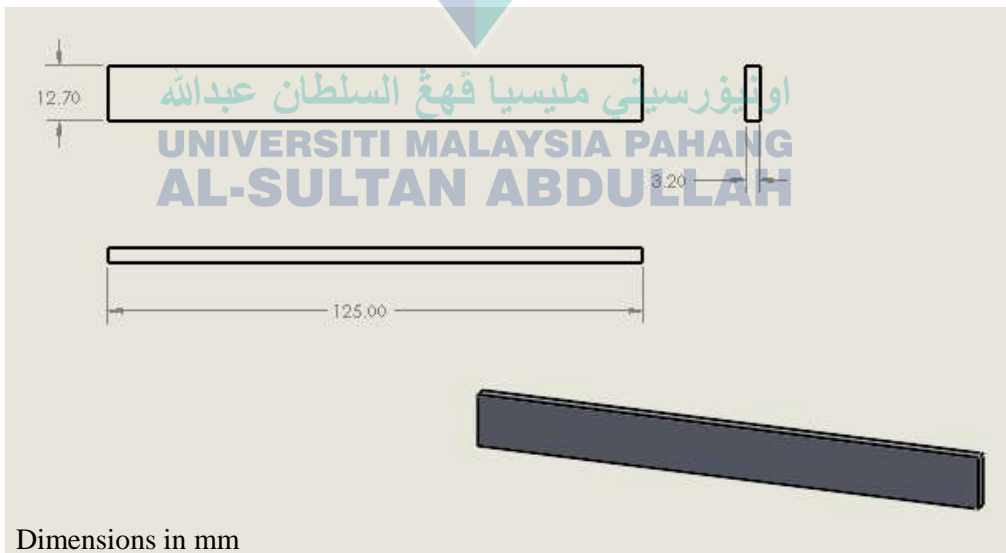


Figure 3.5 Bending sample dimensions (ASTM D790-17)

3.6 Processing Parameter and Sample Condition

Processing parameters play an important role in determining the printed sample properties, whereby selecting the appropriate attributes such as nozzle temperature, bed temperature, nozzle diameter, layer height, infill density, printing speed, infill pattern, and raster angle is vital in view of its substantial impact on the printed samples. In this research, the processing parameters comprised two types, namely the constant and manipulated parameters. Constant parameters consist of nozzle temperature, bed temperature, printing speed, layer height, and infill density, whereas the manipulated parameters are orientation angle and infill pattern as shown in Tables 3.3 and 3.4, respectively. The orientation angles for single plane were 0° , 45° , and 90° while angles $(0^\circ, 0^\circ)$, $(45^\circ, 0^\circ)$, and $(90^\circ, 0^\circ)$ denoted the multiplane. Processing parameter selection was done based on the literature review and the preliminary experiment. The selection of concentric and line patterns could be justified by the fact that they would yield 100% infill density and the outer layer of the printed sample would bear similarities to the infill pattern by using the Ultimaker Cura 4.12.1 software. In contrast, selecting another infill pattern other than these two patterns would result in an infill density of only 99.9%. Therefore, a 100% infill density was achieved and used in this study, whereby the suitable infill patterns were concentric and line patterns.

Table 3.3 Constant processing parameter

Parameter	Value	Source
Nozzle temperature	195°C	(Cojocarú et al., 2022)
Bed temperature	60°C	(Cojocarú et al., 2022)
Layer height	0.2mm	(Cojocarú et al., 2022; R. Kumar et al., 2019)
Printing speed	15mm/s	(Kristiawan et al., 2021)
Infill density	100%	(Gunasekaran et al., 2021)

Table 3.4 Manipulated processing parameter

Parameter	Value
Orientation angle	single-plane - 0°, 45°, 90° multiplane – (0°,0°), (45°,0°), (90°,0°)
Infill pattern	Concentric, Line

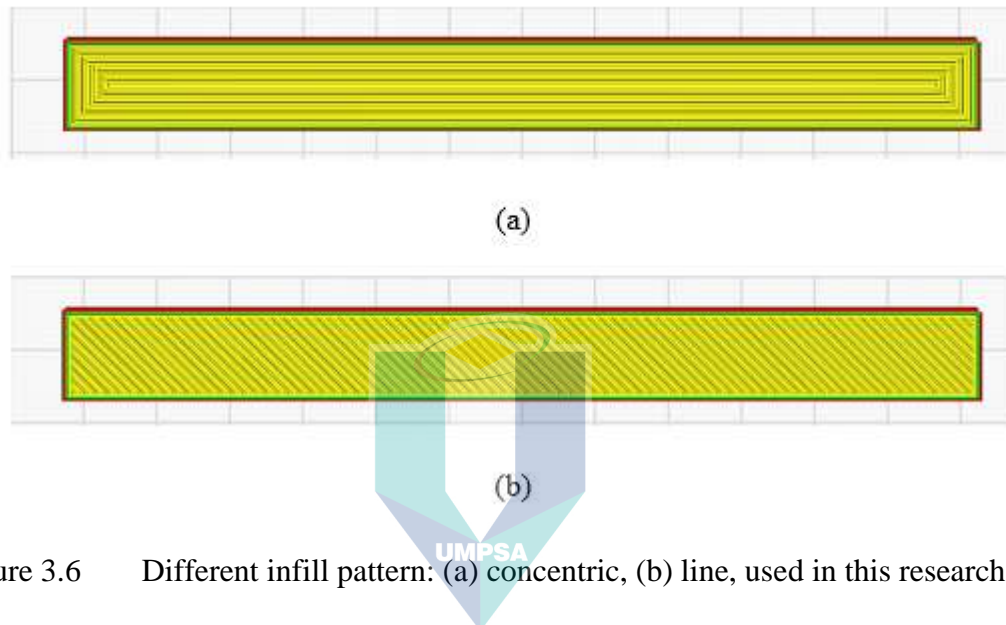


Figure 3.6 Different infill pattern: (a) concentric, (b) line, used in this research

With regard to the sample condition, single plane and multiplane denoted the two types of planes. Here, a total of 12 conditions were printed using the PLA filament in both infill patterns applied (i.e. concentric and line) as shown in Figure 3.6 in which each condition consisted of five samples. Thus, 156 PLA samples as shown in Table 3.5 are printed to assess their properties, comprising 60 samples for tensile and bending testing each, while the remaining 36 printed samples are used to assess the density properties.

Table 3.5 Summary of sample condition for single-plane and multiplane

Plane Type	Sample Condition	Tensile		Bending		Density	
		Concentric	Line	Concentric	Line	Concentric	Line
Single-plane	0	5	5	5	5	3	3
	45	5	5	5	5	3	3
	90	5	5	5	5	3	3
Multi-plane	0,0	5	5	5	5	3	3
	45,0	5	5	5	5	3	3
	90,0	5	5	5	5	3	3
Total		30	30	30	30	18	18

3.7 Sample Fabrication of Single-Plane and Multiplane

Firstly, the tensile and bending samples were drawn using the SOLIDWORKS software and followed by the generation of the CAD model, before the drawing was converted into an STL file. The Ultimaker Cura 4.12.1 slicing software was implemented accordingly for its accuracy in generating a G-code, wherein its use allowed the printing parameters (i.e. infill pattern, infill density, layer height, printing speed, and bed and nozzle temperatures) to be set. Once all parameters were set, the G-code was generated and the file was saved on an SD card. Then, the G-code was transferred to the 3D printer via the SD card, rendering the part ready to print. The 3D printer set the machine parameters based on the G-code selection provided through its interface. Before the part was ready to print, some preparations were needed in the 3D printer, such as heating the bed. During the printing process, the nozzle and bed temperatures remained constant until the sample was fully printed as per set in the software. After the samples were printed, their dimensions were recorded to ensure the dimensional accuracy before they were subjected to the mechanical testing. The uniqueness of multiplane laid in the combination of different planes on one sample, whereby the layering was done on three different building orientations, which are $(0^\circ, 0^\circ)$, $(45^\circ, 0^\circ)$, and $(90^\circ, 0^\circ)$. Here, the printing toolpath was in x-z direction for the $(0^\circ, 0^\circ)$ orientation. For the $(45^\circ, 0^\circ)$ and $(90^\circ, 0^\circ)$ orientations, however, it was vertical for the first layer, (x-y) direction vertical position, and x-z direction horizontal position for the second layer. As for the multiplane printing as shown in Figure 3.7, the first layer $(0^\circ, 45^\circ, 90^\circ)$ of the samples was printed with the thickness of 1.6mm for bending sample and 2mm for tensile sample. Then, the second

layer was printed in 0° orientation with the same thickness for all three type of build orientation. Hence, stopper was placed around the samples to grip the samples during the printing of second layer. Figure 3.8 illustrates the samples during printing and the printed tensile and bending samples for single-plane and multiplane are shown in Figure 3.9 and Figure 3.10.

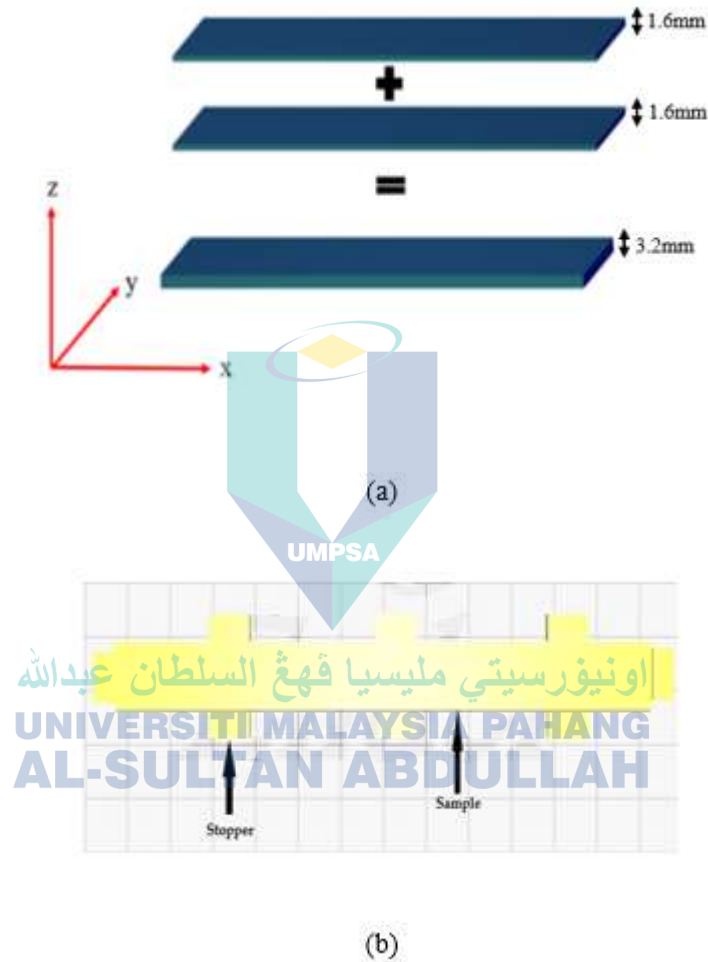


Figure 3.7 Illustration on how (a) multiplane samples are printed, (b) position of stopper

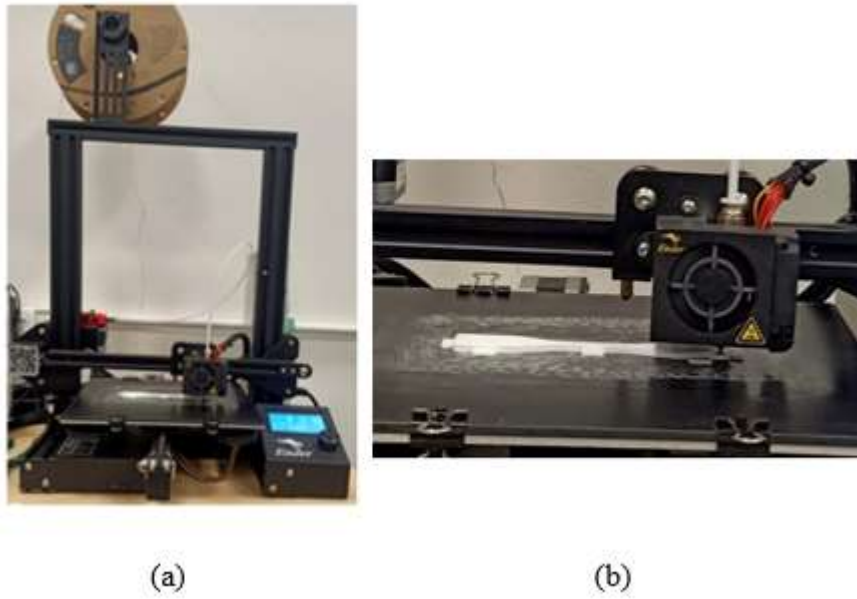


Figure 3.8 (a) Printing of tensile sample, (b) magnified view of sample printing

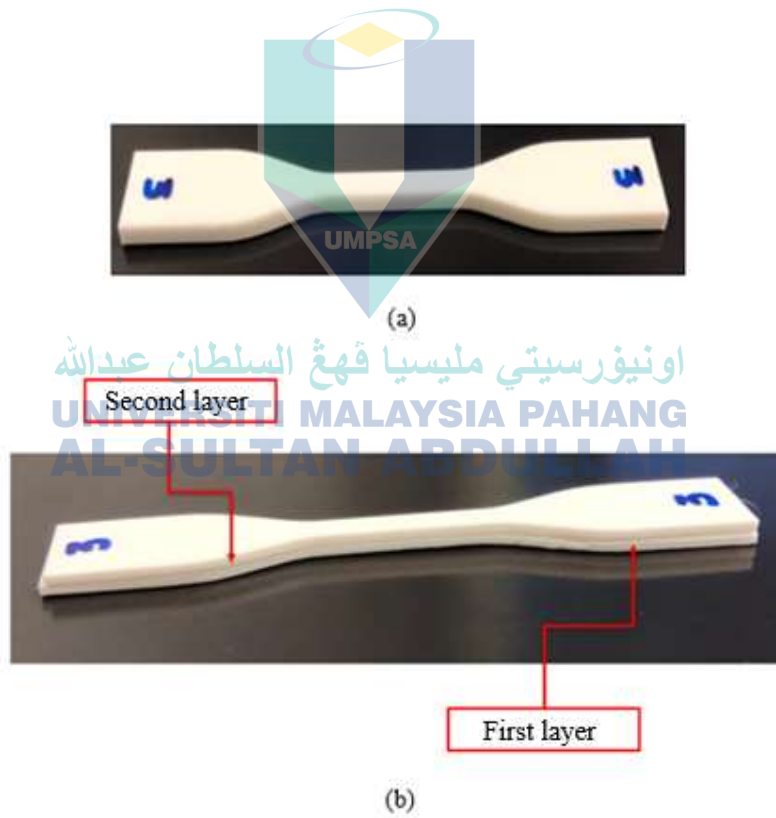


Figure 3.9 (a) single-plane printed tensile sample, (b) multiplane printed tensile sample

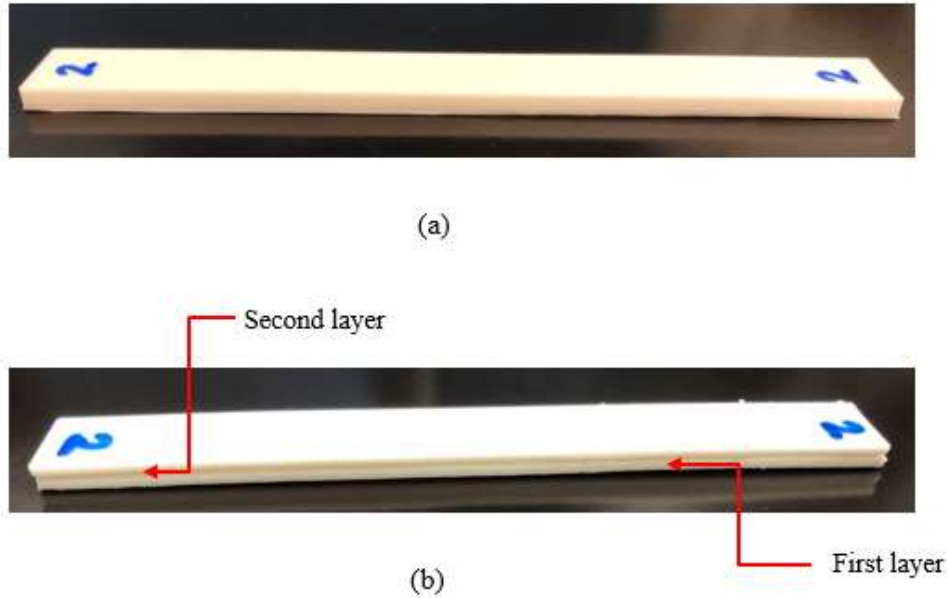


Figure 3.10 (a) single-plane printed bending sample, (b) multiplane printed bending sample

3.8 Mechanical Testing

Mechanical testing such as tensile and bending was done on PLA printed samples to analyse the effect of mechanical properties on the single-plane and multiplane. The tensile tests included the ultimate tensile strength (UTS) and Young's modulus, whereas the bending test was done to analysed the bending strength.

3.8.1 Tensile Test

Evaluation of tensile properties (i.e. UTS and Young's modulus) was carried out by using the INSTRON 3369 universal testing machine as shown in Figure 3.11. Here, the ASTM D638-14 type IV standard was implemented in testing the tensile properties and a minimum of five samples required to be printed to obtain the tensile test data according to ASTM. The machine has a maximum load of 50kN. The testing was conducted at room temperature (25°C), with a crosshead speed of 1mm/min. The built-in Bluehill software within the machine was utilised, allowing the data measurements to be monitored, controlled and recorded. Meanwhile, two types of grips could be used in tensile testing, namely clamp grip and threaded grip, whereby the first type was implemented in this research and the top and bottom jigs tightened the sample. Before testing, sample measurements such as gauge length, width and thickness input were fed

into the software. Then, the sample was placed into the grips and an extensometer was attached to it with a gauge length of 50mm. The extensometer served to measure strain directly on the sample. During testing, a crosshead motion continued until the sample was fractured, following which the raw data generated was saved automatically after each test. Subsequently, all data obtained were subjected to an analysis to comprehend the tensile properties of each sample.

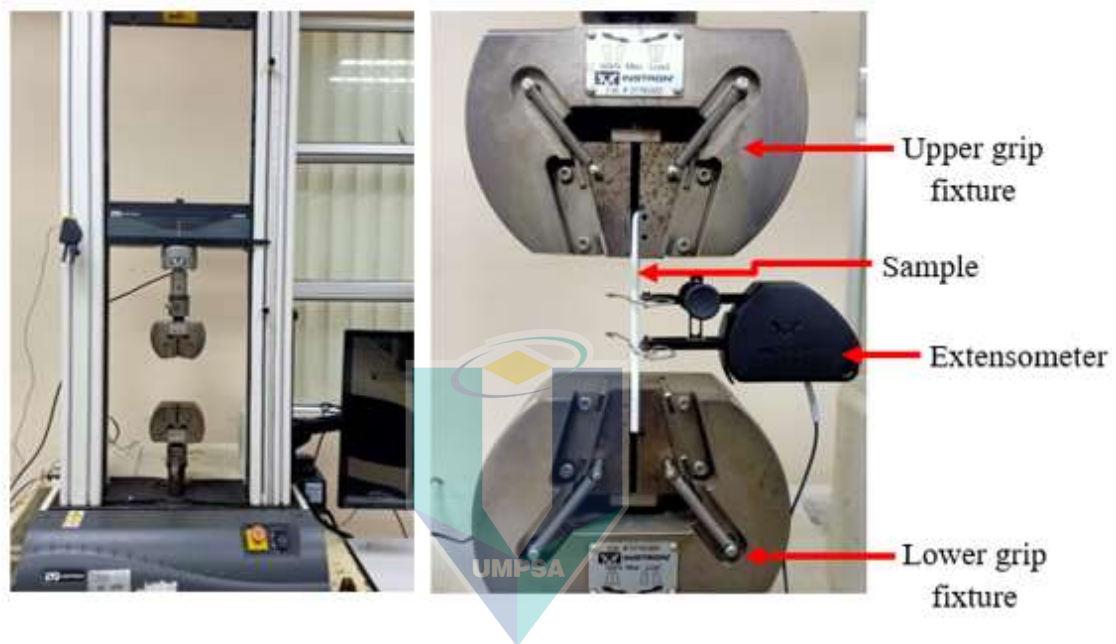


Figure 3.11 (a) INSTRON 3369 universal testing machine, (b) sample during testing

3.8.2 Bending Test

The bending test calculates the force needed to bend a sample under three-point loading conditions, allowing an assessment of the bend strength, ductility and stability held by a material. These characteristics can predict its susceptibility to failure under pressure. Before the testing was initiated in this study, several machinery parameters were necessary, namely support span, force applied and loading speed. Accordingly, the bending test was conducted by using the INSTRON 3369 universal testing machine as shown in Figure 3.12, which has a maximum load of 50kN. Here, the span-to-depth ratio is set to 16:1 and the crosshead motion is calculated using Equation 3.1. Furthermore, determining the bending properties of reinforced and unreinforced polymers was achieved by utilising the ASTM D790-17 standard. During the testing, the sample was supported at both ends and a load was applied at the centre of the sample, causing a three-

point bending at a predetermined rate. Conducted at room temperature (25°C) with a crosshead speed of 1.365mm/min, the test ended when the sample either hit a 5% deflection or broke.

$$R = ZL^2 / 6d \quad 3.1$$

R = Rate of crosshead motion, mm/min

L = Support span, mm

d = Depth of the beam, mm

Z = Rate of straining the outer fibre, mm/m/min (constant = 0.01 mm/mm/min)

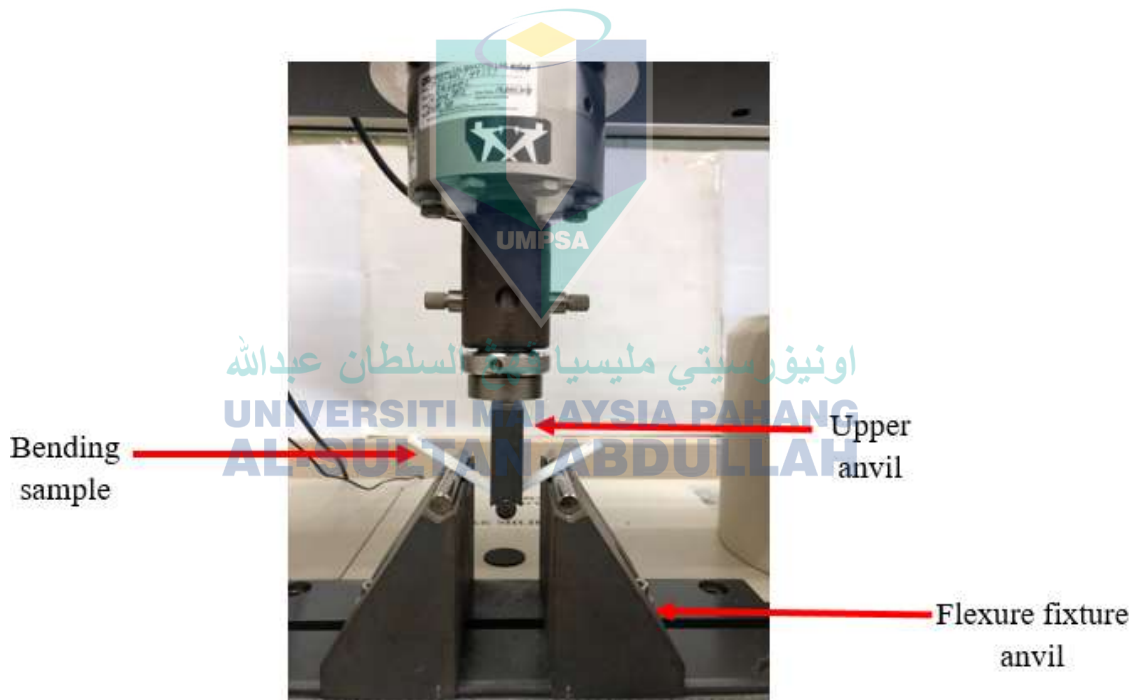


Figure 3.12 Bending sample during testing

3.9 Physical Properties

In this research, physical tests on the dimensional accuracy and density were performed on the PLA-printed samples to calculate their individual density and precision. Testing was done on both single-plane and multiplane to study the effect of both parameters in both planes.

3.9.1 Density

Theoretically, the density of a material denotes its mass per unit of volume. In this study, the printed sample density was measured according to Archimedes' principle. The samples are placed in an ultrasonic machine to remove any air bubbles present within before weighed using a digital weighing scale, as shown in Figure 3.13 below. The setup for density testing is as follows, and the machine used to measure the samples is Precisa Gravimentrics, which is Swiss equipment capable of weighing up to 220g maximum with a 0.1mg resolution. To carry out the test, a beaker was first filled with distilled water and air bubbles formed during the filling were then removed. The beaker was next placed inside the weighing scale machine before a hanging pan was placed in the beaker. The pan has two parts, which were to measure the air and water density, respectively, whereby calculating these values would yield the relative density. Calculations for density is shown in Equation 3.2 accordingly.

$$\rho = \frac{\rho_{PLA}}{5} \times 100 \quad 3.2$$

ρ = Relative density

ρ_{PLA} = Density of PLA samples



Figure 3.13 Density test setup and weighing scale machine (Precisa, Switzerland)

3.9.2 Dimensional Accuracy

The dimensional accuracy of FDM-printed parts is one factor that defines the overall quality of manufactured prototypes due to its impact on the results of future

prototype investigations. The term is further defined as the accuracy indicating how well a production's machine output complies with the tolerance within a given dimension. With CAD data, the assessment of dimensional accuracy determines how accurately the geometrical features of samples are manufactured using FDM. To achieve the sample dimensional accuracy, various measurement points were needed, namely length, width and thickness of the sample. In this research, the bending sample (i.e. length, width and thickness) where three points was chosen to evaluate the dimensional accuracy of the overall samples by using Equation 3.3. In addition, a digital vernier calliper (Mitutoyo, Malaysia) with $\pm 0.01\text{mm}$ tolerance as shown in Figure 3.14 was used to measure the points.

$$\Delta D = \left| \frac{D_{EXP} - D_{CAD}}{(D_{EXP} + D_{CAD}) / 2} \right| \times 100 \quad 3.3$$

ΔD = Percentage difference in dimension

D_{EXP} = Experimental value

D_{CAD} = Designed value of CAD model



Figure 3.14 Digital vernier calliper (Mitutoyo, Malaysia)

3.10 Morphology Analysis

The printed PLA samples comprising density samples were observed under a microscope. First, the density samples were cut in half to analyse the inner structure. Before being observed, they were subjected to grinding and polishing processes to ensure the cut surface was even and smooth. The samples were ground by using a grinding machine (Topper, China) as shown in Figure 3.15, following which an even surface was achieved via various grit designations of sandpaper were used (i.e. P180, P240, P320, P400, P600, P800, P1000, P1200, and P1500) shown in Figure 3.16. As the sandpaper designation increases, its roughness decreases. Here, water was used as a coolant to

reduce friction. Once the grinding process was completed, the polishing process was done on the ground sample by using a polishing pad and distilled water as the polishing liquid. Then, the polished sample was observed under the microscope to analyse the effect of single-plane and multiplane material behaviours, whereby testing under 5x, 10x, and 20x magnification was achieved by using an optical microscope (Olympus, Japan) shown in Figure 3.17.



Figure 3.15 Grinding and polishing machine (Topper, China)



Figure 3.16 Various designations of sandpaper



Figure 3.17 Optical microscope (Olympus, Japan)

Meanwhile, PLA fractured tensile samples were observed under an SEM (HITACHI TM3030 PLUS) in which they were chosen according to the highest and lowest values of tensile strength results obtained by each infill pattern, respectively. First, the samples were cut into small pieces approximately 1cm in size before coated with gold coating, following which they were observed under the microscope. Finally, SEM testing was done to investigate the material behaviour of the fractured samples towards the tensile strength. Magnification of 40x to 200x was used to observe the samples by using the SEM machine, shown in Figure 3.18.



Figure 3.18 Scanning Electron Microscope (HITACHI TM3030 PLUS)

3.11 Preliminary Results of Thermal Analysis

Thermal analysis (TA) is one of the most important research methods in developing and manufacturing polymer materials, being among the crucial research and quality control techniques (Blanco, 2022). TA comprises many techniques, which are DSC, differential thermal analysis (DTA), dynamic mechanical analysis (DMA) and TGA. In this research, the thermal behaviour of PLA materials was characterised by conducting DSC and TGA with a focus on determining the transition temperature and thermal degradation rate of the sample.

3.11.1 Differential Scanning Calorimetry (DSC)

The thermal characteristics of polymer materials are commonly determined using the DSC technique (Kristiawan et al., 2021). The glass transition temperature, crystallisation temperature, and melting temperature of the material are measured using the method to examine any changes in the sample heat capacity. Furthermore, the temperature at which crystals are formed, as well as other endothermic and exothermic factors, may be studied (Vinyas et al., 2019). In this study, the DSC test was conducted using a Perkin Elmer DSC8000 analyser, shown in Figure 3.19. First, the PLA filament was cut into small pieces weighing about 9mg, following which the cut sample pieces were placed in a pan with a surrounding atmosphere of nitrogen gas. The change in heat capacity was observed as the temperature was raised up to 350 °C progressively at 10 °C/min increments. The phenomena were plotted for the fluctuation of heat flux and temperature accordingly.



Figure 3.19 Differential Scanning Calorimetry machine (Perkin Elmer DSC8000, USA)

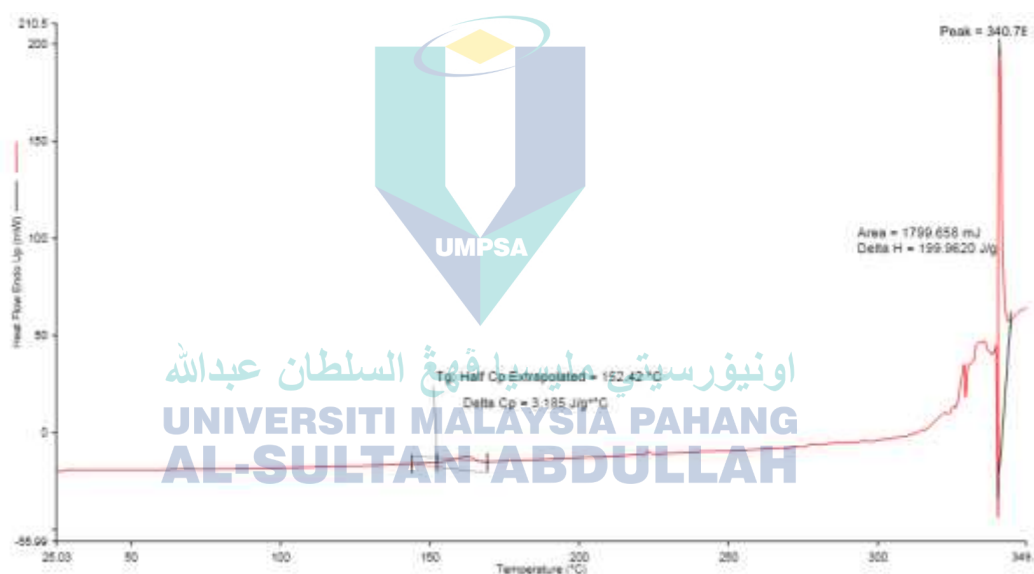


Figure 3.20 Heat flow changes of PLA

The glass transition temperature (T_g) and melting temperature (T_m) of PLA are obtained from Figure 3.19. It is an endothermic process in which heat flows into a sample. The glass transition temperature was observed at 152.42 °C and the material transitioned from a solid state to a rubber-like viscous state. At the melting temperature of 340.78 °C, the material started to degrade.

3.11.2 Thermogravimetric Analysis (TGA)

The mass degradation of a sample concurrent with temperature increases can be measured by using TGA (Khoo et al., 2016). This test reveals various details regarding the sample degradation temperature through information such as phase transitions, adsorption, and thermal decomposition. The rate of mass change is measured using the derivative thermo-gravimetric (DTG) method, which provides data on the amount of sample loss at the degradation temperature (Vinyas et al., 2019). To determine the thermal stability of the PLA material, the TGA test was conducted using the Hitachi STA 7200 machine. First, the filament was cut into small pieces weighing about 15.8 mg and heated from ambient room temperature of 30°C to 700°C at a heating rate of 10°C/min. This allowed an evaluation of the thermal deterioration underwent by the material due to the temperature change. Then, the furnace was purged with nitrogen gas at a constant flow rate of 10 mL/min. The weight loss recorded as a result is shown in Figure 3.21.

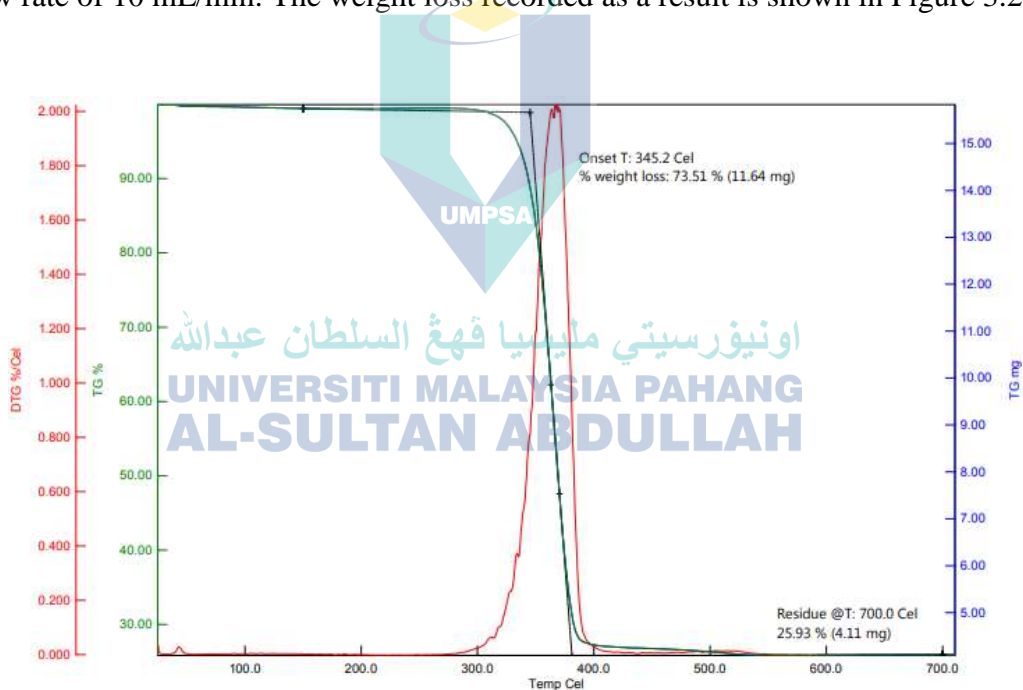


Figure 3.21 Thermogravimetric and DTG curves about temperature variations

According to Vinyas *et al.* (2019), PLA is known to have substantially poor thermal characteristics compared to other polymers which are PET-G, ABS and composite materials based on their research (Vinyas et al., 2019). Figure 3.20 illustrates the thermogravimetric and differential thermogravimetric analysis (DTG) curves. As the material was heated, the sample was measured using a thermal balance in a furnace, following which a broken line could be seen as the material started to decompose. As

seen in Figure 3.20, the sample starts to degrade at a temperature of 345.2°C, undergoes a weight loss of 11.64mg, and records a residual weight of 4.11mg. Due to its distinctive property, PLA is readily biodegradable in heating environments. Hence, the characteristics of material properties could significantly affect the temperature and rate at which polymers degrade (Vinyas et al., 2019). Additionally, thermal experiments using TGA confirm that polymer composites show better thermal properties than pure polymers (Blanco, 2022).



اونيورسيتي مليسيا قهغ السلطان عبدالله
**UNIVERSITI MALAYSIA PAHANG
AL-SULTAN ABDULLAH**

CHAPTER 4

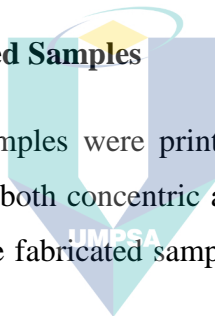
RESULTS AND DISCUSSION

4.1 Introduction

This chapter discusses the results that was obtained from the physical, mechanical, thermal, and morphology testing. In the previous chapter, samples fabricated using the FDM process were shown. Therefore, the discussion initiated depicts these fabricated samples, with a detailed look into the resulting effects of single-plane and multiplane on the mechanical and physical properties throughout the current chapter.

4.2 Conditions of Fabricated Samples

Tensile and bending samples were printed under six different conditions for single-plane and multiplane for both concentric and line patterns. These conditions are presented in Table 4.1 while the fabricated samples for tensile and bending testing are shown in Figure 4.1



اونيورسيتي مليسيا قهغ السلطان عبدالله
UNIVERSITI MALAYSIA PAHANG
AL-SULTAN ABDULLAH

Table 4.1 Parameters of tensile and bending fabricated sample

Infill Pattern	Type of Plane	Condition
Concentric	Single-plane	0°
		45°
		90°
		0°,0°
		45°,0°
Line	Multiplane	90°,0°
		0°
		45°
		90°
		0°,0°
	Single-plane	45°,0°
		90°,0°
		0°,0°



Figure 4.1 Fabricated (a) tensile and (b) bending samples for single-plane and multiplane

4.3 Dimensional Accuracy

Dimensional accuracy denotes the state in which the measured dimensions of a product are relatively near to the nominal value, whereby the nominal value corresponds to the dimensions of the CAD model. Manufacturing complex forms and geometries is one of the main advantages of 3D printing. Here, dimensional accuracy is crucial in determining whether a machine can reliably generate each object according to the desired outcomes (Chand et al., 2022; Hanon, Zsidai, et al., 2021). Bending samples (ASTM D790-17) were chosen for use to investigate the dimensional accuracy for layering (i.e. single-plane and multiplane) and pattern (i.e. concentric and line) both. To examine the dimensional accuracy of FDM-printed samples, the dimensions of the rectangular test samples were measured using a digital vernier calliper of ± 0.01 mm accuracy. The results of single-plane and multiplane are tabulated in Tables 4.2 and 4.3.

Table 4.2 Dimensional accuracy results of single-plane vs multiplane of bending sample for concentric pattern

Type of Plane	Orientation (°)	Error percentage (%)		
		Length	Width	Thickness
Single-plane	0	0.2	0.02	0.01
	45	0.4	0.01	0.01
	90	0.05	0.01	0.01
Multiplane	0,0	0.3	0.2	0.3
	45,0	0.02	0.08	0.3
	90,0	0.3	0.08	0.3

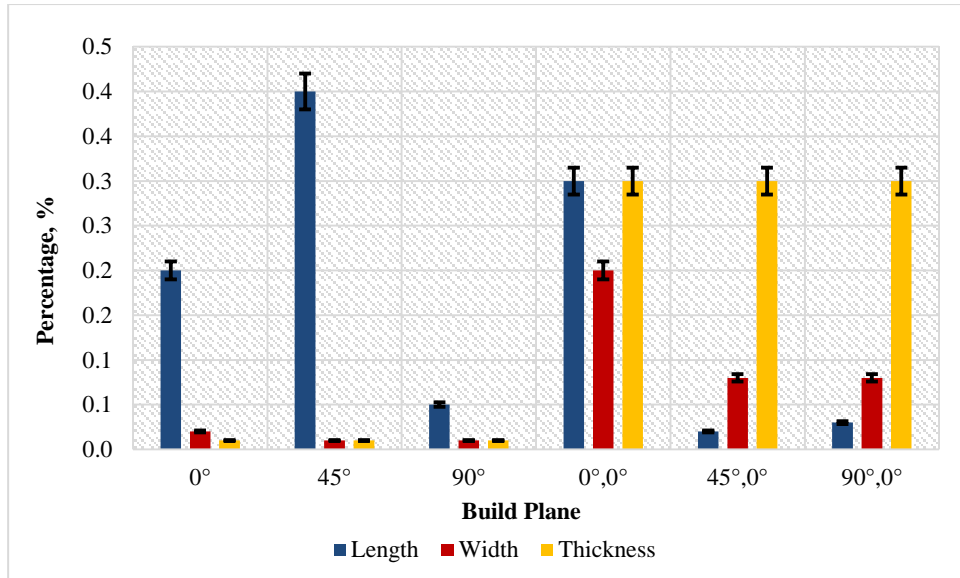


Figure 4.2 Dimensional accuracy of single-plane vs multiplane of bending samples for concentric pattern

Table 4.3 Dimensional accuracy results of single-plane vs multiplane of bending sample for line pattern

Type of Plane	Orientation (°)	Error percentage (%)		
		Length	Width	Thickness
Single-plane	0	0.4	0.08	0.01
	45	0.14	0.08	0.3
	90	0.01	0.2	0.6
Multiplane	0,0	0.4	0.08	0.3
	45,0	0.05	0.01	0.6
	90,0	0.14	0.08	0.3

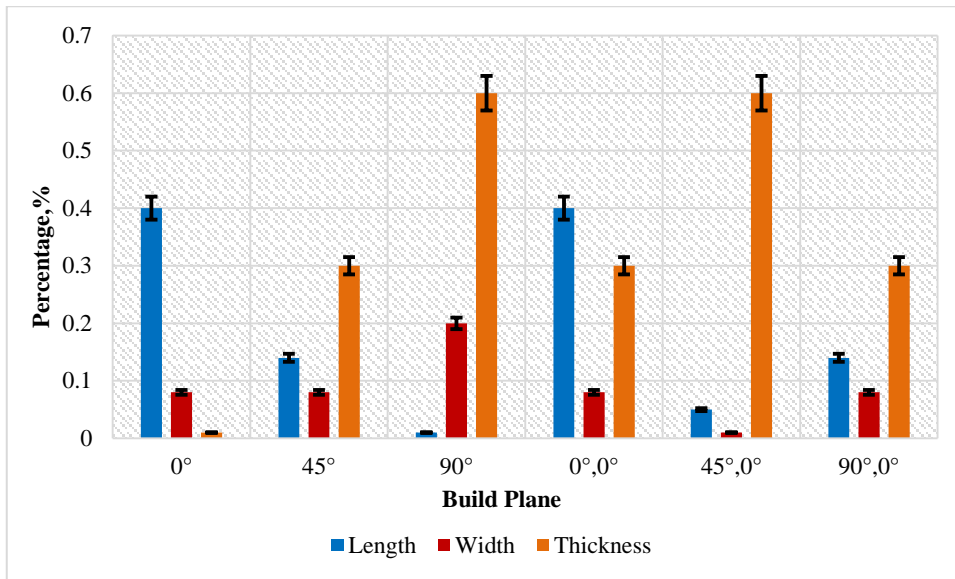


Figure 4.3 Dimensional accuracy of single-plane vs multiplane of bending samples for line pattern

Figures 4.2 and 4.3 depict the dimensional accuracy of single-plane and multiplane bending samples for the concentric and line patterns accordingly. Parts printed by using the FDM technique frequently experience variations in dimensional accuracy as they exhibit shrinkage and distortion in which these unfavourable effects on product quality are brought on by a wide range of circumstances (Choi et al., 2002). Here, a lower percentage of dimensional difference represents a higher dimensional accuracy of the FDM-printed parts (Darsin et al., 2021). From the above graph, it could be stated that single-plane and multiplane layering yield a lower percentage, $\pm 0.5\%$ as seen for both concentric and line patterns. Therefore, the findings demonstrated that the building orientation did pose an impact on the dimensional accuracy. Prior studies have shown that in order to achieve the desired dimensional accuracy, choosing the appropriate processing parameters such as layer height and build orientation are crucial as they influence the resulting accuracy of a part (Kechagias et al., 2022; Mohamed, 2017).

Furthermore, researchers have investigated the dimensional accuracy of FDM-printed parts and came to the conclusion that their accuracy was highly impacted by the build orientation, layer height and air gap (Chung Wang et al., 2007; Nancharaiah et al.,

2010). During the material deposition, the fusion between layers poses an impact on the dimensional accuracy, with discoveries showing that the FDM technique is the least accurate (Chand et al., 2022). Through the right modifications to the process parameters, attempts have been made to increase the dimensional accuracy of such parts (Choi et al., 2002). To conclude the overall research findings on dimensional accuracy, selecting the appropriate processing parameter would ensure that accuracy of FDM-printed samples is achieved, whereby the accuracy is near to its nominal value and both patterns yield very minor differences.

4.4 Density

One critical element in defining the properties of polymer materials is density. Here, the density of PLA is 1.24g/cm^3 . An average of three sample readings was taken to calculate the relative density and investigate the effect of density on printed single-plane and multiplane samples.

4.4.1 Density of Single-Plane and Multiplane for Concentric Pattern

The average density outcomes for concentric-patterned single-plane and multiplane samples are interpreted and shown in Tables 4.4 and Figure 4.4, respectively.

Table 4.4 Density results of single-plane and multiplane for concentric pattern

Type of Plane	Orientation (°)	Average (%)
Single-plane	0	96.6
	45	96.3
	90	97.5
Multiplane	0,0	97.6
	45,0	98.1
	90,0	97.6

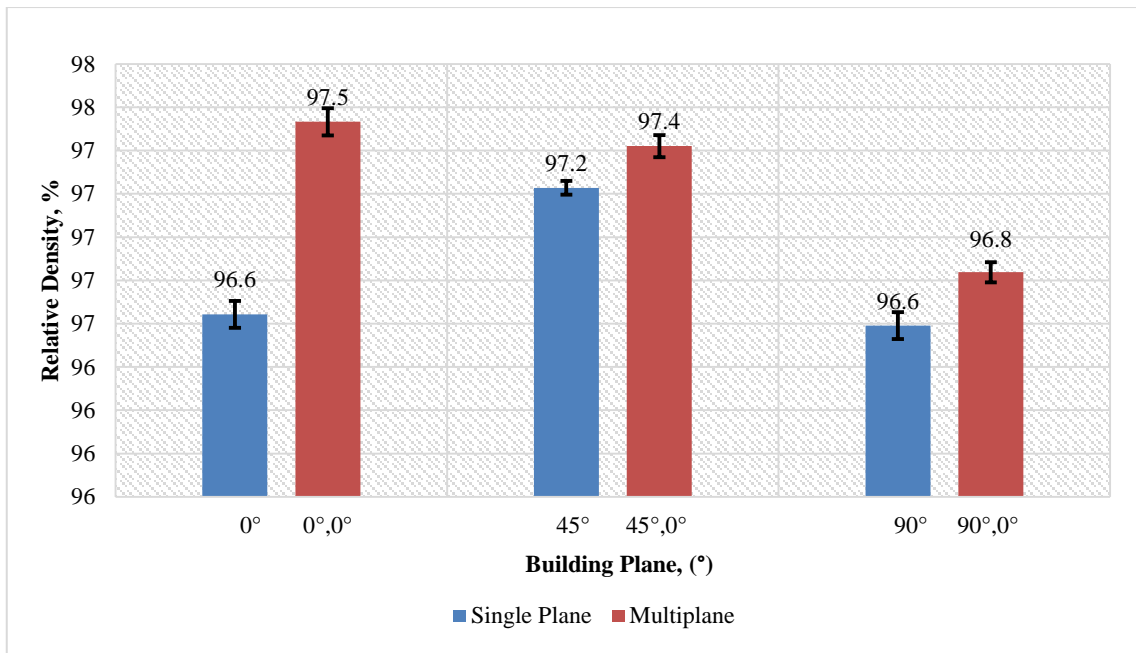


Figure 4.4 Relative density of single-plane vs multiplane for concentric pattern

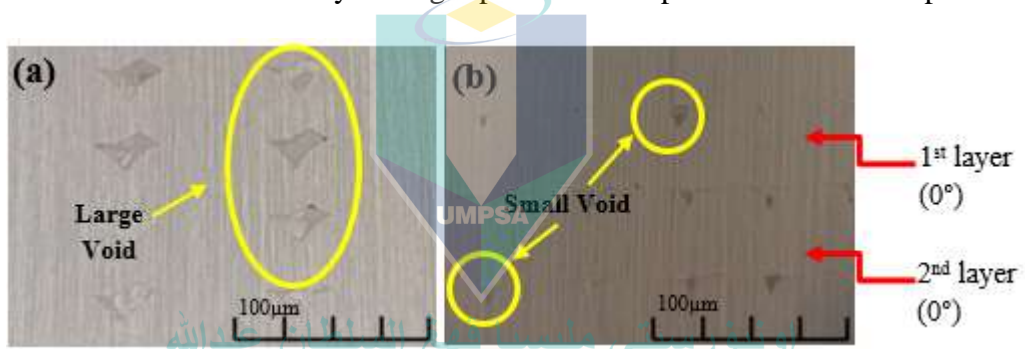


Figure 4.5 Optical micrographs of (a) single-plane 0°, (b) multiplane 0°, 0°

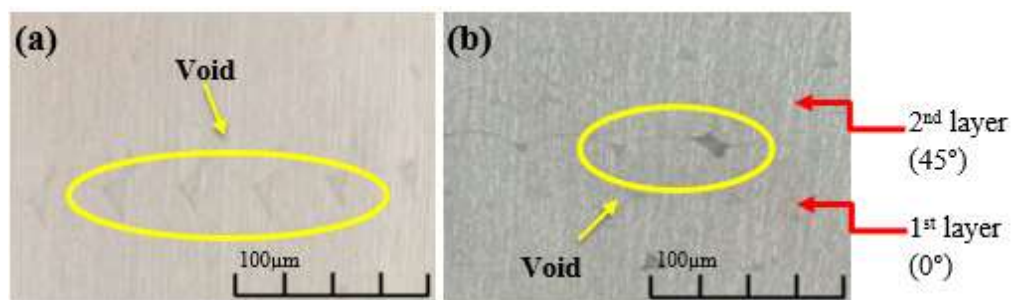


Figure 4.6 Optical micrographs of (a) single-plane 45°, (b) multiplane 45°, 0°

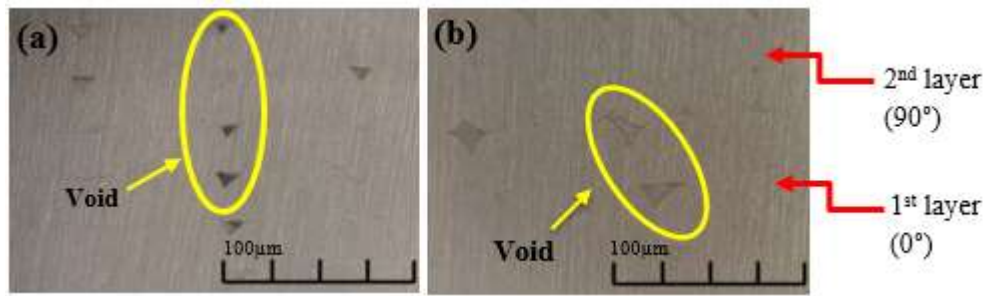


Figure 4.7 Optical micrographs of (a) single-plane 90°, (b) multiplane 90°, 0°

In Figure 4.4, the average values of relative density achieved by concentric-patterned single-plane and multiplane layering: at the 0° single-plane printing orientation, the value is 96.6% while in the multiplane 0°, 0° orientation, 97.5% is attained. From Figure 4.5(a), void formation is more significant and larger than the multiplane shown in Figure 4.5(b), which can be explained to micro-voids present in multiplane (0°, 0°), rendering the density higher. Next, the 45° single plane exhibited 97.2% while the multiplane (45°, 0°) obtained 97.4%. Figure 4.6 shows the voids that was occurred during printing for 45° single-plane and multiplane (45°, 0°). For the printing orientation at 90° and (90°, 0°), the relative density was 96.6% and 96.8% for single-plane and multiplane, respectively. Figure 4.7 displays the higher number of voids seen in the 90° single-plane and multiplane. Even though multiplane has voids, it still exhibits a higher density than a single-plane due to the strong interlayer bond present between planes. Among all building orientations tested, (0°,0°) exhibited the highest relative density at 97.5% while the lowest was observed at 90° single-plane. From the microstructure analysis, the multiplane type evidently depicted less void for each build orientation compared to the single-plane type. The occurrence of voids and poor bonding between each layer indicate that FDM-printed parts suffer from weak and anisotropic mechanical properties (Tao, 2021).

4.4.2 Density of Single-Plane and Multiplane for Line Pattern

The average density outcomes for line-patterned single-plane and multiplane samples are interpreted and shown in Tables 4.5 and Figure 4.8, respectively.

Table 4.5 Density results of single-plane and multiplane for line pattern

Type of Plane	Orientation (°)	Average (%)
Single-plane	0	96.6
	45	97.2
	90	96.6
Multiplane	0,0	97.5
	45,0	97.4
	90,0	96.8

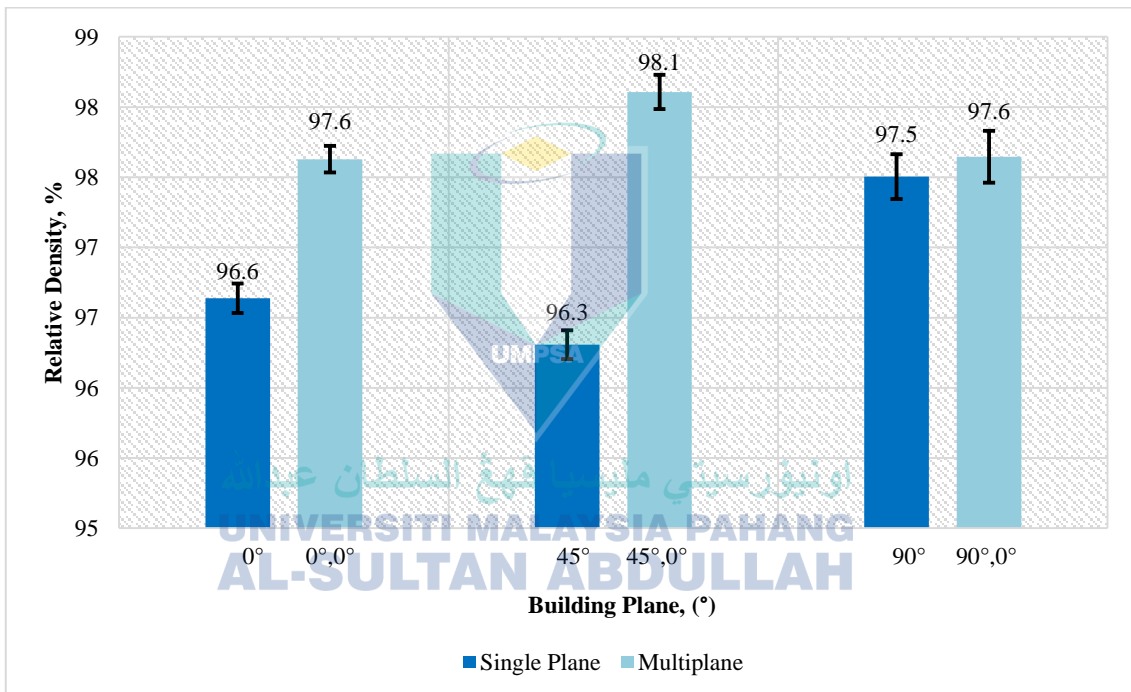


Figure 4.8 Relative density of single-plane vs multiplane for line pattern

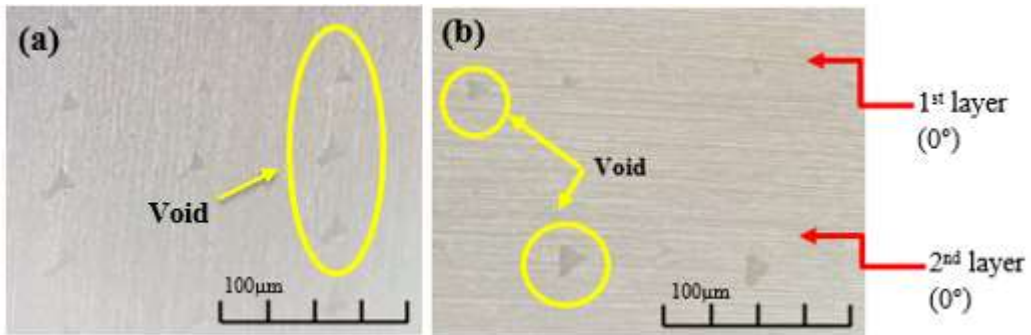


Figure 4.9 Optical micrographs of (a) single-plane 0° , (b) multiplane $0^\circ, 0^\circ$

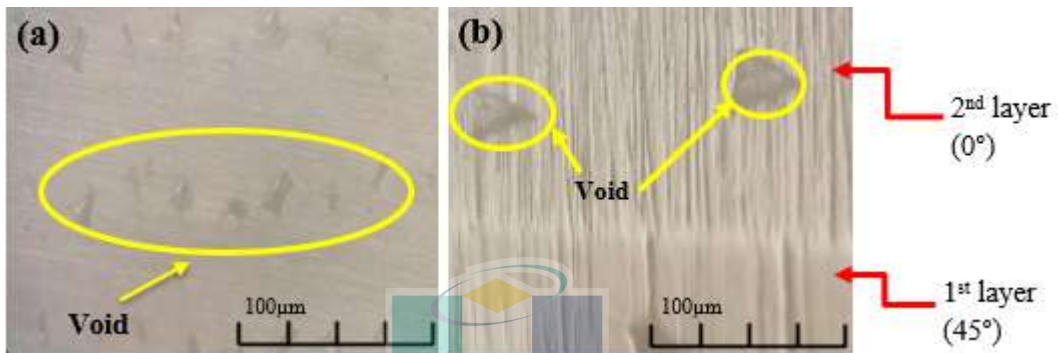


Figure 4.10 Optical micrographs of (a) single-plane 45° , (b) multiplane $45^\circ, 0^\circ$

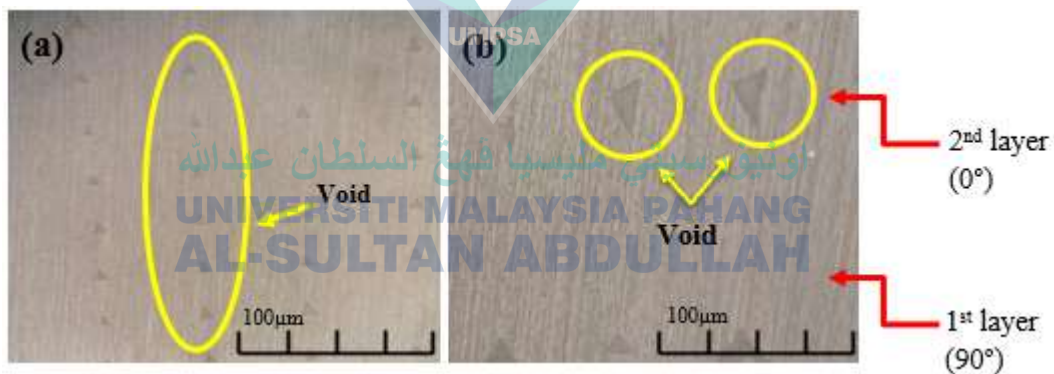


Figure 4.11 Optical micrographs of (a) single-plane 90° , (b) multiplane $90^\circ, 0^\circ$

Figure 4.8, in particular, displays the average outcomes of the relative density achieved by line-patterned single-plane and multiplane sample: at 0° single-plane, the printing orientation is 96.6%, while it is 97.6% at multiplane ($0^\circ, 0^\circ$). From Figure 4.9(a), void formation is more evident compared to the multiplane shown in Figure 4.9(b). At 45° single-plane, the values obtained was 96.3%, while multiplane ($45^\circ, 0^\circ$) generated 98.1%. As seen in Figure 4.10(b), the voids are lesser compared to the single plane. For the printing orientation at 90° and ($90^\circ, 0^\circ$), the relative density is 97.5% and 97.6 % for

single-plane and multiplane, respectively. Figure 4.11 further shows that single-plane 90° has more voids compared to multiplane. Among all building orientations, (45°, 0°) exhibited the highest relative density at 98.1% while the lowest was seen at single-plane 45° which is 96.3%. Evidently, the microstructure analysis revealed a smaller number of voids in a multiplane compared to a single-plane for each build orientation. As the void is a small hole formed between the layers in FDM-printed parts, rendering it prone for weakening the mechanical properties. A previous experiment has revealed that the final parts printed by using FDM had more voids due to the lack of pressure applied during printing (Dawoud et al., 2016). Additionally, the interlayer deformation contributing to micro-voids in the structure could be reduced by minimising the layer thickness, which would enhance the bond between layers.

4.5 Tensile Strength Test

In this study, the tensile test was conducted on each printed sample for respective planes (single-plane and multiplane) and patterns (concentric and line). Five samples were thus evaluated for each layering configuration according to the respective orientation. The samples were printed in accordance with the ASTM D638-14 type IV standard, which is used for testing thermoplastic materials. The resulting outcomes for each category and infill pattern (concentric and line) are summarised in Tables 4.6 and 4.7 accordingly.

Table 4.6 Summary of tensile data for concentric pattern

Type of Plane	Orientation (°)	Ultimate tensile strength (MPa)	Young's modulus (GPa)
Single-plane	0	51.9	1.77
	45	41.8	1.58
	90	35.2	1.57
Multiplane	0,0	52.5	1.78
	45,0	42.3	1.75
	90,0	42.6	1.71

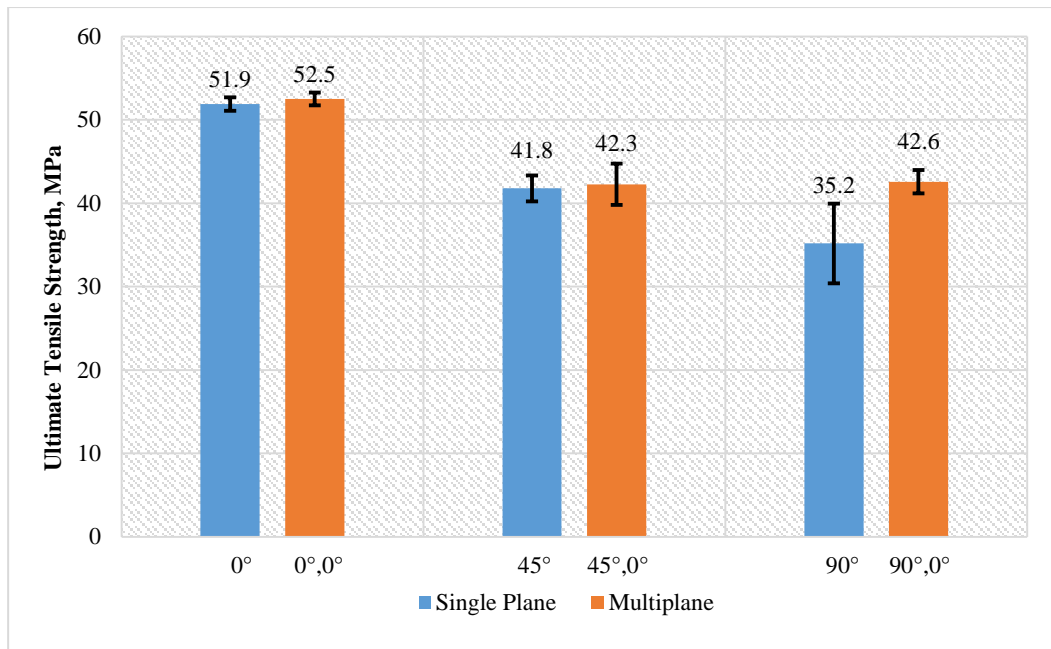


Figure 4.12 Ultimate tensile strength of single-plane vs multiplane for concentric pattern

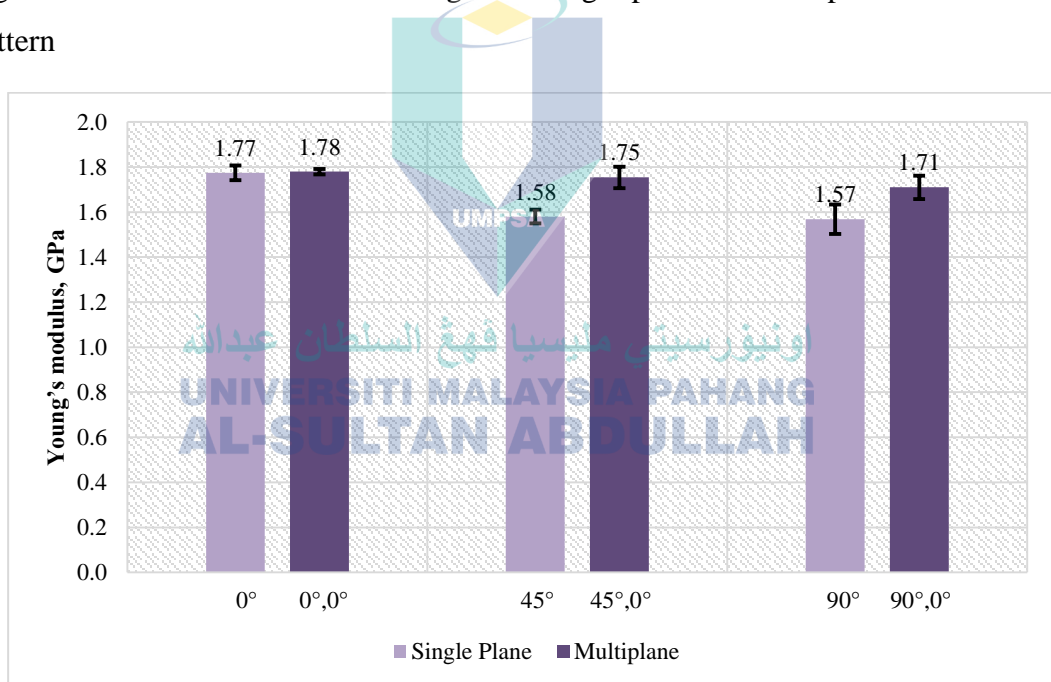


Figure 4.13 Young's modulus of single-plane vs multiplane for concentric pattern

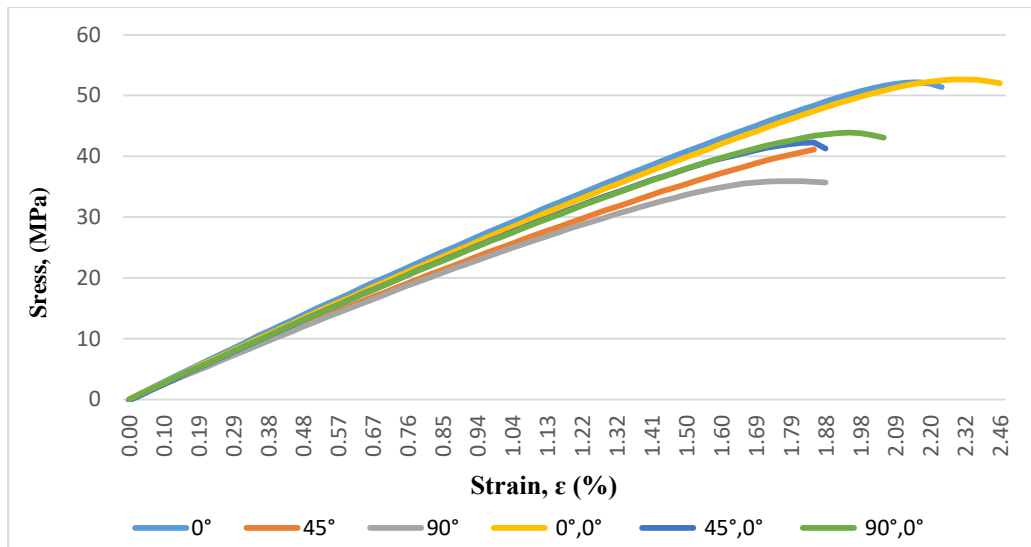


Figure 4.14 Stress-strain curves of concentric pattern for single-plane and multiplane tensile samples

In general, the ultimate tensile strength (UTS) is the maximum stress that can be sustained by a material without undergoing plastic deformation when elongated or pulled. Young's modulus, however, or also referred to as stiffness, is the proportion of force that substance has to the resulting deformation (Hsueh et al., 2021). To give a comprehensive overview of the material behaviour, the average values of each sample set comprising the UTS and Young's modulus are calculated and reported in Figures 4.12 and 4.13 accordingly. A summary of the tensile data results is further tabulated in Table 4.6. A comparison of UTS and Young's modulus outcomes (see Figures 4.12 and 4.13) revealed that the multiplane exhibited the highest results compared to the single-plane. Among all categories of building orientation, multiplane (0°, 0°) obtained the highest UTS and Young's modulus values compared to the single-plane, thus demonstrating the factor's impact on the tensile strength.

The effect of building orientation has been further underpinned as a significant parameter affecting mechanical properties by a researcher, whereby the study observed higher tensile strength for the FDM part with filaments deposited in the load direction one oriented in the transverse direction (Zhou et al., 2017). During the printing of samples in (0°, 0°), beads were deposited throughout the length of the sample in a parallel direction. Thus, the pulling force during tensile testing was parallel with the printing direction and resulted in high tensile strength. This explains the flexibility of samples in

such building orientation without sustaining any noticeable deformation (T. Yao et al., 2020). On the contrary, the UTS and Young's modulus values were lower when printed in the upright direction (90°). This demonstrated the weaker bonding present between the layers than it was within the layers themselves. Such occurrence could be attributed to the intra and inter-layer strength, whereby the intra-layer is superior than the inter-layer as seen in the pattern causing stresses in the inter-layer direction (Spoerk et al., 2017). When tensile loading is applied at 90°, the stress is concentrated in the small intra-layer bond area, thereby resulting in the layers delaminating or separating from the bonded area and displaying failure (Rajpurohit & Dave, 2018). Moreover, the sample became brittle as the pulling force was perpendicular towards the printing direction, which was printed at a 90° angle, and the infill pattern. The brittle and ductile behaviours of the sample is seen in Figure 4.14 as reflected by the difference in elongation to failure.

Table 4.7 Summary of tensile data for line pattern

Type of Plane	Orientation (°)	Ultimate tensile strength (MPa)	Young's modulus (GPa)
Single-plane	0	50.2	1.76
	45	37.6	1.51
	90	30.2	1.60
Multiplane	0,0	51.0	1.79
	45,0	40.9	1.61
	90,0	44.8	1.77

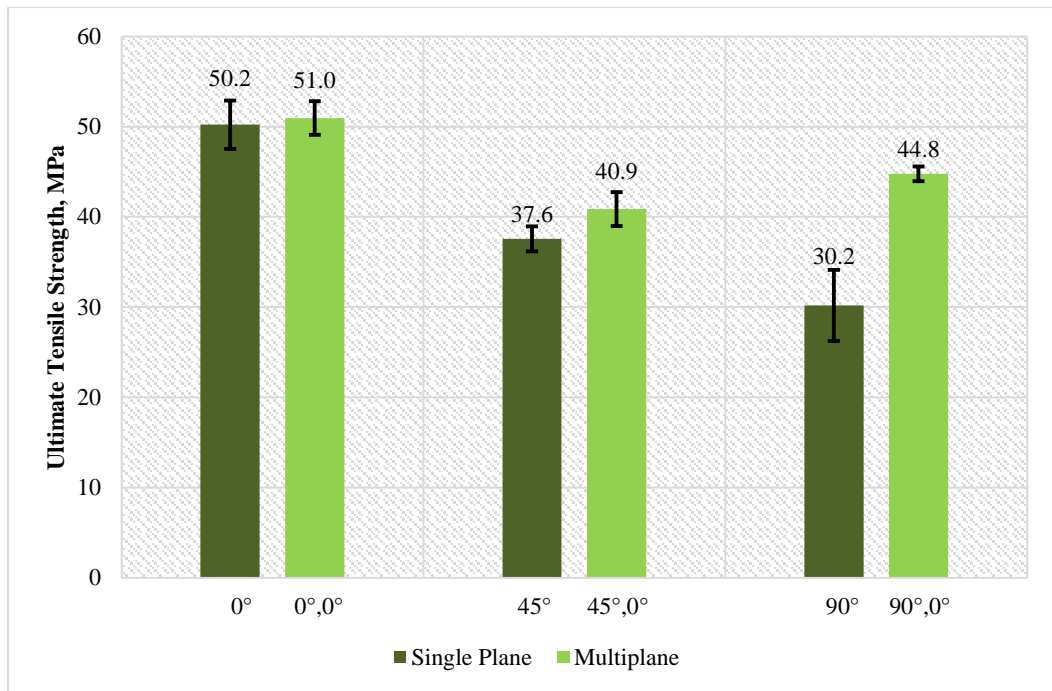


Figure 4.15 Ultimate tensile strength of single-plane vs multiplane for line pattern

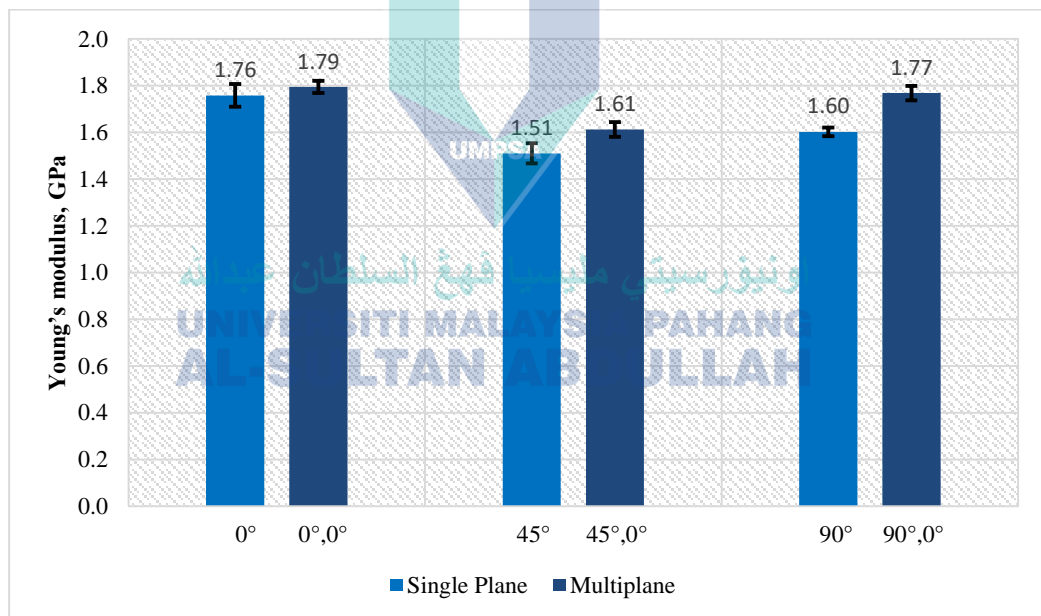


Figure 4.16 Young's modulus of single-plane vs multiplane for line pattern

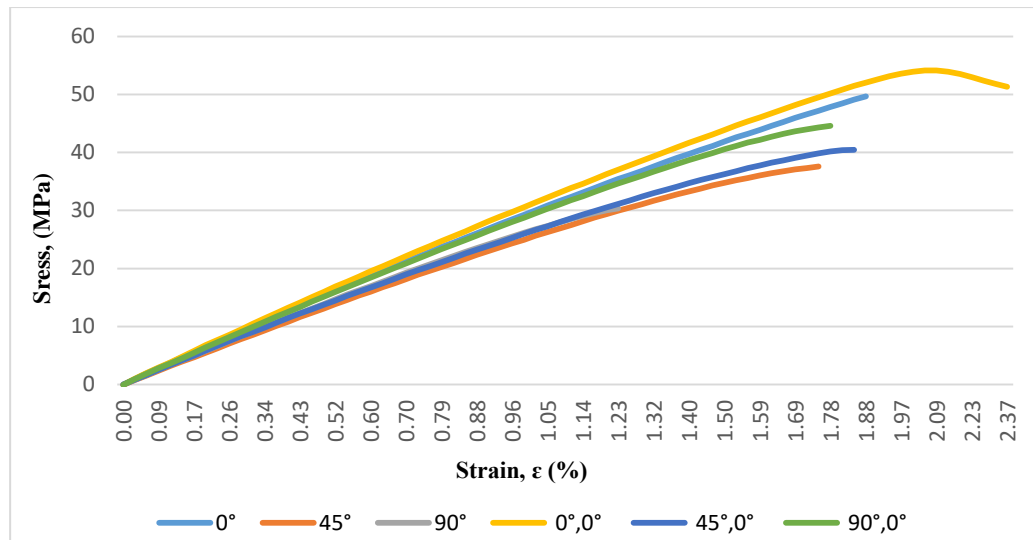


Figure 4.17 Stress-strain curves of line pattern for single-plane and multiplane tensile samples

A summary of the tensile data for the line pattern is further tabulated in Table 4.7. The beads were deposited in parallel lines for each layer in a line pattern. Figures 4.15, 4.16, and 4.17 show that the multiplane yields a higher value of UTS and Young's modulus. In particular, multiplane (0°, 0°) generated the highest UTS (51.9 MPa) and Young's modulus (1.77 GPa), whereas the lowest could be seen at single plane 90° (35.2 MPa). In Figure 4.17, the ductility and brittle behaviour of the sample are evaluated by the difference in elongation. The building orientation significantly affected the sample strength. Meanwhile, Torres *et al.* (2016) have investigated the influence of processing parameters such as printing speed, extrusion temperature, layer height, and infill density on the tensile properties of PLA samples across various building orientations (Torres *et al.*, 2016). Their outcomes have underlined build orientation as one of the most critical factors influencing tensile strength, as well as impacting other tensile properties. Moreover, parts oriented with 0° as in multiplane all the orientations are combined with 0° building orientation either printed vertically or horizontally in the x-y plane has the maximum tensile strength. This is due to the extruded filament parallel to the applied force for such building orientation in which the decrease in tensile strength for single-plane layering could be justified as the weak bonding between layers as these layers are vertical to the load direction and have high void contents. Therefore, fracture occurs predominantly between the layers. High tensile strength in multiplane could be best

explained by the arrangement between layers resulting in good bonding between layers. Another work has also confirmed that the strength is improved by maximising the alignment of the layers towards the load direction (Rodríguez-Panes et al., 2018).

As a result, the tensile outcomes of both patterns for the PLA material were significantly influenced by the building orientation, which was highlighted as a crucial factor in the FDM process. Due to the partially bonded cylindrical build material filaments used in FDM parts, the degree of interlayer and intra-layer bonding is a crucial factor in determining the mechanical qualities, as well as the bonding quality. According to published research, interlayer and intra-layer bonds all affect the component strength (Syrlybayev et al., 2021). The reduction in strength typically seen at a higher value of building orientation is attributable to the failure mode switching from ductile to brittle failure, which is characterised by interface separation. Here, the overall percentage difference between single-plane and multiplane layering for the concentric and line patterns were 10.7% and 24.5%, respectively. Therefore, combinations of different plane orientations led to increased UTS and Young's modulus values compared to single-plane printing. Implementation of multiplane layering thus enhanced the mechanical properties of PLA as the bonds between layers were bonded strongly and reduced voids and air gaps.

4.6 Bending Test

The bending test measures the ability of a material to withstand a bending deflection when force is applied to the sample, which can be determined by using a three-point loading test (Chowdhury & Hossain, 2020). This study utilised the three-point loading test to investigate the bending properties for FDM-printed samples with a total of five samples subjected for each layering at each of the orientations and patterns. The bending test results are presented in Figures 4.18 and 4.19.

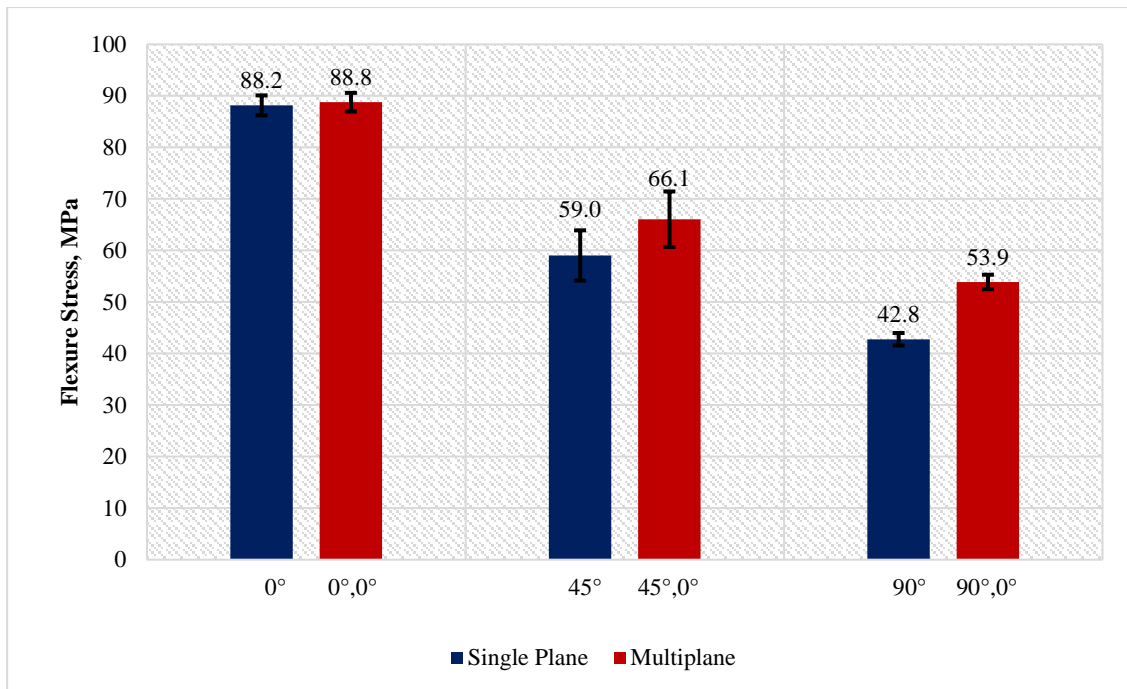


Figure 4.18 Flexure stress of single-plane vs multiplane for concentric pattern

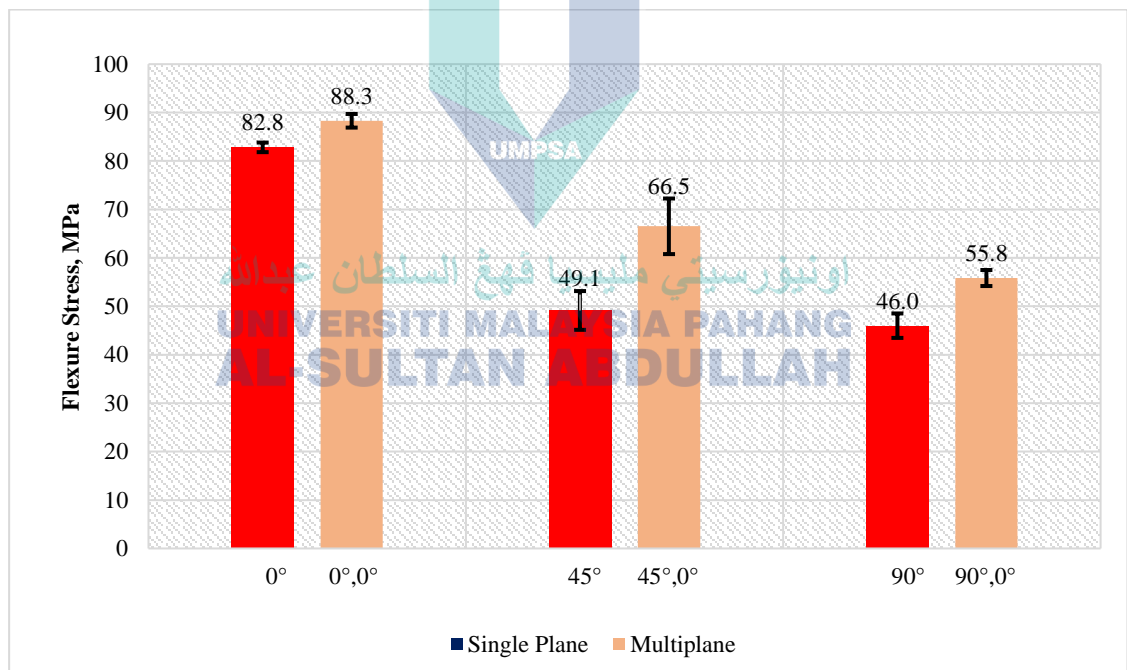


Figure 4.19 Flexure stress of single plane vs multiplane for line pattern

A researcher stated that, in comparison with the tensile and compressive strength testing, the bending strength of the FDM-printed part has received the least amount of research (Sheoran & Kumar, 2020). During bending testing, the samples are exposed to both tensile and compressive stress (Ziemian et al., 2012). Figure 4.18 shows the flexure

stress outcomes for single-plane and multiplane for concentric-patterned samples while Figure 4.19 displays the results for line-patterned single-plane and multiplane samples. From both graphs, one could observe the higher bending strength shown by the multiplane sample than the tensile strength for both layering and patterns. The $(0^\circ, 0^\circ)$ multiplane layering reached the maximum bending strength for both patterns, which were 88.8 MPa (concentric) and 88.3 MPa (line).

Conversely, a 90° single-plane layering attained the minimum bending strength for both patterns, specifically 42.8 MPa (concentric) and 46.0 MPa (line). Similar to the tensile testing outcomes, the building orientation affected the bending strength of the printed samples. According to a researcher, build orientation denote variables posing the most significant impact on the flexural, impact, tensile strength, and anisotropic structure (Ahn et al., 2002). When compared to a flat build orientation, the fracture mode differed from its vertical counterpart. As force was exerted on the sample printed in the vertical position, the bond between each line was weak and interlayer fracture occurred. This was caused by the loading direction that was parallel to the direction of the extruded lines, thus directly affecting the mechanical properties of FDM-printed samples.

Furthermore, as the layers were delaminated, they might lose the ability to bear loads, resulting in low bending strength. Delamination of layers, in particular, could be attributed to deformations brought on by uneven heating and cooling cycles or interlayer porosity (Sood et al., 2012). Conversely, there were two layers with different build orientations printed for the multiplane layering. Samples printed in all three build orientations, namely $(0^\circ, 0^\circ)$, $(45^\circ, 0^\circ)$ and $(90^\circ, 0^\circ)$ obtained higher bending strength compared to those of the single-plane for both patterns. A comparison of all three types of build orientation further showed that the $(0^\circ, 0^\circ)$ multiplane achieved maximum bending strength. Previously, Sheoran *et al.* (2020) have reported that the bending strength is maximum when it is printed in the 0° orientation as the filament is oriented perpendicular to the direction of the applied load (Sheoran & Kumar, 2020). Hence, incorporating two different planes enhance the mechanical properties of the printed samples as the interlayer bonding between layers is strong.

It's crucial to understand the mechanical characteristics of 3D printed materials when it comes to the engineering use of FDM products. Therefore, the selection of various processing parameters, each of which has a value that differs from the experimental processing parameter values, is the cause of the value disparity between the experimental value and the manufacturer data sheet. The omission of testing rates is another possible explanation. This is a crucial piece of information, especially when testing rates are required for bending and tensile testing.

4.7 Scanning Electron Microscope (SEM)

SEM was utilised in this study to investigate the material behaviour towards the mechanical properties of printed PLA samples. To better understand the tensile test findings, assessing the fracture surface for all printed samples was performed using the method in which the highest and lowest values of the tested tensile samples were taken both patterns (concentric and line). Both patterns generated the highest UTS in multiplane (0° , 0°) while the lowest value was observed in single-plane 90° . Identification of the void contents and air gaps for the printed samples are studied through SEM and shown in Figures 4.20, 4.21, 4.22, and 4.23.

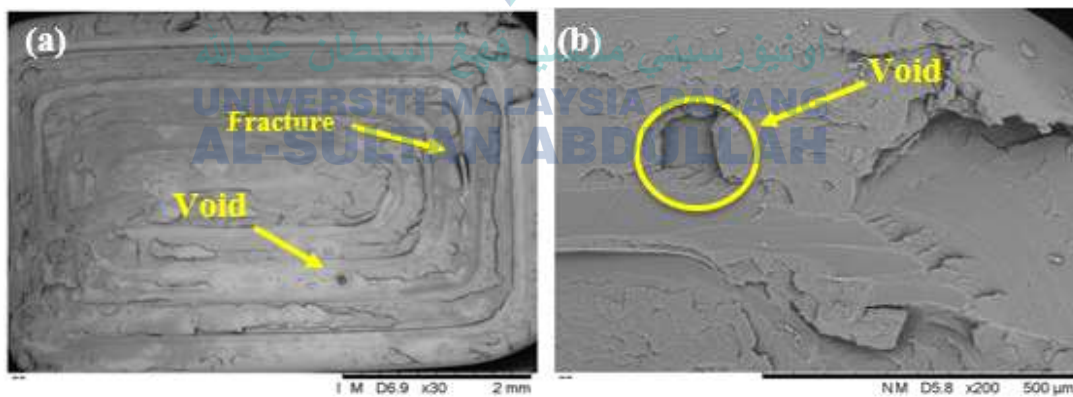


Figure 4.20 Single-plane fractured cross-section SEM images of tensile test samples (a) outer structure of 90° concentric pattern, (b) void in concentric pattern

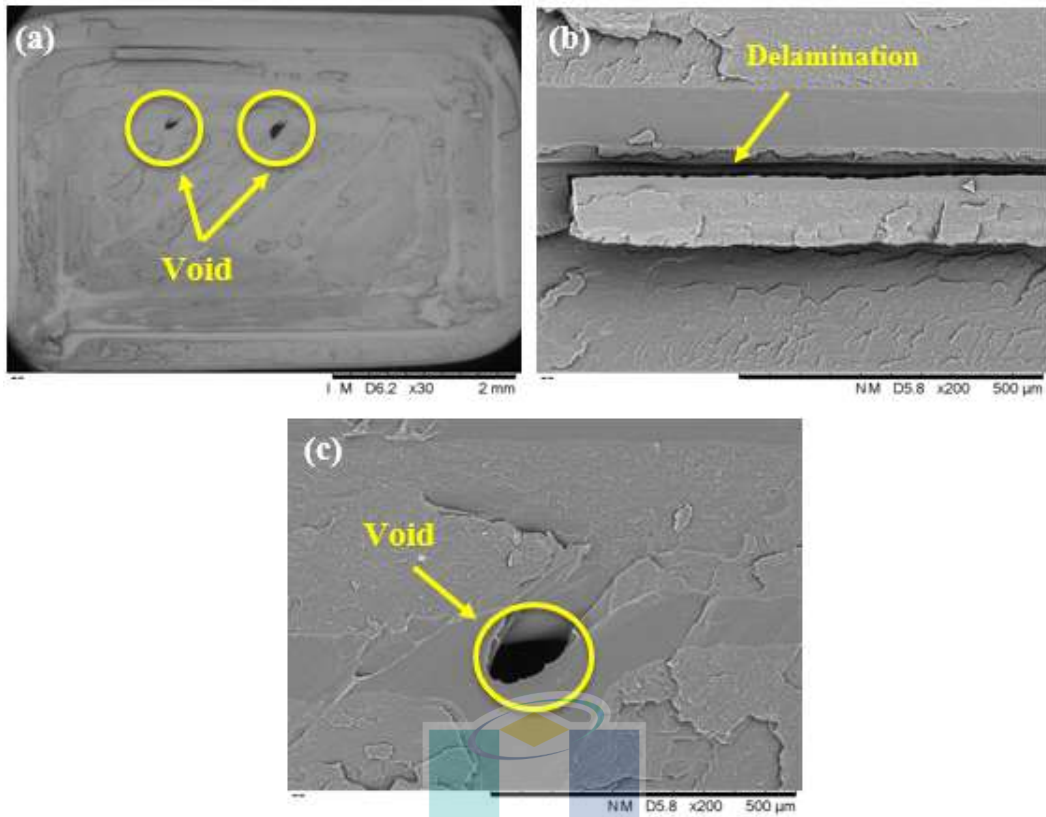


Figure 4.21 Single-plane fractured cross-section SEM images of tensile test samples
 (a) outer structure of 90° lines pattern, (b) delamination between layers, (c) void

اونيورسيتي مليسيا قهغ السلطان عبدالله
 UNIVERSITI MALAYSIA PAHANG
 AL-SULTAN ABDULLAH

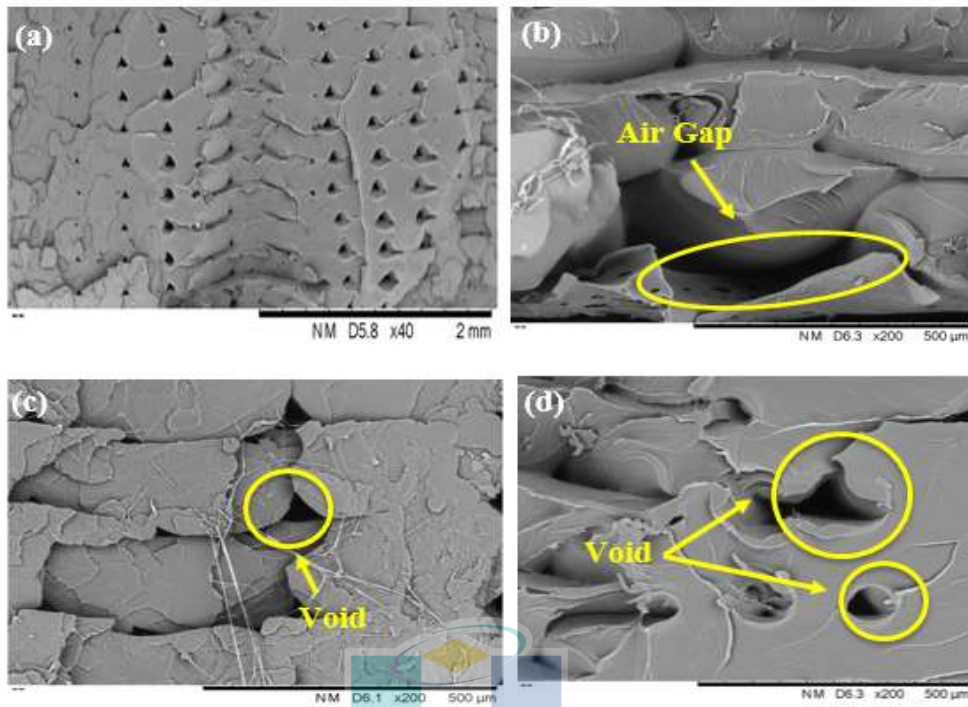


Figure 4.22 Multiplane fractured cross-section SEM images of tensile test samples (a) outer structure of 0°, 0° concentric pattern, (b) air gap between layers, (c) void, (d) magnified view of void

اونيورسيتي مليسيا قهغ السلطان عبدالله
 UNIVERSITI MALAYSIA PAHANG
 AL-SULTAN ABDULLAH

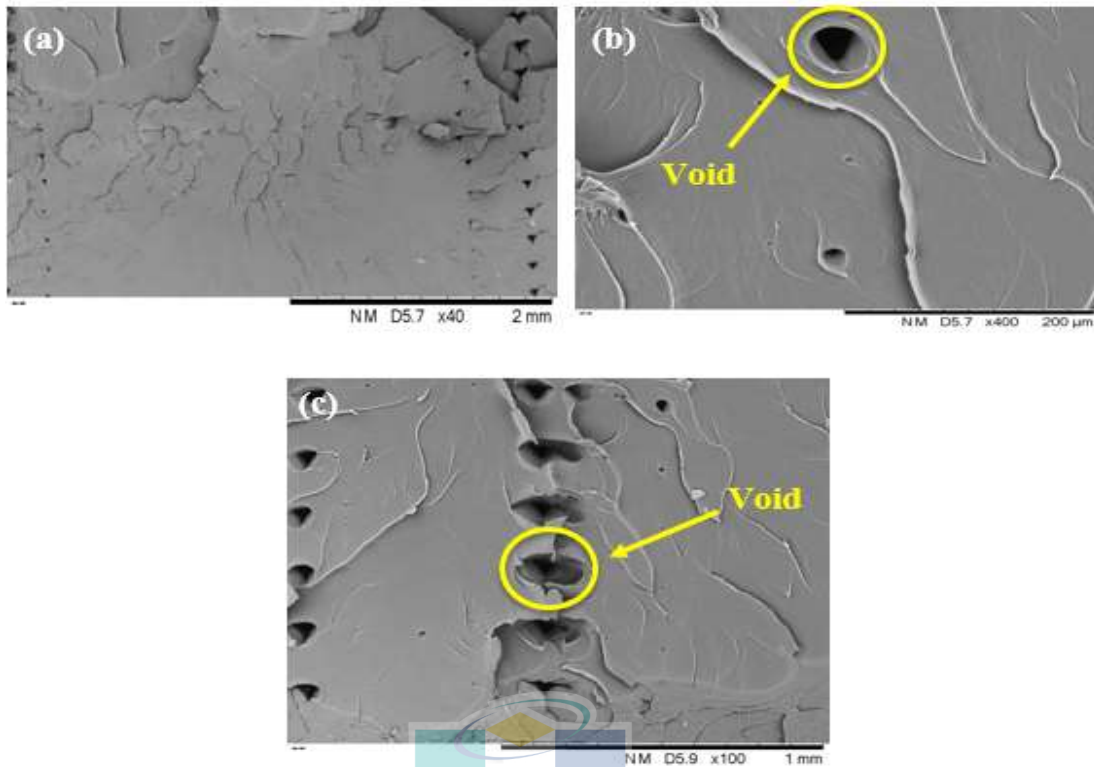


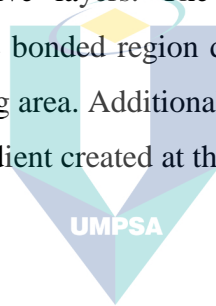
Figure 4.23 Multiplane fractured cross-section SEM images of tensile test samples (a) outer structure of 0° , 0° lines pattern, (b) void, (c) magnified view of the void

Based on Figures 4.20 and 4.21, the SEM images of the single-plane (90°) of both concentric and line patterns are presented while Figures 4.22 and 4.23 show the images of multiplane (0° , 0°) of concentric and lines patterns respectively. Here, the single-plane (90°) concentric and line sample pattern demonstrated the lowest UTS at 35.2 MPa and 30.2 MPa while the multiplane (0° , 0°) concentric and line pattern attained higher values at 52.5 MPa and 51.0MPa.

Voids and air gaps were evidently present in both planes and these defects directly influenced the mechanical strength, thus resulting in weaker samples. Furthermore, a series of triangular voids could be seen between the layers of the multiplane sample in both concentric and line patterns. The differences between an air gap and a void is that an air gap is the separation between two adjacent bead depositions, whereas voids are formed between layers during printing. In FDM, void contents depend on a wide range of variables, including the size and form of the liquefier nozzle, melt flow properties like pressure and velocity gradients, bead orientations, and thermodynamic variables like bed temperature and cooling rate associated with melting solidifications (Papon & Haque,

2018). Moreover, the occurrence of a void between layers is due to the rapid cooling of molten fibres or the absence of overlap between the extruded material and solidified material (Syrlybayev et al., 2021). Although voids were present in both planes, their sizes were small in the case of multiplane, resulting in more robust and efficient bonds between layers. As evidenced by the outcomes of the mechanical testing, this resulted in greater strength. Even though air gaps and inter-voids could be seen clearly in the multiplane, the strength was higher as the pulling force was parallel to the infill pattern. Similarly, inter-voids are usually seen between each bead, which is due to the bead structure that expands outwards (Papon & Haque, 2018).

In contrast, the single-plane sample printed at 90° was characterised with a pulling force perpendicular towards the infill pattern and printing direction during testing, yielding a brittle sample. From Figure 4.21(b), the layers are observed to be separated via delamination between successive layers. The sample failed under the aspect of delamination of layers from the bonded region during tensile testing as the stress was centred on the interlayer bonding area. Additionally, as the polymer was initially melted and cooled, the temperature gradient created at the contact was vital for forming bonds.



اونيورسيتي مليسيا قهغ السلطان عبدالله
UNIVERSITI MALAYSIA PAHANG
AL-SULTAN ABDULLAH

CHAPTER 5

CONCLUSION

5.1 Introduction

This chapter presents the conclusion of the overall research. The first part includes the concluding remarks, which summarises the research findings with regard to the stated objectives. The second section contains recommendations for future works.

5.2 Conclusion

This research aimed to assess the anisotropic properties of PLA-FDM printed samples by implementing multiplane, whereby investigating the physical and mechanical behaviours of PLA-3D printed samples and increasing the knowledge of AM were thus attained. Experimental evaluations were done accordingly regarding the physical and mechanical behaviours of 3D printed samples for both single-plane and multiplane by varying the building orientations and infill pattern. The objectives of this research were henceforth achieved.

In 3D printing, the infill pattern poses an important influence on the structure and strength of the printed sample. Two patterns, namely concentric and line patterns, were then selected and designed by using CAD with the same infill density. These pattern structures adhered to the same arrangement under different conditions as FDM machine-printed patterns. The first research objective denoted assessing the effect of the infill pattern towards the mechanical and physical properties of PLA-printed samples. Based on the results obtained, each infill pattern yielded different effects on the mechanical and physical properties, which was attributable to its role in controlling the motion of the nozzle along the XY axis when filling the region of the layer. By comparing the infill pattern, concentric and line patterns independently almost offered identical values for all examined conditions, except for the type of planes, whereby multiplane layering resulted in higher values for both patterns. In contrast, dimensional accuracy for both types of

layering resulted near their nominal value as the infill pattern had no major impact on the factor. Moreover, the efficiency of each infill pattern was influenced by the number of contact points used in such specific pattern. Due to the inter-layer bonding between two successive layers, the physical behaviour of the printed samples was enhanced at the high infill density while their mechanical properties were impacted by the infill pattern design during printing.

In a nutshell, the mechanical properties of the FDM-printed samples depended on the building orientation. The tensile test as reflected by the UTS and Young's modulus values exhibited higher results for multiplane ($0^\circ, 0^\circ$) across both concentric and line patterns compared to the single-plane layering. In particular, the values for both aspects for the building orientation ($0^\circ, 0^\circ$) of concentric pattern were 52.5 MPa and 1.78 GPa, respectively, while the line-patterned samples obtained 51.0 MPa and 1.79 GPa, respectively. Meanwhile, the lowest tensile properties were seen at the single-plane 90° building orientation for both patterns. Therefore, higher results outcomes could be attributed to the sample's flexibility, allowing them to be twisted without suffering any discernible harm or distortion to their overall shape where the beads are arranged along with the sample length in a direction parallel to the applied load. Similar to the tensile properties, high bending strength was achieved in multiplane, whereby the bending strength obtained in concentric and line patterns were 88.8 MPa and 88.3 MPa, respectively. The reduction in strength occurred mainly in the upright printing orientation (90°) and caused by the weak line between each layer, leading to interlayer fracture as force was applied to the printed sample. Similarly, the loading direction being perpendicular to the extruded line direction was also a cause as it directly impacted the mechanical properties of the samples.

Lastly, the relationship between the building orientations with the properties of PLA was investigated through a morphological approach for ascertaining the physical and mechanical properties. The high and low tensile strength results were explained and proved from the SEM images obtained, following which one could deduce that low tensile strength in single-plane was due to delamination and the presence of more voids compared to multiplane. Next, relative density and dimensional accuracy were calculated for each orientation angle for both single-plane and multiplane layering. The resulting

analysis allowed the conclusion that the highest relative density was achieved in multiplane, whereas both types of layering yielded almost identical values for dimensional accuracy. Here, the occurrence of voids between layers was the primary reason for the value differences and supported by the optical images obtained.

In summary, building orientation directly influenced the mechanical properties of printed samples and resulted in anisotropic properties. Therefore, the implementation of multiplane layering would enhance the mechanical properties of these samples, particularly those printed in the loading direction would yield improved properties such as tensile and bending strength. Stronger bonds between layers and fewer voids in the printed samples also resulted in better mechanical properties. Comparatively, multiplane layering resulted in superior mechanical and physical properties alike, which could be explained by the implementation of various orientation angles in one single sample. In comparison with the experimental value and manufacturer data sheet, the value discrepancy is due to the selection of different processing parameters, each of which has a value that deviates from the experimental processing parameter values. Another potential reason is the exclusion of testing rate's. This is an essential fact, particularly in the case where testing rate are necessary for the tensile and bending testing. Finally, it should be noted that multiplane printing was achieved by utilising the Creality Ender-3 machine in printing a 3D part.

5.3 Recommendation

This study focused on overcoming the anisotropic properties shown by PLA-printed samples and assessing their mechanical properties following the implementation of multiplane layering. Two process parameters were manipulated, namely building orientation and infill pattern. Thus, it is recommended that future works focus on enhancing the mechanical properties by attempting the following:

- i. Varying the processing parameters, whereby an investigation into different nozzle temperatures, layer heights, infill patterns, and raster angles can be done
- ii. Ascertaining the response of different types of mechanical properties such as impact and compression strength

- iii. Parameter optimisation for composite materials by reinforcing fillers with pure PLA in order to improve the mechanical properties of FDM-printed parts
- iv. Implementation of multiplane layering on composite materials to enhance their mechanical and physical properties for future application



اونيورسيتي مليسيا قهغ السلطان عبدالله
**UNIVERSITI MALAYSIA PAHANG
AL-SULTAN ABDULLAH**

REFERENCES

- Abbas, T. F., Othman, F. M., & Ali, H. B. (2018). Influence of layer thickness on impact property of 3D-printed PLA. *Int. Res. J. Eng. Technol.(Irjet)*, 5, 1-4.
- Abbott, A., Tandon, G., Bradford, R., Koerner, H., & Baur, J. (2018). Process-structure-property effects on ABS bond strength in fused filament fabrication. *Additive Manufacturing*, 19, 29-38.
- Abeykoon, C., Sri-Amphorn, P., & Fernando, A. (2020). Optimization of fused deposition modeling parameters for improved PLA and ABS 3D printed structures. *International Journal of Lightweight Materials and Manufacture*, 3(3), 284-297.
- Ahangar, P., Cooke, M. E., Weber, M. H., & Rosenzweig, D. H. (2019). Current biomedical applications of 3D printing and additive manufacturing. *Applied sciences*, 9(8), 1713.
- Ahmed, J., Zhang, J.-X., Song, Z., & Varshney, S. (2009). Thermal properties of polylactides. *Journal of Thermal Analysis and Calorimetry*, 95(3), 957-964.
- Ahn, S. H., Montero, M., Odell, D., Roundy, S., & Wright, P. K. (2002). Anisotropic material properties of fused deposition modeling ABS. *Rapid Prototyping Journal*.
- Akhoundi, B., & Behravesh, A. H. (2019). Effect of filling pattern on the tensile and flexural mechanical properties of FDM 3D printed products. *Experimental Mechanics*, 59(6), 883-897.
- Alafaghani, A. a. (2018). Investigating the effect of fused deposition modeling processing parameters using taguchi design of experiment method
- Aliheidari, N., Christ, J., Tripuraneni, R., Nadimpalli, S., & Ameli, A. (2018). Interlayer adhesion and fracture resistance of polymers printed through melt extrusion additive manufacturing process. *Materials & Design*, 156, 351-361.
- Alsharhan, A. T., Centea, T., & Gupta, S. K. (2017). Enhancing mechanical properties of thin-walled structures using non-planar extrusion based additive manufacturing. International Manufacturing Science and Engineering Conference,
- Ansari, A. A. (2021). Effect of print speed and extrusion temperature on properties of 3D printed PLA using fused deposition modeling process
- Attaran, M. (2017). The rise of 3-D printing: The advantages of additive manufacturing over traditional manufacturing. *Business Horizons*, 60(5), 677-688.
- Awasthi, P., & Banerjee, S. S. (2021). Fused deposition modeling of thermoplastic elastomeric materials: challenges and opportunities. *Additive Manufacturing*, 46. <https://doi.org/10.1016/j.addma.2021.102177>
- Aworinde, A. K., Adeosun, S. O., Oyawale, F. A., Akinlabi, E. T., & Akinlabi, S. A. (2019). Parametric effects of fused deposition modelling on the mechanical properties of polylactide composites: a review. *Journal of Physics: Conference Series*,
- Baich, L., & Manogharan, G. (2015). Study of infill print parameters on mechanical strength

and production cost-time of 3D printed ABS parts. 2014 International Solid Freeform Fabrication Symposium,

- Baker, A. M., McCoy, J., Majumdar, B. S., Rumley-Ouellette, B., Wahry, J., Marchi, A. N., Bernardin, J. D., & Spornjak, D. (2017). Measurement and modelling of thermal and mechanical anisotropy of parts additively manufactured using fused deposition modelling (FDM). 11th International Workshop on Structural Health Monitoring 2017,
- Barrios, J. M., & Romero, P. E. (2019). Improvement of surface roughness and hydrophobicity in PETG parts manufactured via fused deposition modeling (FDM): An application in 3D printed self-cleaning parts. *Materials*, 12(15), 2499.
- Behzadnasab, M., Yousefi, A. A., Ebrahimibagha, D., & Nasiri, F. (2020). Effects of processing conditions on mechanical properties of PLA printed parts. *Rapid Prototyping Journal*, 26(2), 381-389.
- Bellehumeur, C., Li, L., Sun, Q., & Gu, P. (2004). Modeling of bond formation between polymer filaments in the fused deposition modeling process. *Journal of Manufacturing Processes*, 6(2), 170-178.
- Bertrand, P., Bayle, F., Combe, C., Gœuriot, P., & Smurov, I. (2007). Ceramic components manufacturing by selective laser sintering. *Applied Surface Science*, 254(4), 989-992.
- Bhagia, S., Bornani, K., Agarwal, R., Sandlewal, A., Durkovic, J., Lagana, R., Bhagia, M., Yoo, C. G., Zhao, X., & Kunc, V. (2021). Critical review of FDM 3D printing of PLA biocomposites filled with biomass resources, characterization, biodegradability, upcycling and opportunities for biorefineries. *Applied Materials Today*, 24, 101078.
- Bikas, H., Stavropoulos, P., & Chryssolouris, G. (2016). Additive manufacturing methods and modelling approaches: a critical review. *The International Journal of Advanced Manufacturing Technology*, 83(1-4), 389-405.
- Bin Ishak, I., Fisher, J., & Laroche, P. (2016). Robot arm platform for additive manufacturing using multi-plane toolpaths. International Design Engineering Technical Conferences and Computers and Information in Engineering Conference.
- Blanco, I. (2022). A brief review of the applications of selected thermal analysis methods to 3D printing. *Thermo*, 2(1), 74-83.
- Blazdell, P. (2003). Solid free-forming of ceramics using a continuous jet printer. *Journal of Materials Processing Technology*, 137(1-3), 49-54.
- Blazdell, P., & Evans, J. (2000). Application of a continuous ink jet printer to solid freeforming of ceramics. *Journal of Materials Processing Technology*, 99(1-3), 94-102.
- Blazdell, P., Evans, J., Edirisinghe, M., Shaw, P., & Binstead, M. (1995). The computer aided manufacture of ceramics using multilayer jet printing. *Journal of materials science letters*, 14(22), 1562-1565.
- Bledzki, A., & Jaskiewicz, A. (2010). Mechanical performance of biocomposites based on PLA and PHBV reinforced with natural fibres—A comparative study to PP. *Composites Science and Technology*, 70(12), 1687-1696.

- Bourell, D., Kruth, J. P., Leu, M., Levy, G., Rosen, D., Beese, A. M., & Clare, A. (2017). Materials for additive manufacturing. *CIRP annals*, 66(2), 659-681.
- Calvert, P. (2001). Inkjet printing for materials and devices. *Chemistry of materials*, 13(10), 3299-3305.
- Camacho, D. D., Clayton, P., O'Brien, W. J., Seepersad, C., Juenger, M., Ferron, R., & Salamone, S. (2018). Applications of additive manufacturing in the construction industry—A forward-looking review. *Automation in construction*, 89, 110-119.
- Cano-Vicent, A., Tambuwala, M. M., Hassan, S. S., Barh, D., Aljabali, A. A., Birkett, M., Arjunan, A., & Serrano-Aroca, Á. (2021a). Fused deposition modelling: Current status, methodology, applications and future prospects. *Additive Manufacturing*, 47, 102378.
- Cano-Vicent, A., Tambuwala, M. M., Hassan, S. S., Barh, D., Aljabali, A. A. A., Birkett, M., Arjunan, A., & Serrano-Aroca, Á. (2021b). Fused deposition modelling: Current status, methodology, applications and future prospects. *Additive Manufacturing*, 47. <https://doi.org/10.1016/j.addma.2021.102378>
- Chacón, J., Caminero, M. A., García-Plaza, E., & Núñez, P. J. (2017). Additive manufacturing of PLA structures using fused deposition modelling: Effect of process parameters on mechanical properties and their optimal selection. *Materials & Design*, 124, 143-157.
- Chand, R., Sharma, V. S., Trehan, R., Gupta, M. K., & Sarikaya, M. (2022). Investigating the dimensional accuracy and surface roughness for 3D printed parts using a multi-jet printer. *Journal of Materials Engineering and Performance*, 1-15.
- Chia, H. N., & Wu, B. M. (2015). Recent advances in 3D printing of biomaterials. *J Biol Eng*, 9, 4. <https://doi.org/10.1186/s13036-015-0001-4>
- Chockalingam, K., Jawahar, N., & Praveen, J. (2016). Enhancement of anisotropic strength of fused deposited ABS parts by genetic algorithm. *Materials and Manufacturing Processes*, 31(15), 2001-2010.
- Choi, J.-Y., Choi, J.-H., Kim, N.-K., Kim, Y., Lee, J.-K., Kim, M.-K., Lee, J.-H., & Kim, M.-J. (2002). Analysis of errors in medical rapid prototyping models. *International journal of oral and maxillofacial surgery*, 31(1), 23-32.
- Chowdhury, M. A., & Hossain, S. (2020). A review on tensile and flexural properties of fiber-reinforced polymer composites. *J. Polym. Sci. A Polym. Chem*, 7, 16-26.
- Christ, J. F., Aliheidari, N., Ameli, A., & Pötschke, P. (2017). 3D printed highly elastic strain sensors of multiwalled carbon nanotube/thermoplastic polyurethane nanocomposites. *Materials & Design*, 131, 394-401.
- Chung Wang, C., Lin, T. W., & Hu, S. S. (2007). Optimizing the rapid prototyping process by integrating the taguchi method with the gray relational analysis. *Rapid Prototyping Journal*, 13(5), 304-315.
- Cojocar, V., Frunzaverde, D., Miclosina, C.-O., & Marginean, G. (2022). The influence of the process parameters on the mechanical properties of PLA specimens produced by fused filament fabrication—A review. *Polymers*, 14(5), 886.

- Cooke, W., Anne Tomlinson, R., Burguete, R., Johns, D., & Vanard, G. (2011). Anisotropy, homogeneity and ageing in an SLS polymer. *Rapid Prototyping Journal*, 17(4), 269-279.
- Cuan-Urquizo, E., Barocio, E., Tejada-Ortigoza, V., Pipes, R. B., Rodriguez, C. A., & Roman-Flores, A. (2019). Characterization of the mechanical properties of FFF structures and materials: A review on the experimental, computational and theoretical approaches. *Materials*, 12(6), 895.
- Damanpack, A. R., Sousa, A., & Bodaghi, M. (2021). Porous PLAs with controllable density by FDM 3D printing and chemical foaming agent. *Micromachines (Basel)*, 12(8). <https://doi.org/10.3390/mi12080866>
- Daminabo, S. C., Goel, S., Grammatikos, S. A., Nezhad, H. Y., & Thakur, V. K. (2020). Fused deposition modeling-based additive manufacturing (3D printing): techniques for polymer material systems. *Materials today chemistry*, 16, 100248.
- Darsin, M., Mahardika, N. A., Jatisukanto, G., Edoward, M., Fachri, B. A., & Hussin, M. S. (2021). Effect of 3D printing parameters on dimensional accuracy using steel filaments. *J. 3D Print. Addit. Manuf*, 1(1), 1-7.
- Dawoud, M., Taha, I., & Ebeid, S. J. (2016). Mechanical behaviour of ABS: An experimental study using FDM and injection moulding techniques. *Journal of Manufacturing Processes*, 21, 39-45.
- De Ciurana, J., Serenó, L., & Vallès, È. (2013). Selecting process parameters in rewrap additive manufacturing system for PLA scaffolds manufacture. *Procedia CIRP*, 5, 152-157. <https://doi.org/10.1016/j.procir.2013.01.031>
- De Gans, B. J., Duineveld, P. C., & Schubert, U. S. (2004). Inkjet printing of polymers: state of the art and future developments. *Advanced materials*, 16(3), 203-213.
- De Toro, E. V., Sobrino, J. C., Martínez, A. M., & Eguía, V. M. (2019). Analysis of the influence of the variables of the fused deposition modeling (FDM) process on the mechanical properties of a carbon fiber-reinforced polyamide. *Procedia Manufacturing*, 41, 731-738.
- Deckers, J., Shahzad, K., Vleugels, J., & Kruth, J.-P. (2012). Isostatic pressing assisted indirect selective laser sintering of alumina components. *Rapid prototyping journal*.
- Dey, A., & Yodo, N. (2019). A systematic survey of FDM process parameter optimization and their influence on part characteristics. *Journal of Manufacturing and Materials Processing*, 3(3), 64.
- Dhinakaran, V., Kumar, K. M., Ram, P. B., Ravichandran, M., & Vinayagamorthy, M. (2020). A review on recent advancements in fused deposition modeling. *Materials Today: Proceedings*, 27, 752-756.
- Dilberoglu, U. M., Gharehpapagh, B., Yaman, U., & Dolen, M. (2017). The role of additive manufacturing in the era of industry 4.0. *Procedia Manufacturing*, 11, 545-554.
- Dizon, J. R. C., Espera Jr, A. H., Chen, Q., & Advincula, R. C. (2018). Mechanical characterization of 3D-printed polymers. *Additive Manufacturing*, 20, 44-67.

- Domingo-Espin, M., Puigoriol-Forcada, J. M., Garcia-Granada, A.-A., Llumà, J., Borros, S., & Reyes, G. (2015). Mechanical property characterization and simulation of fused deposition modeling polycarbonate parts. *Materials & Design*, 83, 670-677.
- Dorgan, J. R., Lehermeier, H. J., Palade, L. I., & Cicero, J. (2001). Polylactides: properties and prospects of an environmentally benign plastic from renewable resources. *macromolecular symposia*,
- Durgun, I., & Ertan, R. (2014). Experimental investigation of FDM process for improvement of mechanical properties and production cost. *Rapid Prototyping Journal*.
- Elliott, A. M., Ivanova, O. S., Williams, C. B., & Campbell, T. A. (2013). Inkjet printing of quantum dots in photopolymer for use in additive manufacturing of nanocomposites. *Advanced engineering materials*, 15(10), 903-907.
- Farah, S., Anderson, D. G., & Langer, R. (2016). Physical and mechanical properties of PLA, and their functions in widespread applications—A comprehensive review. *Advanced drug delivery reviews*, 107, 367-392.
- Farazin, A., & Mohammadimehr, M. (2022). Effect of different parameters on the tensile properties of printed polylactic acid samples by FDM: Experimental design tested with MDs simulation. *The International Journal of Advanced Manufacturing Technology*, 118(1-2), 103-118.
- Fekete, I., Ronkay, F., & Lendvai, L. (2021). Highly toughened blends of poly (lactic acid)(PLA) and natural rubber (NR) for FDM-based 3D printing applications: The effect of composition and infill pattern. *Polymer Testing*, 99, 107205.
- Feng, L., Wang, Y., & Wei, Q. (2019). PA12 Powder recycled from SLS for FDM. *Polymers*, 11(4), 727.
- Forster, A. M., & Forster, A. M. (2015). Materials testing standards for additive manufacturing of polymer materials: state of the art and standards applicability.
- Gao, W., Zhang, Y., Ramanujan, D., Ramani, K., Chen, Y., Williams, C. B., Wang, C. C., Shin, Y. C., Zhang, S., & Zavattieri, P. D. (2015). The status, challenges, and future of additive manufacturing in engineering. *Computer-Aided Design*, 69, 65-89.
- Garg, A., & Bhattacharya, A. (2017). An insight to the failure of FDM parts under tensile loading: finite element analysis and experimental study. *International Journal of Mechanical Sciences*, 120, 225-236.
- Garlotta, D. (2001). A literature review of poly (lactic acid). *Journal of Polymers and the Environment*, 9(2), 63-84.
- Ghorbani, J., Koirala, P., Shen, Y.-L., & Tehrani, M. (2022). Eliminating voids and reducing mechanical anisotropy in fused filament fabrication parts by adjusting the filament extrusion rate. *Journal of Manufacturing Processes*, 80, 651-658.
- González, C., Vilatela, J., Molina-Aldareguía, J., Lopes, C., & LLorca, J. (2017). Structural composites for multifunctional applications: Current challenges and future trends. *Progress in Materials Science*, 89, 194-251.

- Gruber, P., Drumright, R., & Henton, D. (2000). Polylactic acid technology. *Adv. Mater*, 12(23), 1841-1846.
- Gu, S. H., Nicolas, V., Lalis, A., Sathirapongsasuti, N., & Yanagihara, R. (2013). Complete genome sequence and molecular phylogeny of a newfound hantavirus harbored by the Doucet's musk shrew (*Crocidura douceti*) in Guinea. *Infection, Genetics and Evolution*, 20, 118-123.
- Gülcan, O., Günaydın, K., & Tamer, A. (2021). The state of the art of material jetting- A critical review. *Polymers*, 13(16), 2829.
- Gunasekaran, K., Aravinth, V., Kumaran, C. M., Madhankumar, K., & Kumar, S. P. (2021). Investigation of mechanical properties of PLA printed materials under varying infill density. *Materials Today: Proceedings*, 45, 1849-1856.
- Hanon, M. M., Marczis, R., & Zsidai, L. (2021). Influence of the 3D printing process settings on tensile strength of PLA and HT-PLA. *Periodica Polytechnica Mechanical Engineering*, 65(1), 38-46.
- Hanon, M. M., Zsidai, L., & Ma, Q. (2021). Accuracy investigation of 3D printed PLA with various process parameters and different colors. *Materials Today: Proceedings*, 42, 3089-3096.
- Harun, W., Manam, N., Kamariah, M., Sharif, S., Zulkifly, A., Ahmad, I., & Miura, H. (2018). A review of powdered additive manufacturing techniques for Ti-6al-4v biomedical applications. *Powder Technology*, 331, 74-97.
- Hernandez-Contreras, A., Ruiz-Huerta, L., Caballero-Ruiz, A., Moock, V., & Siller, H. R. (2020). Extended CT void analysis in FDM additive manufacturing components. *Materials*, 13(17), 3831.
- Hodzic, D., Pandzic, A., Hajro, I., & Tasić, P. (2020). Strength comparison of FDM 3D printed PLA made by different manufacturers. *TEM J*, 9, 966-970.
- Hsueh, M.-H., Lai, C.-J., Chung, C.-F., Wang, S.-H., Huang, W.-C., Pan, C.-Y., Zeng, Y.-S., & Hsieh, C.-H. (2021). Effect of printing parameters on the tensile properties of 3d-printed polylactic acid (Pla) based on fused deposition modeling. *Polymers*, 13(14), 2387.
- Ian Gibson, I. G. (2015). Additive manufacturing technologies 3D printing, rapid prototyping, and direct digital manufacturing. In: Springer.
- Ishak, I. B., Fleming, D., & Larochelle, P. (2019). Multiplane fused deposition modeling: A study of tensile strength. *Mechanics Based Design of Structures and Machines*.
- Jain, P., & Kuthe, A. (2013). Feasibility study of manufacturing using rapid prototyping: FDM approach. *Procedia Engineering*, 63, 4-11.
- Jaya Christiyani, K., Chandrasekhar, U., & Venkateswarlu, K. (2018). Flexural properties of PLA components under various test condition manufactured by 3D Printer. *Journal of The Institution of Engineers (India): Series C*, 99, 363-367.
- Jerez-mesa. (2017). Fatigue lifespan study of PLA parts obtained by additive manufacturing.

Procedia Manufacturing, 13, 872-879.

- Kabir, S. F., Mathur, K., & Seyam, A.-F. M. (2020). A critical review on 3D printed continuous fiber-reinforced composites: history, mechanism, materials and properties. *Composite Structures*, 232, 111476.
- Kačergis, L., Mitkus, R., & Sinapius, M. (2019). Influence of fused deposition modeling process parameters on the transformation of 4D printed morphing structures. *Smart Materials and Structures*, 28(10), 105042.
- Keating, S., & Oxman, N. (2013). Compound fabrication: A multi-functional robotic platform for digital design and fabrication. *Robotics and Computer-Integrated Manufacturing*, 29(6), 439-448.
- Kechagias, J., Chaidas, D., Vidakis, N., Salonitis, K., & Vaxevanidis, N. (2022). Key parameters controlling surface quality and dimensional accuracy: A critical review of FFF process. *Materials and Manufacturing Processes*, 1-22.
- Khoo, R., Ismail, H., & Chow, W. (2016). Thermal and morphological properties of poly (lactic acid)/nanocellulose nanocomposites. *Procedia Chemistry*, 19, 788-794.
- Khosravani, M. R., & Reinicke, T. (2020). Effects of raster layup and printing speed on strength of 3D-printed structural components. *Procedia Structural Integrity*, 28, 720-725.
- Ko, S. H., Chung, J., Hotz, N., Nam, K. H., & Grigoropoulos, C. P. (2010). Metal nanoparticle direct inkjet printing for low-temperature 3D micro metal structure fabrication. *Journal of Micromechanics and Microengineering*, 20(12), 125010.
- Kristiawan, R. B., Imaduddin, F., Ariawan, D., & Arifin, Z. (2021). A review on the fused deposition modeling (FDM) 3D printing: Filament processing, materials, and printing parameters. *Open Engineering*, 11(1), 639-649.
- Kumar, L. J., & Nair, C. K. (2017). Current trends of additive manufacturing in the aerospace industry. In *Advances in 3D printing & additive manufacturing technologies* (pp. 39-54). Springer.
- Kumar, M., Ramakrishnan, R., & Omarbekova, A. (2019). 3D printed polycarbonate reinforced acrylonitrile–butadiene–styrene composites: Composition effects on mechanical properties, micro-structure and void formation study. *Journal of Mechanical Science and Technology*, 33, 5219-5226.
- Kumar, R., Ul Haq, M. I., Raina, A., & Anand, A. (2019). Industrial applications of natural fibre-reinforced polymer composites—challenges and opportunities. *International Journal of Sustainable Engineering*, 12(3), 212-220.
- Kumar, S., Singh, R., Singh, T., & Batish, A. (2021). 3D printed tensile and flexural prototypes of thermoplastic matrix reinforced with multi-materials: A statistical analysis. *Materials Today: Proceedings*, 44, 79-85.
- Laureto, J. J., & Pearce, J. M. (2018). Anisotropic mechanical property variance between ASTM D638-14 type i and type iv fused filament fabricated specimens. *Polymer Testing*, 68, 294-301.

- Le, H. P. (1998). Progress and trends in ink-jet printing technology. *Journal of Imaging Science and Technology*, 42(1), 49-62.
- Lee, J.-Y. (2017). Fundamentals and applications of 3D printing for novel materials.
- Lee, J.-Y., An, J., & Chua, C. K. (2017). Fundamentals and applications of 3D printing for novel materials. *Applied Materials Today*, 7, 120-133.
- Li, V. C.-F., Kuang, X., Hamel, C. M., Roach, D., Deng, Y., & Qi, H. J. (2019). Cellulose nanocrystals support material for 3D printing complexly shaped structures via multi-materials-multi-methods printing. *Additive Manufacturing*, 28, 14-22.
- Ligon, S. C., Liska, R., Stampfl, J., Gurr, M., & Mülhaupt, R. (2017). Polymers for 3D printing and customized additive manufacturing. *Chemical reviews*, 117(15), 10212-10290.
- Lipton, J., Cutler, M., Nigl, F., Cohen, D., & Lipson, H. (2015). Additive manufacturing for the food industry, vol. 43. In: Elsevier Ltd.
- Liu, Z., Wang, Y., Wu, B., Cui, C., Guo, Y., & Yan, C. (2019). A critical review of fused deposition modeling 3D printing technology in manufacturing polylactic acid parts. *The International Journal of Advanced Manufacturing Technology*, 102(9), 2877-2889.
- Luzanin, O., Movrin, D., Stathopoulos, V., Pandis, P., Radusin, T., & Guduric, V. (2019). Impact of processing parameters on tensile strength, in-process crystallinity and mesostructure in FDM-fabricated PLA specimens. *Rapid Prototyping Journal*, 25(8), 1398-1410.
- Masood, S. H. (2014). 10.04 - Advances in fused deposition modeling. In S. Hashmi, G. F. Batalha, C. J. Van Tyne, & B. Yilbas (Eds.), *Comprehensive Materials Processing* (pp. 69-91). Elsevier. [https://doi.org/https://doi.org/10.1016/B978-0-08-096532-1.01002-5](https://doi.org/10.1016/B978-0-08-096532-1.01002-5)
- Melchels, F. P., Feijen, J., & Grijpma, D. W. (2009). A poly (D, L-lactide) resin for the preparation of tissue engineering scaffolds by stereolithography. *Biomaterials*, 30(23-24), 3801-3809.
- Meteyer, S., Xu, X., Perry, N., & Zhao, Y. F. (2014). Energy and material flow analysis of binder-jetting additive manufacturing processes. *Procedia Cirp*, 15, 19-25.
- Mitchell, A., Lafont, U., Hołyńska, M., & Semprimoschnig, C. (2018). Additive manufacturing—A review of 4D printing and future applications. *Additive Manufacturing*, 24, 606-626.
- Mogan, J., Sandanamsamy, L., Halim, N., Harun, W., Kadirgama, K., & Ramasamy, D. (2021). A review of FDM and graphene-based polymer composite. IOP Conference Series: Materials Science and Engineering,
- Mohamed, O. A. (2017). Analytical modeling and experimental investigation of product quality and mechanical properties in FDM additive manufacturing [Swinburne University of Technology].
- Mohamed, O. A., Masood, S. H., & Bhowmik, J. L. (2015). Optimization of fused deposition modeling process parameters: a review of current research and future prospects. *Advances in manufacturing*, 3(1), 42-53.

- Mohammed, A., & Abdullah, A. (2018). Scanning electron microscopy (SEM): A review. Proceedings of the 2018 International Conference on Hydraulics and Pneumatics-HERVEX, Baile Govora, Romania,
- Monzón, M., Ortega, Z., Hernández, A., Paz, R., & Ortega, F. (2017). Anisotropy of photopolymer parts made by digital light processing. *Materials*, 10(1), 64.
- Morissette, S. L., Lewis, J. A., Cesarano, J., Dimos, D. B., & Baer, T. (2000). Solid freeform fabrication of aqueous alumina-poly (vinyl alcohol) gelcasting suspensions. *Journal of the American Ceramic Society*, 83(10), 2409-2416.
- Muñoz, J. (2020). 3D-printed biosensors for electrochemical and optical applications.
- Murphy, C. A., & Collins, M. N. (2018). Microcrystalline cellulose reinforced polylactic acid biocomposite filaments for 3D printing. *Polymer Composites*, 39(4), 1311-1320.
- Nabipour, M., & Akhondi, B. (2021). An experimental study of FDM parameters effects on tensile strength, density, and production time of ABS/Cu composites. *Journal of Elastomers & Plastics*, 53(2), 146-164.
- Nampoothiri, K. M., Nair, N. R., & John, R. P. (2010). An overview of the recent developments in polylactide (PLA) research. *Bioresource technology*, 101(22), 8493-8501.
- Nancharaiah, T., Raju, D. R., & Raju, V. R. (2010). An experimental investigation on surface quality and dimensional accuracy of FDM components. *International Journal on Emerging Technologies*, 1(2), 106-111.
- Navarro, M., Aparicio, C., Charles-Harris, M., Ginebra, M., Engel, E., & Planell, J. (2006). Development of a biodegradable composite scaffold for bone tissue engineering: physicochemical, topographical, mechanical, degradation, and biological properties. *Ordered Polymeric Nanostructures at Surfaces*, 209-231.
- Ngo, T. D. (2018). Additive manufacturing (3D printing)_ A review of materials, methods, applications and challenges.
- Ngo, T. D., Kashani, A., Imbalzano, G., Nguyen, K. T., & Hui, D. (2018). Additive manufacturing (3D printing): A review of materials, methods, applications and challenges. *Composites Part B: Engineering*, 143, 172-196.
- NKOMO, N., Gwamuri, J., Sibanda, N. R., & NKIWANE, L. (2017). A study of applications of 3D printing technology and potential applications in the plastic thermoforming industry. *IOSR Journal of Engineering*.
- Nyiranzeyimana, G., Mutua, J., Mose, B., & Mbuya, T. (2021). Optimization of process parameters in fused deposition modelling of thermoplastics: A review. *Materialwissenschaft und Werkstofftechnik*, 52(6), 682-694.
- Papon, E. A., & Haque, A. (2018). Tensile properties, void contents, dispersion and fracture behaviour of 3D printed carbon nanofiber reinforced composites. *Journal of Reinforced Plastics and Composites*, 37(6), 381-395.
- Pappu, A., Thakur, V. K., Patidar, R., Asolekar, S. R., & Saxena, M. (2019). Recycling marble wastes and Jarosite wastes into sustainable hybrid composite materials and validation

- through Response Surface Methodology. *Journal of Cleaner Production*, 240, 118249.
- Patil, P., Singh, D., Raykar, S. J., & Bhamu, J. (2021). Multi-objective optimization of process parameters of fused deposition modeling (FDM) for printing polylactic acid (PLA) polymer components. *Materials Today: Proceedings*, 45, 4880-4885.
- Petersmann, S., Spoerk-Erdely, P., Feuchter, M., Wieme, T., Arbeiter, F., & Spoerk, M. (2020). Process-induced morphological features in material extrusion-based additive manufacturing of polypropylene. *Additive Manufacturing*, 35, 101384.
- Popescu, D., Zapciu, A., Amza, C., Baci, F., & Marinescu, R. (2018). FDM process parameters influence over the mechanical properties of polymer specimens: A review. *Polymer Testing*, 69, 157-166. <https://doi.org/10.1016/j.polymertesting.2018.05.020>
- Priya, M. S., Naresh, K., Jayaganthan, R., & Velmurugan, R. (2019). A comparative study between in-house 3D printed and injection molded ABS and PLA polymers for low-frequency applications. *Materials Research Express*, 6(8), 085345.
- Qattawi, A., Alrawi, B., & Guzman, A. (2017). Experimental optimization of fused deposition modelling processing parameters: a design-for-manufacturing approach. *Procedia Manufacturing*, 10, 791-803.
- Rajan, K., Samykano, M., Kadirgama, K., Harun, W. S. W., & Rahman, M. (2022). Fused deposition modeling: Process, materials, parameters, properties, and applications. *The International Journal of Advanced Manufacturing Technology*, 1-40.
- Rajpurohit, S. R., & Dave, H. K. (2018). Effect of process parameters on tensile strength of FDM printed PLA part. *Rapid Prototyping Journal*.
- Rajpurohit, S. R., & Dave, H. K. (2019). Analysis of tensile strength of a fused filament fabricated PLA part using an open-source 3D printer. *The International Journal of Advanced Manufacturing Technology*, 101(5), 1525-1536.
- Rasal, R. M., Janorkar, A. V., & Hirt, D. E. (2010). Poly (lactic acid) modifications. *Progress in polymer science*, 35(3), 338-356.
- Rayegani, F., & Onwubolu, G. C. (2014). Fused deposition modelling (FDM) process parameter prediction and optimization using group method for data handling (GMDH) and differential evolution (DE). *The International Journal of Advanced Manufacturing Technology*, 73(1), 509-519.
- Rezaei, R., Karamooz Ravari, M. R., Badrossamay, M., & Kadkhodaei, M. (2016). Mechanical characterization and finite element modeling of polylactic acid BCC-Z cellular lattice structures fabricated by fused deposition modeling. *Proceedings of the Institution of Mechanical Engineers, Part C: Journal of Mechanical Engineering Science*, 231(11), 1995-2004. <https://doi.org/10.1177/0954406215626941>
- Rezwan, K., Chen, Q., Blaker, J. J., & Boccaccini, A. R. (2006). Biodegradable and bioactive porous polymer/inorganic composite scaffolds for bone tissue engineering. *Biomaterials*, 27(18), 3413-3431.
- Ribeiro, K. S., Mariani, F. E., & Coelho, R. T. (2020). A study of different deposition strategies in direct energy deposition (DED) processes. *Procedia Manufacturing*, 48, 663-670.

- Riddick, J. C., Haile, M. A., Von Wahlde, R., Cole, D. P., Bamiduro, O., & Johnson, T. E. (2016). Fractographic analysis of tensile failure of acrylonitrile-butadiene-styrene fabricated by fused deposition modeling. *Additive Manufacturing*, *11*, 49-59.
- Roberson, D. A., Perez, A. R. T., Shemelya, C. M., Rivera, A., MacDonald, E., & Wicker, R. B. (2015). Comparison of stress concentrator fabrication for 3D printed polymeric izod impact test specimens. *Additive Manufacturing*, *7*, 1-11.
- Rodríguez-Panes, A., Claver, J., & Camacho, A. M. (2018). The influence of manufacturing parameters on the mechanical behaviour of PLA and ABS pieces manufactured by FDM: A comparative analysis. *Materials*, *11*(8), 1333.
- Rodríguez, J. F., Thomas, J. P., & Renaud, J. E. (2001). Mechanical behavior of acrylonitrile butadiene styrene (ABS) fused deposition materials. Experimental investigation. *Rapid Prototyping Journal*.
- Saba, N., Jawaid, M., & Sultan, M. (2019). An overview of mechanical and physical testing of composite materials. *Mechanical and physical testing of biocomposites, fibre-reinforced composites and hybrid composites*, 1-12.
- Sachs, E. (1992). CAD-casting: the direct fabrication of ceramic shells and cores by three-dimensional printing. *Manuf Rev*, *5*, 118-126.
- Samykan, M. (2021). Mechanical property and prediction model for FDM-3D printed polylactic acid (PLA). *Arabian Journal for Science and Engineering*, *46*, 7875-7892.
- Saroia, J., Wang, Y., Wei, Q., Lei, M., Li, X., Guo, Y., & Zhang, K. (2019). A review on 3D printed matrix polymer composites: its potential and future challenges. *The International Journal of Advanced Manufacturing Technology*, *106*(5-6), 1695-1721. <https://doi.org/10.1007/s00170-019-04534-z>
- Sathies, T., Senthil, P., & Anoop, M. (2020). A review on advancements in applications of fused deposition modelling process. *Rapid Prototyping Journal*.
- Scheithauer, U., Schwarzer, E., Richter, H. J., & Moritz, T. (2015). Thermoplastic 3D printing—an additive manufacturing method for producing dense ceramics. *International journal of applied ceramic technology*, *12*(1), 26-31.
- Shanmugam, V., Das, O., Babu, K., Marimuthu, U., Veerasimman, A., Johnson, D. J., Neisiany, R. E., Hedenqvist, M. S., Ramakrishna, S., & Berto, F. (2021). Fatigue behaviour of FDM-3D printed polymers, polymeric composites and architected cellular materials. *International Journal of Fatigue*, *143*. <https://doi.org/10.1016/j.ijfatigue.2020.106007>
- Shembekar, A. V., Yoon, Y. J., Kanyuck, A., & Gupta, S. K. (2018). Trajectory planning for conformal 3d printing using non-planar layers. International design engineering technical conferences and computers and information in engineering conference.
- Sheoran, A. J., & Kumar, H. (2020). Fused Deposition modeling process parameters optimization and effect on mechanical properties and part quality: Review and reflection on present research. *Materials Today: Proceedings*, *21*, 1659-1672.
- Shih, R. H. (2013). *Parametric Modeling with Creo Parametric 2.0*. Sdc Publications.

- Singh, J., Goyal, K. K., & Kumar, R. (2022). Effect of filling percentage and raster style on tensile behavior of FDM produced PLA parts at different build orientation. *Materials Today: Proceedings*.
- Singh, R., Gupta, A., Tripathi, O., Srivastava, S., Singh, B., Awasthi, A., Rajput, S., Sonia, P., Singhal, P., & Saxena, K. K. (2020). Powder bed fusion process in additive manufacturing: An overview. *Materials Today: Proceedings*, 26, 3058-3070.
- Singh, S., Ramakrishna, S., & Singh, R. (2017). Material issues in additive manufacturing: A review. *Journal of Manufacturing Processes*, 25, 185-200.
- Slade, C. (1998). Freeforming ceramics using a thermal jet printer. *Journal of materials science letters*, 17(19), 1669-1671.
- Smay, J. E., & Lewis, J. A. (2012). Solid free-form fabrication of 3-D ceramic structures. *Ceramics and composites processing methods, 1st edn. Wiley, New Jersey*, 459-484.
- Solomon, I. J., Sevel, P., & Gunasekaran, J. (2021). A review on the various processing parameters in FDM. *Materials Today: Proceedings*, 37, 509-514.
- Sood, A. K., Ohdar, R., & Mahapatra, S. S. (2009). Improving dimensional accuracy of fused deposition modelling processed part using grey Taguchi method. *Materials & Design*, 30(10), 4243-4252.
- Sood, A. K., Ohdar, R. K., & Mahapatra, S. S. (2012). Experimental investigation and empirical modelling of FDM process for compressive strength improvement. *Journal of Advanced Research*, 3(1), 81-90.
- Soundararajan, B., Sofia, D., Barletta, D., & Poletto, M. (2021). Review on modeling techniques for powder bed fusion processes based on physical principles. *Additive Manufacturing*, 47, 102336.
- Spoerk, M., Arbeiter, F., Cajner, H., Sapkota, J., & Holzer, C. (2017). Parametric optimization of intra-and inter-layer strengths in parts produced by extrusion-based additive manufacturing of poly (lactic acid). *Journal of Applied Polymer Science*, 134(41), 45401.
- Sun, Q., Rizvi, G., Bellehumeur, C., & Gu, P. (2008). Effect of processing conditions on the bonding quality of FDM polymer filaments. *Rapid prototyping journal*.
- Syrlybayev, D., Zharylkassyn, B., Seisekulova, A., Akhmetov, M., Perveen, A., & Talamona, D. (2021). Optimisation of strength properties of FDM printed parts—A critical review. *Polymers*, 13(10), 1587.
- Tagliaferri, V., Trovalusci, F., Guarino, S., & Venettacci, S. (2019). Environmental and economic analysis of FDM, SLS and MJF additive manufacturing technologies. *Materials*, 12(24), 4161.
- Taib, N.-A. A. B., Rahman, M. R., Huda, D., Kuok, K. K., Hamdan, S., Bakri, M. K. B., Julaihi, M. R. M. B., & Khan, A. (2022). A review on poly lactic acid (PLA) as a biodegradable polymer. *Polymer Bulletin*, 1-35.
- Takezawa, A. (2017). Design methodology for porous composites with tunable thermal

expansion produced by multi-material topology optimization and additive manufacturing.

- Tao, Y. (2021). A review on voids of 3D printed parts by fused filament fabrication *Journal of Materials Research and Technology*, 15, 4860-4879.
- Thakur, A. K., Pappu, A., & Thakur, V. K. (2019). Synthesis and characterization of new class of geopolymer hybrid composite materials from industrial wastes. *Journal of Cleaner Production*, 230, 11-20.
- Tofail, S. A., Koumoulos, E. P., Bandyopadhyay, A., Bose, S., O'Donoghue, L., & Charitidis, C. (2018). Additive manufacturing: scientific and technological challenges, market uptake and opportunities. *Materials today*, 21(1), 22-37.
- Torres, J., Cole, M., Owji, A., DeMastry, Z., & Gordon, A. P. (2016). An approach for mechanical property optimization of fused deposition modeling with polylactic acid via design of experiments. *Rapid Prototyping Journal*.
- Travitzky, N., Bonet, A., Dermeik, B., Fey, T., Filbert-Demut, I., Schlier, L., Schlordt, T., & Greil, P. (2014). Additive manufacturing of ceramic-based materials. *Advanced engineering materials*, 16(6), 729-754.
- Tronvoll, S. A., Welo, T., & Elverum, C. W. (2018). The effects of voids on structural properties of fused deposition modelled parts: a probabilistic approach. *The International Journal of Advanced Manufacturing Technology*, 97(9-12), 3607-3618. <https://doi.org/10.1007/s00170-018-2148-x>
- Turner, B. N., Strong, R., & Gold, S. A. J. R. P. J. (2014). A review of melt extrusion additive manufacturing processes: I. Process design and modeling.
- Valvez, S., Santos, P., Parente, J., Silva, M., & Reis, P. (2020). 3D printed continuous carbon fiber reinforced PLA composites: A short review. *Procedia Structural Integrity*, 25, 394-399.
- van Manen, T., Janbaz, S., & Zadpoor, A. A. (2018). Programming the shape-shifting of flat soft matter. *Materials Today*, 21(2), 144-163.
- Vatani, M., Lu, Y., Engeberg, E. D., & Choi, J.-W. (2015). Combined 3D printing technologies and material for fabrication of tactile sensors. *International Journal of Precision Engineering and Manufacturing*, 16(7), 1375-1383.
- Vink, E. T., Rabago, K. R., Glassner, D. A., & Gruber, P. R. (2003). Applications of life cycle assessment to NatureWorks polylactide (PLA) production. *Polymer Degradation and stability*, 80(3), 403-419.
- Vinyas, M., Athul, S., Harursampath, D., & Thoi, T. N. (2019). Experimental evaluation of the mechanical and thermal properties of 3D printed PLA and its composites. *Materials Research Express*, 6(11), 115301.
- Wang, L., & Gardner, D. J. (2017). Effect of fused layer modeling (FLM) processing parameters on impact strength of cellular polypropylene. *Polymer*, 113, 74-80.
- Wang, L., Gramlich, W. M., & Gardner, D. J. (2017). Improving the impact strength of Poly

- (lactic acid)(PLA) in fused layer modeling (FLM). *Polymer*, 114, 242-248.
- Wang, T.-M., Xi, J.-T., & Jin, Y. (2007). A model research for prototype warp deformation in the FDM process. *The International Journal of Advanced Manufacturing Technology*, 33(11), 1087-1096.
- Wickramasinghe, S., Do, T., & Tran, P. (2020). FDM-based 3D printing of polymer and associated composite: A review on mechanical properties, defects and treatments. *Polymers*, 12(7), 1529.
- Wickramasinghe, S., Do, T., & Tran, P. (2020). FDM-Based 3D Printing of Polymer and Associated Composite: A Review on mechanical properties, defects and treatments. *Polymers (Basel)*, 12(7). <https://doi.org/10.3390/polym12071529>
- Williams, C. B., Cochran, J. K., & Rosen, D. W. (2011). Additive manufacturing of metallic cellular materials via three-dimensional printing. *The International Journal of Advanced Manufacturing Technology*, 53(1), 231-239.
- Wilson, J. M., Piya, C., Shin, Y. C., Zhao, F., & Ramani, K. (2014). Remanufacturing of turbine blades by laser direct deposition with its energy and environmental impact analysis. *Journal of Cleaner Production*, 80, 170-178.
- Wong, K. V., & Hernandez, A. (2012). A review of additive manufacturing. *International scholarly research notices*, 2012.
- Wu, W., Geng, P., Li, G., Zhao, D., Zhang, H., & Zhao, J. (2015). Influence of layer thickness and raster angle on the mechanical properties of 3D-printed PEEK and a comparative mechanical study between PEEK and ABS. *Materials*, 8(9), 5834-5846.
- XinWang. (2017). 3D printing of polymer matrix composites-A review and prospective.
- Xiong, Z., Yan, Y., Wang, S., Zhang, R., & Zhang, C. (2002). Fabrication of porous scaffolds for bone tissue engineering via low-temperature deposition. *Scripta Materialia*, 46(11), 771-776.
- Yang, T. C., & Yeh, C. H. (2020). Morphology and mechanical properties of 3D printed wood fiber/polylactic acid composite parts using fused deposition modeling (FDM): The effects of printing speed. *Polymers (Basel)*, 12(6). <https://doi.org/10.3390/polym12061334>
- Yao, T., Ye, J., Deng, Z., Zhang, K., Ma, Y., & Ouyang, H. (2020). Tensile failure strength and separation angle of FDM 3D printing PLA material: Experimental and theoretical analyses. *Composites Part B: Engineering*, 188, 107894.
- Yao, X., Ge, P., Li, J., Wang, Y., Li, T., Liu, W., & Zhang, Z. (2020). Controlling the solidification process parameters of direct energy deposition additive manufacturing considering laser and powder properties. *Computational Materials Science*, 182, 109788.
- Ye, X., & Shin, Y. C. (2014). Synthesis and characterization of Fe-based amorphous composite by laser direct deposition. *Surface and Coatings Technology*, 239, 34-40.
- Zhang, Y., Wu, L., Guo, X., Kane, S., Deng, Y., Jung, Y.-G., Lee, J.-H., & Zhang, J. (2018).

Additive manufacturing of metallic materials: a review. *Journal of Materials Engineering and Performance*, 27(1), 1-13.

Zhao, X., Evans, J., Edirisinghe, M., & Song, J. (2003). Formulation of a ceramic ink for a wide-array drop-on-demand ink-jet printer. *Ceramics International*, 29(8), 887-892.

Zharylkassyn, B., Perveen, A., & Talamona, D. (2021). Effect of process parameters and materials on the dimensional accuracy of FDM parts. *Materials Today: Proceedings*, 44, 1307-1311.

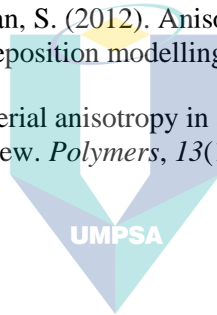
Zhou, Y.-G., Su, B., & Turng, L.-s. (2017). Deposition-induced effects of isotactic polypropylene and polycarbonate composites during fused deposition modeling. *Rapid Prototyping Journal*.

Zhu, J., Zhu, H., Njuguna, J., & Abhyankar, H. (2013). Recent development of flax fibres and their reinforced composites based on different polymeric matrices. *Materials*, 6(11), 5171-5198.

Ziaee, M., & Crane, N. B. (2019). Binder jetting: A review of process, materials, and methods. *Additive Manufacturing*, 28, 781-801.

Ziemian, C., Sharma, M., & Ziemian, S. (2012). Anisotropic mechanical properties of ABS parts fabricated by fused deposition modelling. *Mechanical engineering*, 23, 159-180.

Zohdi, N., & Yang, R. (2021). Material anisotropy in additively manufactured polymers and polymer composites: a review. *Polymers*, 13(19), 3368.

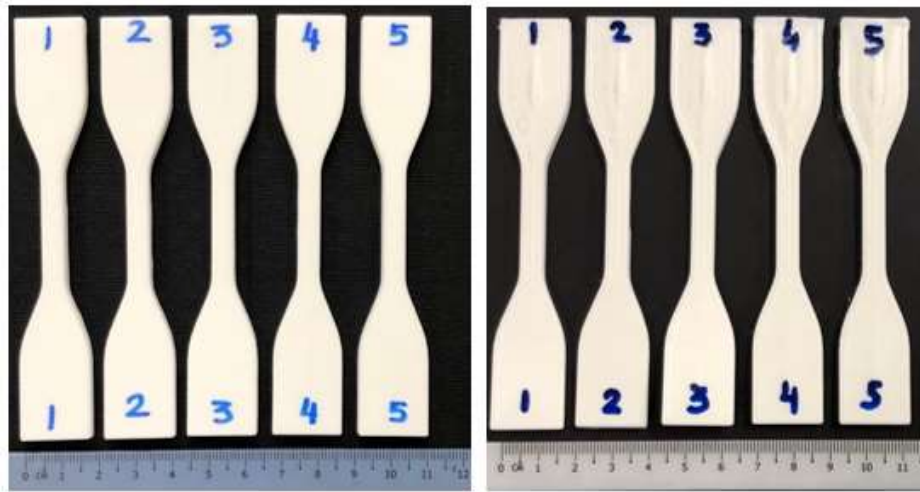


اونيورسيتي مليسيا قهغ السلطان عبدالله
UNIVERSITI MALAYSIA PAHANG
AL-SULTAN ABDULLAH



اونيورسيتي مليسيا قهغ السلطان عبدالله
UNIVERSITI MALAYSIA PAHANG
AL-SULTAN ABDULLAH

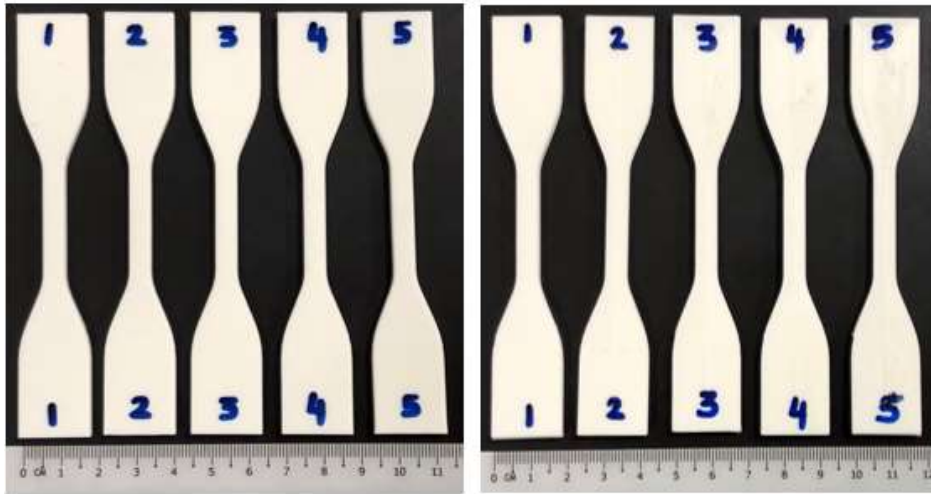
Appendix A: Fabricated tensile samples for concentric pattern



Fabricated tensile samples of Single Plane (0°) and Multiplane ($0^\circ, 0^\circ$) for Concentric Pattern



Fabricated tensile samples of Single Plane (45°) and Multiplane ($45^\circ, 0^\circ$) for Concentric Pattern

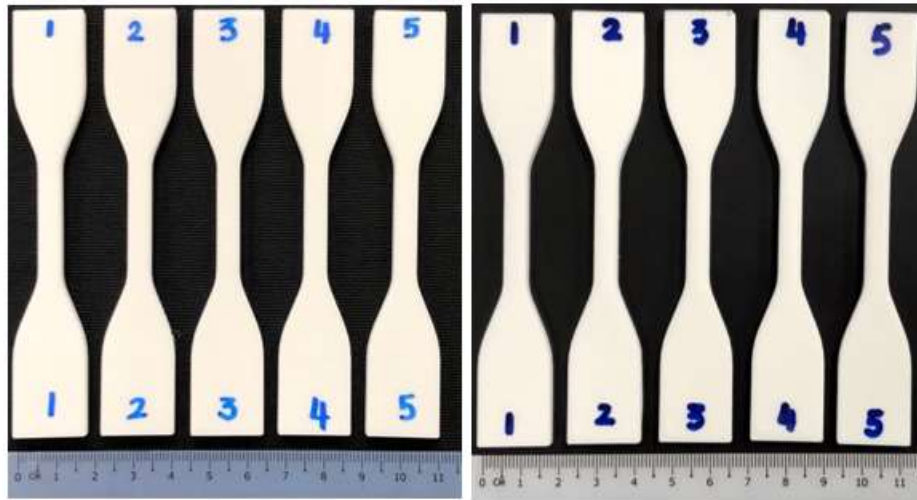


Fabricated tensile samples of Single Plane (0°) and Multiplane ($90^\circ, 0^\circ$) for Concentric Pattern



اونيورسيتي مليسيا قهغ السلطان عبدالله
UNIVERSITI MALAYSIA PAHANG
AL-SULTAN ABDULLAH

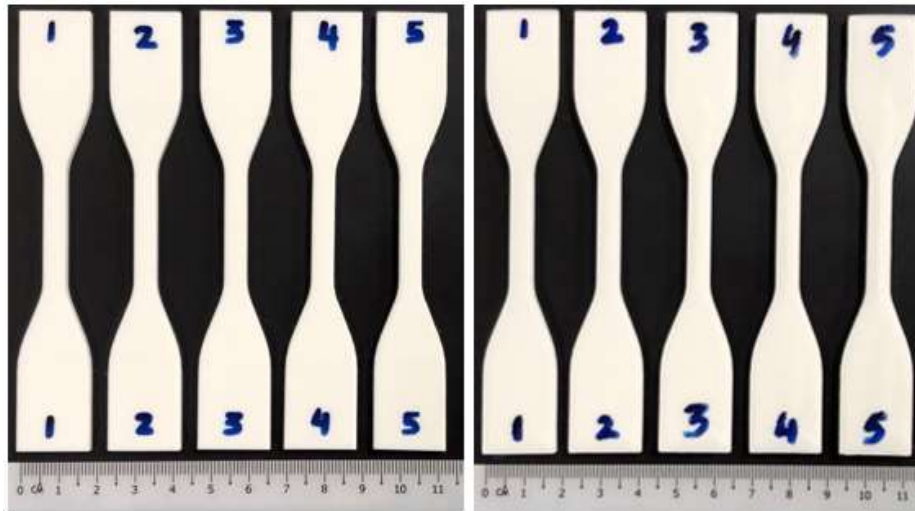
Appendix B: Fabricated tensile samples for line pattern



Fabricated tensile samples of Single Plane (0°) and Multiplane ($0^\circ, 0^\circ$) for Line Pattern



Fabricated tensile samples of Single Plane (45°) and Multiplane ($45^\circ, 0^\circ$) for Line Pattern

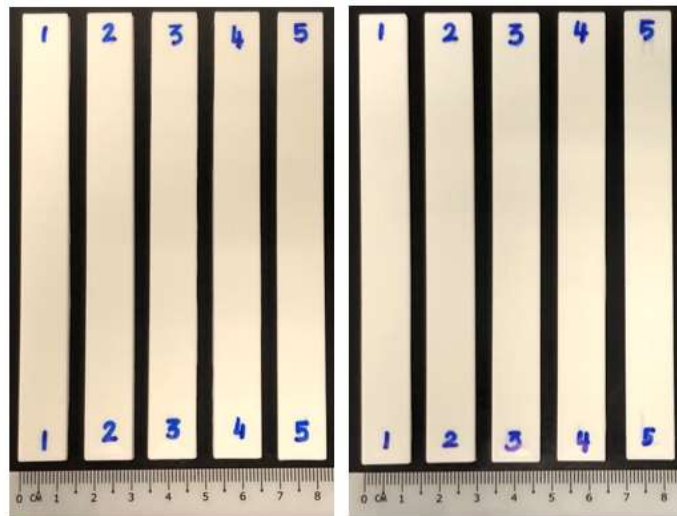


Fabricated tensile samples of Single Plane (90°) and Multiplane ($90^\circ, 0^\circ$) for Line Pattern



اونيورسيتي مليسيا قهغ السلطان عبدالله
UNIVERSITI MALAYSIA PAHANG
AL-SULTAN ABDULLAH

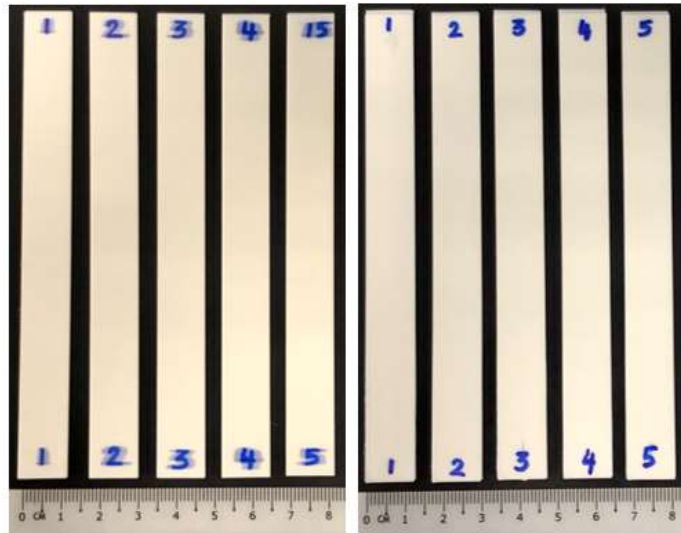
Appendix C: Fabricated bending samples for concentric pattern



Fabricated bending samples of Single Plane (0°) and Multiplane ($0^\circ, 0^\circ$) for Concentric Pattern



Fabricated bending samples of Single Plane (45°) and Multiplane ($45^\circ, 0^\circ$) for Concentric Pattern

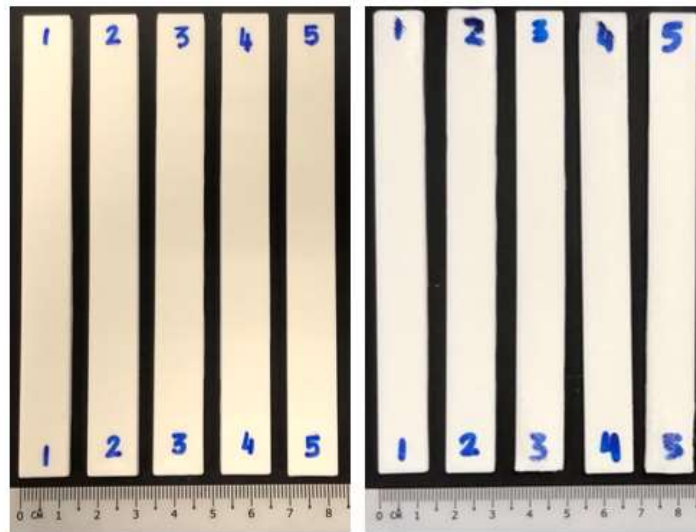


Fabricated bending samples of Single Plane (90°) and Multiplane ($90^\circ, 0^\circ$) for Concentric Pattern



اونيورسيتي مليسيا قهغ السلطان عبدالله
UNIVERSITI MALAYSIA PAHANG
AL-SULTAN ABDULLAH

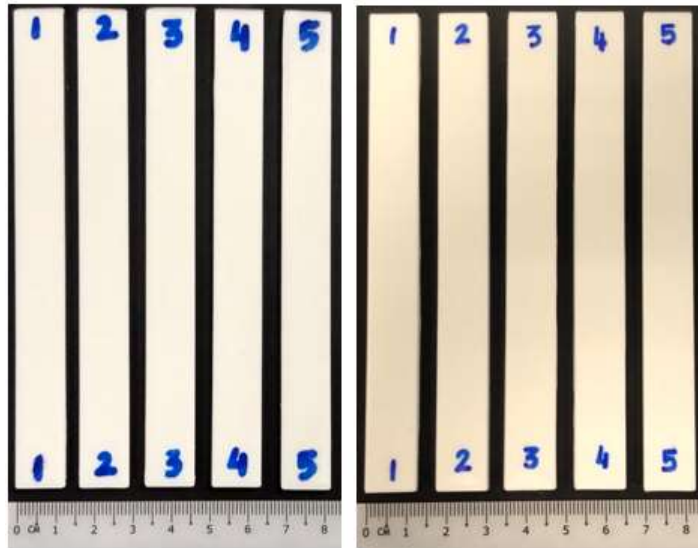
Appendix D: Fabricated bending samples for line pattern



Fabricated bending samples of Single Plane (0°) and Multiplane ($0^\circ, 0^\circ$) for Line Pattern



Fabricated bending samples of Single Plane (45°) and Multiplane ($45^\circ, 0^\circ$) for Line Pattern



Fabricated bending samples of Single Plane (90°) and Multiplane (90° , 0°) for Line Pattern



اونيورسيتي مليسيا قهغ السلطان عبدالله
UNIVERSITI MALAYSIA PAHANG
AL-SULTAN ABDULLAH

Appendix E: Density results of concentric pattern for single-plane and multiplane

Single-plane 0° concentric pattern

Sample	SP-0-C-01	SP-0-C-02	SP-0-C-03
Weight in air (g)	1.1757	1.1730	1.1760
Weight in water (g)	0.1937	0.1949	0.1943
Water temperature (°C)	28.0	28.0	28.0
Δ Weight	0.9820	0.9781	0.9817
Volume (cm ³)	0.9867	0.9828	0.9864
Density (g/cm ³)	1.1973	1.1993	1.1979
Water density (g/cm ³)	0.9952	0.9952	0.9952
Relative density (%)	96.6	96.7	97.6
Average (%)	96.6		

Single-plane 45° concentric pattern

Sample	SP-45-C-01	SP-45-C-02	SP-45-C-03
Weight in air (g)	1.1865	1.1847	1.1866
Weight in water (g)	0.2020	0.2022	0.2026
Water temperature (°C)	28.0	28.0	28.0
Δ Weight	0.9845	0.9825	0.9840
Volume (cm ³)	0.9892	0.9872	0.9887
Density (g/cm ³)	1.2052	1.2058	1.2059
Water density (g/cm ³)	0.9952	0.9952	0.9952
Relative density (%)	97.2	97.2	97.2
Average (%)	97.2		

Single-plane 90° concentric pattern

Sample	SP-90-C-01	SP-90-C-02	SP-90-C-03
Weight in air (g)	1.1755	1.1765	1.1747
Weight in water (g)	0.1945	0.1935	0.1942
Water temperature (°C)	28.0	28.0	28.0
Δ Weight	0.9810	0.9830	0.9805
Volume (cm ³)	0.9857	0.9877	0.9852
Density (g/cm ³)	1.1983	1.1968	1.1981
Water density (g/cm ³)	0.9952	0.9952	0.9952
Relative density (%)	96.6	96.5	96.6
Average (%)	96.6		

Multiplane 0°,0° concentric pattern

Sample	MP-0,0-C-01	MP-0,0-C-02	MP-0,0-C-03
Weight in air (g)	1.1891	1.1874	1.1886
Weight in water (g)	0.2064	0.2058	0.2051
Water temperature (°C)	28.0	28.0	28.0
Δ Weight	0.9827	0.9816	0.9835
Volume (cm ³)	0.9874	0.9863	0.9882
Density (g/cm ³)	1.2100	1.2097	1.2085
Water density (g/cm ³)	0.9952	0.9952	0.9952
Relative density (%)	97.6	97.3	97.5
Average (%)	97.5		

Multiplane 45°,0° concentric pattern

Sample	MP-45,0-C-01	MP-45,0-C-02	MP-45,0-C-03
Weight in air (g)	1.1864	1.1898	1.1901
Weight in water (g)	0.2047	0.2043	0.2051
Water temperature (°C)	28.0	28.0	28.0
Δ Weight	0.9817	0.9855	0.9850
Volume (cm ³)	0.9864	0.9902	0.9897
Density (g/cm ³)	1.2085	1.2073	1.2082
Water density (g/cm ³)	0.9952	0.9952	0.9952
Relative density (%)	97.5	97.3	97.4
Average (%)	97.4		

Multiplane 90°,0° concentric pattern

Sample	MP-90,0-C-01	MP-90,0-C-02	MP-90,0-C-03
Weight in air (g)	1.1733	1.1718	1.1798
Weight in water (g)	0.1962	0.1964	0.1968
Water temperature (°C)	28.0	28.0	28.0
Δ Weight	0.9771	0.9754	0.9830
Volume (cm ³)	0.9818	0.9800	0.9977
Density (g/cm ³)	1.2008	1.2014	1.2002
Water density (g/cm ³)	0.9952	0.9952	0.9952
Relative density (%)	96.8	96.8	96.8
Average (%)	96.8		

Appendix F: Density results of line pattern for single-plane and multiplane

Single-plane 0° line pattern

Sample	SP-0-L-01	SP-0-L-02	SP-0-L-03
Weight in air (g)	1.1731	1.1710	1.1799
Weight in water (g)	0.1937	0.1950	0.1945
Water temperature (°C)	29.0	29.0	29.0
Δ Weight	0.9794	0.9760	0.9854
Volume (cm ³)	0.9843	0.9801	0.9903
Density (g/cm ³)	1.1978	1.1998	1.1974
Water density (g/cm ³)	0.9950	0.9950	0.9950
Relative density (%)	96.5	96.8	96.5
Average (%)	96.6		

Single-plane 45° line pattern

Sample	SP-45-L-01	SP-45-L-02	SP-45-L-03
Weight in air (g)	1.1942	1.1905	1.1891
Weight in water (g)	0.1937	0.1929	0.1946
Water temperature (°C)	29.0	29.0	29.0
Δ Weight	1.0005	0.9976	0.9945
Volume (cm ³)	1.0055	1.0026	0.9995
Density (g/cm ³)	1.1936	1.1934	1.1957
Water density (g/cm ³)	0.9950	0.9950	0.9950
Relative density (%)	96.3	96.2	96.4
Average (%)	96.3		

Single-plane 90° lines pattern

Sample	SP-90-L-01	SP-90-L-02	SP-90-L-03
Weight in air (g)	1.1952	1.1850	1.1928
Weight in water (g)	0.2055	0.2042	0.2081
Water temperature (°C)	29.0	29.0	29.0
Δ Weight	0.9837	0.9778	0.9847
Volume (cm ³)	0.9897	0.9808	0.9847
Density (g/cm ³)	1.2076	1.2082	1.2113
Water density (g/cm ³)	0.9950	0.9950	0.9950
Relative density (%)	97.3	97.4	97.7
Average (%)	97.5		

Multiplane 0°,0° line pattern

Sample	MP-0,0-L-01	MP-0,0-L-02	MP-0,0-L-03
Weight in air (g)	1.1770	1.1778	1.1765
Weight in water (g)	0.2048	0.2058	0.2037
Water temperature (°C)	29.0	29.0	29.0
Δ Weight	0.9722	0.9720	0.9728
Volume (cm ³)	0.9770	0.9769	0.9777
Density (g/cm ³)	1.2107	1.2117	1.2094
Water density (g/cm ³)	0.9950	0.9950	0.9950
Relative density (%)	97.6	97.7	97.5
Average (%)	97.6		

Multiplane 45°,0° line pattern

Sample	MP-45,0-L-01	MP-45,0-L-02	MP-45,0-L-03
Weight in air (g)	1.1854	1.1873	1.1905
Weight in water (g)	0.2096	0.2122	0.2124
Water temperature (°C)	29.0	29.0	29.0
Δ Weight	0.9758	0.9751	0.9781
Volume (cm ³)	0.9807	0.9800	0.9830
Density (g/cm ³)	1.2148	1.2176	1.2172
Water density (g/cm ³)	0.9950	0.9950	0.9950
Relative density (%)	98.0	98.2	98.2
Average (%)	98.1		

Multiplane 90°,0° line pattern

Sample	MP-90,0-L-01	MP-90,0-L-02	MP-90,0-L-03
Weight in air (g)	1.1782	1.1789	1.1798
Weight in water (g)	0.2038	0.2045	0.2075
Water temperature (°C)	29.0	29.0	29.0
Δ Weight	0.9744	0.9744	0.9723
Volume (cm ³)	0.9793	0.9793	0.9772
Density (g/cm ³)	1.2092	1.2099	1.2134
Water density (g/cm ³)	0.9950	0.9950	0.9950
Relative density (%)	97.5	97.5	97.9
Average (%)	97.6		

LIST OF PUBLICATIONS

1. A comprehensive review on fused deposition modelling of polylactic acid, Progress in Additive Manufacturing, Springer, L. Sandanamsamy, W. S. W. Harun, I. Ishak, F. R. M. Romlay, K. Kadirgama, D. Ramasamy, S. R. A. Idris & F. Tsumori
2. Effect of Process Parameter on Tensile Properties of FDM Printed PLA, Materials Today: Proceedings, L.Sandanamsamy, J.Mogan, K.Rajan, W.S.W Harun, I.Ishak, F.R.M Romlay, M.Samykano, K.Kadirgama
3. Investigation of Mechanical Properties of 3D-printed PLA, Materials Today: Proceedings, L Sandanamsamy, WSW Harun, I Ishak and F.R.M Romlay (Submitted for conference publishing)
4. Thermo-mechanical Properties of ABS/Stainless steel composite using FDM, Materials Today Proceedings, J Mogan, L Sandanamsamy, WSW Harun, I Ishak, FRM Romlay, K Kadirgama, D Ramasamy (submitted for conference publishing)
5. A review on 3D printing bio-based polymer composite, IOP Conference Series: Materials Science and Engineering, (IPCME 2021), L Sandanamsamy, J Mogan, N A Halim, W S W Harun, K Kadirgama, D Ramasamy
6. A review of FDM and graphene-based polymer composite, IOP Conference Series: Materials Science and Engineering, (IPCME 2021), J Mogan, L Sandanamsamy, N A Halim, W S W Harun, K Kadirgama, D Ramasamy
7. A review on 3D printed polymer-based composite for thermal applications, IOP Conference Series: Materials Science and Engineering, (IPCME 2021), N A Halim, J Mogan, L Sandanamsamy, W S W Harun, K Kadirgama, D Ramasamy, F Tarlochan